LITHUANIAN UNIVERSITY OF HEALTH SCIENCES
MEDICAL ACADEMY

Milda Pucėtaitė

THE DIAGNOSTIC VALUE OF CONTRAST-ENHANCED ULTRASOUND IN ASSESSING LARYNGEAL CANCER INVASION INTO NON-OSSIFIED THYROID CARTILAGE

Doctoral Dissertation
Medical and Health Sciences,
Medicine (M 001)

Kaunas, 2026

The dissertation was prepared at the Department of Radiology, Faculty of Medicine, Medical Academy, Lithuanian University of Health Sciences during the period of 2021–2025.

Scientific Supervisor

Prof. Dr. Saulius Vaitkus (Lithuanian University of Health Sciences, Medical and Health Sciences, Medicine – M 001).

Consultant

Prof. Dr. Davide Farina (University of Brescia, Medical and Health Sciences, Medicine – M 001).

Dissertation is defended at the Medical Research Council of the Lithuanian University of Health Sciences:

Chairperson

Prof. Dr. Algidas Basevičius (Lithuanian University of Health Sciences, Medical and Health Sciences, Medicine – M 001).

Members:

Prof. Dr. Vykintas Liutkevičius (Lithuanian University of Health Sciences, Medical and Health Sciences, Medicine – M 001);
Prof. Dr. Arturas Inčiūra (Lithuanian University of Health Sciences, Medical and Health Sciences, Medicine – M 001);
Prof. Dr. Nomeda Rima Valevičienė (Vilnius University, Medical and Health Sciences, Medicine – M 001);
Dr. Monika Radikė (North West School of Radiology, Medical and Health Sciences, Medicine – M 001).

Dissertation will be defended at the open session of the Medical Research Council of the Lithuanian University of Health Sciences on the 11th of June 2026 at noon in the 106 auditorium of the Faculty of Nursing, Medical Academy, Lithuanian University of Health Sciences.
Address: Eivenių 2, LT-50161 Kaunas, Lithuania.

LIETUVOS SVEIKATOS MOKSLŲ UNIVERSITETAS
MEDICINOS AKADEMIJA

Milda Pucėtaitė

KONTRASTINIO ULTRAGARSINIO TYRIMO DIAGNOSTINĖ VERTĖ TIRIANT GERKLŲ VĖŽIO IŠPLITIMĄ Į NESUKAULĖJUSIĄ SKYDINĘ KREMZLĘ

Daktaro disertacija
Medicinos ir sveikatos mokslai,
medicina (M 001)

Kaunas, 2026

Disertacija rengta 2021–2025 metais Lietuvos sveikatos mokslų universiteto Medicinos akademijos Medicinos fakulteto Radiologijos klinikoje.

Mokslinis vadovas

prof. dr. Saulius Vaitkus (Lietuvos sveikatos mokslų universitetas, medicinos ir sveikatos mokslai, medicina – M 001).

Konsultantas

prof. dr. Davide Farina (Brešos universitetas, medicinos ir sveikatos mokslai, medicina – M 001).

Disertacija ginama Lietuvos sveikatos mokslų universiteto Medicinos mokslo krypties taryboje:

Pirmininkas

prof. dr. Algidas Basevičius (Lietuvos sveikatos mokslų universitetas, medicinos ir sveikatos mokslai, medicina – M 001).

Nariai:

prof. dr. Vykintas Liutkevičius (Lietuvos sveikatos mokslų universitetas, medicinos ir sveikatos mokslai, medicina – M 001);
prof. dr. Arturas Inčiūra (Lietuvos sveikatos mokslų universitetas, medicinos ir sveikatos mokslai, medicina – M 001);
prof. dr. Nomeda Rima Valevičienė (Vilniaus universitetas, medicinos ir sveikatos mokslai, medicina – M 001);
dr. Monika Radikė (Šiaurės vakarų radiologijos mokykla, medicinos ir sveikatos mokslai, medicina – M 001).

Disertacija bus ginama viešame medicinos mokslo krypties tarybos posėdyje 2026 m. birželio 11 d. 12 val. Lietuvos sveikatos mokslų universiteto Medicinos akademijos Slaugos fakulteto 106 auditorijoje.
Disertacijos gynimo vietos adresas: Eivenių g. 2, LT-50161 Kaunas, Lietuva.

CONTENTS

ABBREVIATIONS

ADC	–	apparent diffusion coefficient
AI	–	artificial intelligence
AJCC	–	American Joint Committee on Cancer
AT	–	arrival time
AUC	–	area under the curve
AUCROC	–	area under the receiver operating characteristic curve
BF	–	blood flow
BRAF	–	B-Raf proto-oncogene, serine/threonine kinase
BV	–	blood volume
CEUS	–	contrast-enhanced ultrasound
CI	–	confidence interval
CRT	–	chemoradiation therapy
cT	–	clinical tumor staging
CT	–	computed tomography
DCE-CT	–	dynamic contrast-enhanced computed tomography
DCE-MRI	–	dynamic contrast-enhanced magnetic resonance imaging
DECT	–	dual-energy computed tomography
DS	–	descending slope
DWI	–	diffusion-weighted imaging
EDTA	–	ethylenediaminetetraacetic acid
EFSUMB	–	European Federation of Societies for Ultrasound in Medicine and Biology
FN	–	false negative
FP	–	false positive
HU	–	Hounsfield units
IMAX	–	maximum intensity
Kep	–	rate constant (contrast reflux from extravascular extracellular space to plasma)
Ktrans	–	volume transfer constant (contrast movement from plasma to extravascular extracellular space)
kVp	–	kilovolt peak
LSCC	–	laryngeal squamous cell carcinoma
MaxEn	–	maximum enhancement
MI	–	mechanical index
MRI	–	magnetic resonance imaging
MTT	–	mean transit time
NNP	–	nuclear notch protein
NOTC	–	non-ossified thyroid cartilage
NPV	–	negative predictive value
NUT	–	nuclear protein in testis
OR	–	odds ratio
PACS	–	Picture Archiving and Communication System
PAS	–	periodic acid–Schiff
PCT	–	perfusion computed tomography
PE	–	peak enhancement
PI	–	peak intensity
PPV	–	positive predictive value

PS – permeability–surface area product
pT – pathological tumor staging
RBV – relative blood volume
ROC – receiver operating characteristic
ROI – region of interest
RS – rise slope
RT – rise time
SCC – squamous cell carcinoma
SECT – single-energy computed tomography
STIR – short tau inversion recovery
TIC – time–intensity curve
TN – true negative
TNM – tumor–node–metastasis
TO – time to onset
ToA – time of arrival
TOLMS – transoral laser microsurgery
TP – true positive
TTP – time to peak
UCA – ultrasound contrast agent
UICC – Union for International Cancer Control
US – ultrasound
Ve – extravascular extracellular volume fraction
VMIs – virtual monochromatic images
Vp – plasma volume
WHO – World Health Organization
WiR/WIR – wash-in rate
WIS – wash-in slope
WIT – wash-in time
WiWoAUC – wash-in/wash-out area under the curve
WoR – wash-out rate (minimum slope)
WOR – wash-out rate
WOT – wash-out time
ΔAUC – difference in area under the curve between tumor and thyroid cartilage
ΔPI – difference in peak intensity between tumor and thyroid cartilage
ΔTTP – difference in time to peak between tumor and thyroid cartilage
ΔWIS – difference in wash-in slope between tumor and thyroid cartilage

INTRODUCTION

Over the last decade, cases of laryngeal cancer have increased by roughly 23% worldwide [1], and it is still significantly more common in men than women [1, 2]. Moreover, the vast majority of malignant laryngeal tumors (about 90%–95%) are squamous cell carcinomas (SCCs), which remain the most common histological type [3, 4].

Accurate imaging assessment of tumor spread, particularly its invasion in thyroid and cricoid cartilages, plays a crucial role in determining the true extent of disease and selecting the most appropriate treatment strategy for an individual patient. It directly influences the extent of surgical management, i.e. whether total laryngectomy, open partial laryngectomy, or transoral laser microsurgery (TOLMS) is performed or whether a conservative approach with radiotherapy and/or chemotherapy is selected [5–9]. These therapeutic decisions have a direct impact on treatment efficacy, prognosis after radiotherapy, and patient's quality of life.

From this point of view, imaging becomes most important in differentiating between T stages according to the Tumor–Node–Metastasis (TNM) classification [10]. Computed tomography (CT) and magnetic resonance imaging (MRI) are the main imaging modalities for staging laryngeal carcinoma for many years [7, 11–16]. Although both CT and MRI are recommended by current guidelines, each modality has intrinsic limitations and strengths. Moreover, the choice of modality often depends on local protocols and scanner availability. CT is effective for evaluating laryngeal cartilage invasion, particularly in regions where the cartilage is already ossified, and it is also advantageous for patients with respiratory difficulties because of its rapid image acquisition. However, a significant diagnostic challenge remains – tumor tissue and non-ossified thyroid cartilage often demonstrate similar tissue densities, making it difficult to reliably assess the presence and extent of tumor invasion [17]. In these cases, MRI is the choice of modality according to the revised MRI criteria by Becker et al. [18] published in 2008. However, even if it is relatively a long time standing reliable radiological modality, the issue of false-positive findings remains. Although the diagnostic accuracy of MRI and dual-energy computed tomography (DECT) has improved, no cross-sectional imaging method has consistently outperformed the others in detecting tumor invasion into non-ossified thyroid cartilage [14, 16–23].

Therefore, researchers continue to investigate new imaging properties and technologies aimed at improving the accuracy of radiologic staging in laryngeal cancer. Contrast-enhanced ultrasound (CEUS) has recently gained

interest in oncological imaging due to its high spatial resolution, excellent acoustic window, and ability to assess and quantify microvascular perfusion in real time [24, 25]. One of the advantages is that CEUS images can be analyzed not only qualitatively but also quantitatively, using perfusion-derived parameters, providing an opportunity to objectify the assessment [24, 26–37]. The knowledge that non-ossified thyroid cartilage is composed of avascular hyaline cartilage rises a hypothesis that it can be differentiated from vascularized tumor tissue based on perfusion patterns observed during CEUS [38–40]. In this field, we found only one study by Hu et al. [41], who have shown that CEUS has potential for detecting laryngeal cartilage invasion in patients with laryngeal cancer. However, this study included all laryngeal cartilages and qualitative CEUS analysis. Overall, the diagnostic role of CEUS in assessing non-ossified thyroid cartilage invasion remains insufficiently investigated, with no studies incorporating quantitative analysis, making it an attractive direction for further research.

The aim of the study

The aim of this study was to determine the diagnostic value of qualitative and quantitative analysis of CEUS in assessing laryngeal squamous cell carcinoma invasion into non-ossified thyroid cartilage, comparing with postoperative histopathological findings.

The objectives of the study

1. To determine the specificity and sensitivity of qualitative (visual) CEUS in assessing laryngeal carcinoma invasion into non-ossified thyroid cartilage.
2. To evaluate the added diagnostic value of CEUS when combined with CT and MRI in assessing laryngeal carcinoma invasion into non-ossified thyroid cartilage.
3. To analyze and determine the diagnostic value of CEUS quantitative time–intensity curve (TIC) parameters in assessing laryngeal carcinoma invasion into non-ossified thyroid cartilage.
4. To determine which combination of TIC parameters provides the highest diagnostic performance in assessing laryngeal carcinoma invasion into non-ossified thyroid cartilage.

The novelty of the study

To this day, the diagnosis of non-ossified thyroid cartilage invasion remains a major challenge in radiological diagnostics with misdiagnosis cases still being present. That is why we decided to look for an additional way to solve this problem. To our knowledge, this is the first scientific CEUS study examining specifically non-ossified thyroid cartilage invasion in patients with laryngeal SCC. Although a similar scientific study was conducted a few years ago, the researchers [41] investigated the invasion of laryngeal cancer into all laryngeal cartilages, without specifically focusing on non-ossified thyroid cartilage. Moreover, the above-mentioned study was based only on visual (qualitative) CEUS assessment [41]. According to the current published literature, we are pioneers in our research topic in several aspects. First, the focus of the CEUS study was non-ossified thyroid cartilage. Second, not only qualitative but also quantitative analysis of CEUS images was performed. Third, the diagnostic values of TIC parameters of non-ossified thyroid cartilage with and without invasion and tumor tissue were determined for the first time. Fourth, for comparison, patients underwent not only CT, but also MRI. Fifth, the added diagnostic value of CEUS combining it with CT and MRI was evaluated. Finally, these aspects of novelty in our research were enhanced by using the histopathological examination as the gold standard, with an accurate target site indicated in our specific Assessment Scheme of Local Spread ("Lokalaus išplitimo ištyrimo schema", Appendix 1), based on CT images.

This study provides novel evidence supporting the potential of CEUS as a complementary, non-invasive imaging modality to CT and MRI for the preoperative assessment of non-ossified thyroid cartilage invasion. These findings may contribute to refining diagnostic algorithms, improving staging accuracy, and reducing diagnostic overestimation, thereby facilitating more appropriate and potentially less traumatic treatment planning in patients with laryngeal squamous cell carcinoma.

1. LITERATURE REVIEW

1.1. Routine imaging modalities

1.1.1. Computed tomography

Computed tomography (CT) is a non-invasive radiological examination that utilizes ionizing radiation. In many institutions, it is most performed as the first-line imaging modality in the diagnosis of laryngeal cancer, especially for patients with locally advanced cancer and dyspnea. It is used to assess tumor localization, local extension, and lymphadenopathy.

According to the established literature guidelines, high-quality diagnostic images should be obtained using a high-resolution multidetector CT scanner with a dedicated head and neck protocol [7]. The examination recommended to be performed both with and without intravenous iodinated contrast administration. Contrast enhancement provides crucial additional information by differentiating between normal and pathological tissues based on their enhancement characteristics [42]. During the examination, images are acquired with a patient positioned supine and breathing gently. The neck should be slightly extended, with the head aligned along the cephalocaudal axis to ensure accurate comparison of bilateral anatomical structures [14]. Following image acquisition, additional multiplanar reconstructions should be done using both soft tissue and bone window settings. High-resolution reconstructions with thin slices and optimal contrast phases are essential for the accurate evaluation of local laryngeal tumor spread in small anatomical regions avoiding misinterpretation. Axial images are parallel to the true vocal cords, whereas sagittal and coronal images are perpendicular. Thin-slice bone multiplanar reconstructions further enhance the evaluation of laryngeal cartilages and potential osseous invasion. CT by offering an exceptional evaluation of the infrahyoid neck with the short scanning time (typically 6–8 s) enables the patient to remain relatively still with low probability of swallowing. Thus, motion artifacts are minimized as compared to imaging modalities longer in duration such as MRI, leaving CT particularly recommended as the first-choice imaging technique in patients with respiratory distress, respiratory failure, or claustrophobia [16, 43].

On CT scans, laryngeal SCCs typically show mild-to-moderate enhancement, though in some cases, enhancement may be stronger [42]. This helps in clearly defining tumor boundaries and evaluating the extent of deep tissue invasion, which is critical for accurate staging. Without extension to soft tissues, tumor invasion to laryngeal cartilages plays an important role [44]. The primary CT characteristics indicative of cartilage invasion include

sclerosis, lysis or erosion, and extra-laryngeal spread. Sclerosis manifests as bony remodeling showing increased density or thickening of the cartilage on CT due to direct invasion or adjacent presence of neoplastic cells; however, specificity to identify cartilage invasion in the presence of sclerosis on CT is the low. As lysis appears as areas of cartilage erosion or destruction, in some cases, it is challenging to evaluate when variable and asymmetrical degrees of cartilage ossification persist [42, 44]. It is important to note that the diagnosis of cartilage invasion is not always straightforward. Notably, the evaluation non-ossified cartilage invasion could be almost indistinguishable on CT, due to the similar densities with enhanced tumor tissue; therefore, normal variations can be mistakenly reported as tumor invasion [14, 17]. However, the suspicion of tumor invasion into non-ossified cartilage typically should be risen when there is proximity between the tumor and the cartilage [11, 14, 17, 42].

Even CT is often preferred over MRI due to its wider availability, lower cost, and faster scanning times, the specificity of CT can be variable and even lower than that of MRI [45]. The results of studies by Becker et al. [18, 46] and other researchers [13, 17, 20, 45] have indicated that the CT-based diagnosis of laryngeal cartilage invasion remains a subject of debate up to this day [13, 17, 18, 20, 45, 46].

1.1.2. Magnetic resonance imaging

MRI is a sophisticated medical imaging technique that provides detailed images without the use of ionizing radiation. This non-invasive examination relies on the interaction between a powerful magnetic field and radiofrequency waves to generate high-resolution images of organs, tissues, and physiological processes within the body. The magnetic field aligns the hydrogen atoms in the body, and when radiofrequency pulses are applied, these atoms emit signals that are detected and processed to create detailed cross-sectional images [47].

One of the key advantages of MRI is its ability to produce images with excellent soft tissue contrast, making it particularly useful for the anatomically difficult head and neck region [6, 9, 16, 43, 44]. Laryngeal MRI should be performed in axial, coronal, and sagittal planes using the vocal cords as strict orientation, providing a comprehensive view of the area of interest. Additionally, institutions should follow the imaging protocol recommendations provided by leaders in head and neck radiology [9].

Primary laryngeal SCCs typically demonstrate intermediate signal intensity on T1, T2, and short tau inversion recovery (STIR)-weighted sequences with moderate contrast enhancement. They may appear as mass-like lesions,

extend along mucosal surfaces, or exhibit diffuse infiltration [9]. One of the main radiological challenges is the assessment of peritumoral infiltration from laryngeal cancer. Peritumoral inflammation usually shows higher T2/STIR signal intensity and stronger contrast enhancement; however, not so rare it mimics a tumor tissue, often leading to overestimation of tumor size and stage [9]. In such cases, advanced imaging techniques such as diffusion-weighted imaging (DWI), which is added to a routine protocol, play an important role in differentiating SCC from peritumoral inflammation. Restricted diffusion is characteristic of tumor tissue, with the mean ADC values of 0.9–1.3 × 10^{-3} mm^2/s, correlating with tumor cellularity and stromal composition. In contrast, peritumoral infiltration shows no restricted diffusion, with higher ADC values of 1.4–1.9 × 10^{-3} mm^2/s [9]. In cases where MRI is not the first-line imaging modality for laryngeal cancer assessment, it serves as a complementary tool for evaluating local tumor spread, including cartilage invasion and extralaryngeal extension, with greater accuracy than CT [9, 18, 45]. On MRI, normal non-ossified thyroid cartilage appears markedly hypointense on T1- and T2-weighted images and, without contrast enhancement, exhibits low-signal intensity on high b-value DWI images and ADC maps [9]. By utilizing the multiparametric diagnostic criteria for tumors, inflammation, normal non-ossified ossified cartilage as previously described, MRI enhances the accuracy of diagnosing cartilage abnormalities, thereby preventing diagnostic errors associated with CT, making it possible to use it as the primary examination in the diagnosis of laryngeal cancer for patients without respiratory distress [13, 18, 42, 45, 48].

To summarize, if the cartilage near a tumor shows a moderately high signal intensity on T2-weighted images, moderate enhancement on contrast-enhanced T1-weighted images, and restricted diffusion (similar to tumor), it should be considered invaded. Conversely, if the cartilage near a tumor exhibits a higher signal intensity on T2-weighted images and greater enhancement than the adjacent tumor, without restricted diffusion, it should be defined as peritumoral cartilage inflammation [9, 18]. It is important to recognize that DWI images might not always be helpful for diagnosis due to issues such as geometric distortion and reduced spatial resolution. Consequently, if the quality of DWI images is insufficient for diagnostic purposes, Becker et al. suggest relying on standard morphologic MR imaging based on experience [9].

Therefore, to obtain high-quality diagnostic images, which are important for cancer staging, MRI should be performed according to the expert-recommended guidelines. Despite its significant advantages, MRI also has other limitations, the main ones being the long scanning time (which may last up to 45 min) and its sensitivity to metal and motion artifacts. For this reason,

MRI is not the first-choice examination for patients with breathing difficulties, respiratory insufficiency, claustrophobia, or those who are unable to remain still for a longer period [6, 11, 49].

1.2. Other imaging modalities

1.2.1. Dynamic contrast-enhanced and perfusion computed tomography

Dynamic contrast-enhanced CT (DCE-CT) is an emerging functional imaging technique in oncological imaging. Unlike conventional CT, which provides mainly anatomical information, DCE-CT offers insight into tumor physiology by tracking the temporal changes in contrast enhancement following intravenous injection of iodinated contrast material and offers a qualitative and quantitative overview of tumor vascularity [19].

Perfusion CT (PCT) is a specific application within the broader category of DCE-CT techniques. It utilizes mathematical models, such as deconvolution or compartmental analysis, to calculate quantitative hemodynamic parameters such as blood flow (BF), blood volume (BV), mean transit time (MTT), and capillary permeability–surface area product (PS) described in Table 1.2.1.1 [50].

Table 1.2.1.1. *Quantitative hemodynamic parameters of perfusion computed tomography [50]*

Perfusion parameter	Description
Blood flow (BF)	expressed in mL/min/100 g of tissue, it is the flow rate of blood through vasculature in a tissue region. BF includes flow information from large vessels, arterioles, capillaries, and venules as well as arteriovenous shunts, which are more common in neoplastic tissue than in healthy tissue
Blood volume (BV)	expressed in mL/100 g of tissue, it represents the volume of blood that flows within vasculature in a tissue region
Mean transit time (MTT)	expressed in s, it represents the mean time blood takes to pass through microvasculature from the arterial to the venous end. MTT is inversely correlated to BF
Permeability–surface (PS) products	expressed in mL/min/100 g of tissue, it measures the product between the permeability and the total surface area of capillary endothelium in a unit mass of tissue (usually 100 g of tissue). It is considered as a surrogate marker of immature leaky vessels, which are more common in neoplastic tissue

Technically, DCE-CT and perfusion CT share the same acquisition principles, involving rapid sequential imaging during the first pass of intravenous contrast administration. However, DCE-CT may employ pharmacokinetic modeling to assess parameters such as the transfer constant (K_{trans}) and extracellular volume fraction (Ve), whereas perfusion CT focuses on the direct quantification of blood flow dynamics within a defined region of interest (ROI) [51]. Despite these methodological distinctions, both techniques are frequently used interchangeably in literature as they serve a common purpose, i.e. functional evaluation of tumor perfusion.

There are some technical considerations worth mentioning. CT scans of the head and neck work best on multi-detector CT machines using a beam collimation as wide as possible to maximize anatomic coverage on the z-axis, achieving an optimal trade-off between radiation dose, image noise, and both spatial and temporal resolution – all this is essential for reliable results [50].

For dynamic scanning, the scan range can be adjusted based on the scanner setup: a 2-cm range for a 16-row CT scanner, a 4-cm range for a 64-row CT scanner, or a range of 8 to 16 cm for a 128- or 320-row CT detector [50]. This helps capture both the main tumor and nearby lymph nodes. The scan settings need to balance radiation exposure and image quality, usually using 80–100 kVp and 20–100 mAs per rotation. Motion correction and standard software are important for consistent results [51].

Quick CT images are taken after injecting contrast into a vein. The dynamic CT acquisition time varies among institutions. For example, the article by Razek et al. [50] mentions a total time of 40–60 s, and for permeability measurements, a second phase is obtained after 2–10 min [50]. These images help create time-attenuation curves for each small area [50–52]. The choice of PCT acquisition parameters depends on the anatomical area being examined, the technical characteristics of the scanner, and the method used for data analysis.

In head and neck oncology, from a scientific perspective, DCECT/PCT has been not very widely applied in the evaluation of tumor infiltration, treatment response, and characterization of tumor aggressiveness, and only few studies investigated laryngeal cartilage invasion [19, 50–53]. To our knowledge, existing studies have not shown a significant diagnostic value of DCECT/PCT in assessing local tumor invasion of the larynx (including thyroid cartilage), although these studies have not specifically investigated non-ossified thyroid cartilage [19, 53]. DCECT/PCT faces several challenges; moreover, in some cases, achieving adequate image quality does not effectively cover large or multifocal tumors. Additionally, variations currently exist in the implementation protocols and software used, which has implications for diagnostic standardization. Furthermore, the technique may

involve increased radiation exposure [51]. To establish the efficacy of DCE-CT in diagnosing and staging laryngeal cancer, large multicenter studies and standardized protocols are required.

1.2.2. Dual-energy computed tomography

DECT represents a significant advancement in imaging technology, specifically enhancing the evaluation of head and neck cancer by obtaining images at two different X-ray energy levels rather than conventional single-energy CT (SECT) [54]. DECT allows for superior tissue characterization and differentiation between malignant and non-malignant tissues, which is essential for precise diagnosis and treatment planning. This technology not only improves visualization of tumors but also aids in assessing their extent and potential invasion into critical structures, paving the way for more targeted therapeutic approaches. Understanding the underlying techniques and a range of applications further underscores the pivotal role DECT plays in modern oncological imaging [54, 55].

It is important to mention that several DECT scanners are utilized in clinical practice, each with unique features and capabilities. These scanners employ different technological approaches to achieve dual-energy imaging, including dual-source systems, rapid kVp switching, and dual-layer detectors (Fig. 1.2.2.1) [54]. Dual-source scanners use two X-ray tubes and detector pairs, allowing for simultaneous acquisition of high- and low-energy data. Rapid kVp switching systems alternate between high- and low-tube voltages during a single rotation, while dual-layer detectors use a single X-ray source with two detector layers sensitive to different energy levels [54–58].

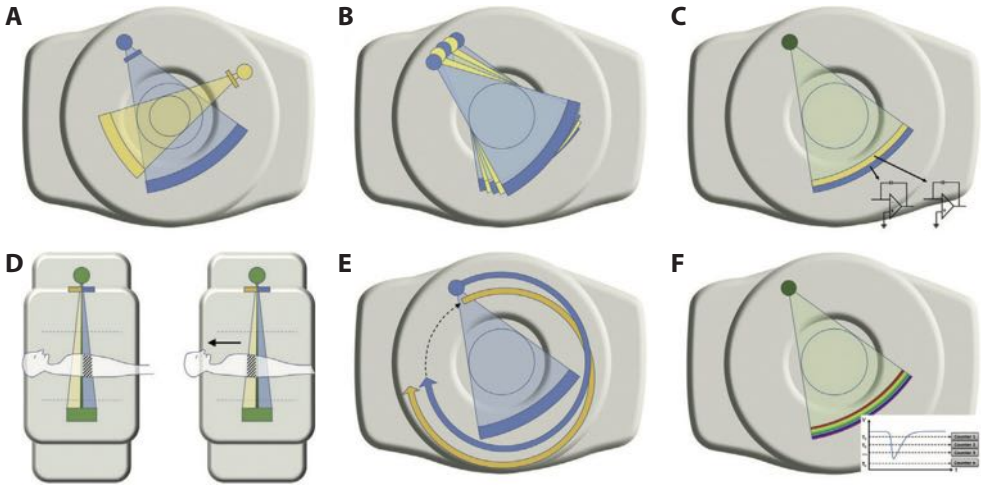

Fig. 1.2.2.1. *Different DECT scanners*

For optimal DECT scanning, projection data should be obtained simultaneously or nearly simultaneously at 2 different peak energies, represented by different colors. Description: **(A)** Dual-source DECT (Siemens AG). This system consists of 2 source x-ray tubes with 2 corresponding detectors at a nearly orthogonal angle, enabling the same slice to be imaged simultaneously at high and low energies. **(B)** Single source DECT with rapid kV switching (GE Healthcare). Projection data are collected twice for every projection, 1 at high- and 1 at low-tube voltage, by very fast switching between low-energy and high-energy spectra combined with fast sampling capabilities of a proprietary, garnet-based scintillator detector with low afterglow for spectral separation at each successive axial or spiral view. **(C)** Dual-layer or sandwich detector DECT (Philips Healthcare). This system consists of a single source and detector, but the detector is composed of 2 scintillation layers. With this system, separation of high-energy and low-energy spectra produced by a single source occurs at the level of the detector. **(D)** TwinBeam DECT (Siemens AG). This system consists of a single source-detector combination in which a split filter at the output of the tube results in separation of the beam into low-energy and high-energy spectra. **(E)** Sequential scanning approach for DECT is one of the earliest and simplest ways to obtain DECT scans. Data at 2 different energies are acquired sequentially at the same positions using different tube voltages. However, there can be significant limitations using this approach because of effects of motion and temporal misregistration that may limit successful use of this technology to certain niche areas. **(F)** A photon-counting scanner, one of the most advanced spectral CT systems currently under development and only available for experimental use at this time. These scanners use photon-counting detectors to resolve the energy of individual photons or photon bins. Theoretically, narrow selectable subranges (or bins) of the spectrum can then be used to classify materials based on their spectral characteristics, enabling multienergy material characterization.
Reproduced from Sananmuang et al. [58] with permission.

The choice of DECT scanner in a clinical setting depends on various factors including specific imaging requirements, patient population, and institutional preferences. Each type of scanner offers distinct advantages in terms of temporal resolution, spatial resolution, and material differentiation capabilities. Understanding the strengths and limitations of different DECT technologies is crucial for optimizing image quality, diagnostic accuracy, and radiation dose management in clinical practice [54].

In clinical practice, DECT examinations should deliver radiation doses that are acceptable and, ideally, not greater than those from SECT. While early adoption of DECT raised concerns about higher exposure, multiple studies have shown that comparable, and sometimes even lower, doses can be achieved without compromising image quality. For adult patients with head and neck cancer, maintaining high-quality imaging is essential to allow accurate staging, treatment planning, and precise delineation of tumor extent for optimal surgical management when indicated. In these cases, a priority should be given to obtaining diagnostically robust images, with radiation exposure kept as low as reasonably achievable rather than focusing on minor dose reductions that do not impact clinical outcomes [54–56]. The different energy levels used in DECT are crucial for image reconstructions and material characterization (Table 1.2.2.1) [54–56, 58].

Table 1.2.2.1. *Most common reconstructions of DECT images [58]*

Image reconstruction type	Basic principles
Virtual monochromatic images (VMIs)	• VMIs can be reconstructed at energies typically ranging from 40 keV to 140 keV or higher • 65- or 70-keV VMIs are considered similar to standard 120-kVp SECT scans • On the low-energy VMIs (e.g., 40 keV) enhance tumor visibility and soft tissue contrast • High-energy VMIs (e.g., 95 keV or higher) are useful for distinguishing non-ossified thyroid cartilage from tumors and reducing metallic artifacts
Material decomposition/ iodine map	• DECT is typically best suited for the decomposition of 2 constituent elements, such as iodine-water for generating an iodine map • Iodine, the main constituent of CT contrast agents, has a k-edge of 33.2 keV • Low-energy VMIs approaching this k-edge increase the attenuation of enhancing tissues
Weighted average images	• Typically blend 30% of the low-energy and 70% of the high-energy attenuation data to simulate standard 120-kVp SECT and used for routine clinical interpretation

keV – kilo-electron-volt; CT – computed tomography; DECT – dual-energy computed tomography; kVp – kilovolt peak; SECT – single-energy computed tomography.

The ability to manipulate these energy levels allows DECT to provide enhanced tissue characterization, improved tumor visualization, artifact reduction, and quantitative analysis capabilities.

DECT has shown a significant promise in assessing thyroid cartilage invasion in laryngeal and hypopharyngeal cancers. The technology leverages the different spectral characteristics of non-ossified thyroid cartilage and tumor tissue to improve diagnostic accuracy. High-energy VMIs are particularly useful in this context as they enhance the distinction between non-ossified thyroid cartilage and the tumor. This differentiation is possible because non-ossified thyroid cartilage maintains its high attenuation at higher energies, while tumor attenuation decreases due to iodine suppression (most evident at VMI energies of 95 HU or higher) [59]. Studies have demonstrated that the addition of iodine maps to standard SECT-equivalent DECT images can increase sensitivity for detecting thyroid cartilage invasion without compromising specificity [60]. Furthermore, DECT with iodine overlay maps has shown a higher specificity and an acceptable sensitivity in diagnosing laryngeal cartilage invasion compared to MRI [61]. It is essential to verify that the display settings are accurate to prevent incorrect identification of iodine levels in the targeted area. Combining this interpretation with traditional imaging is crucial and typically helps in identifying potential errors [58].

Although DECT offers notable advantages, its integration into worldwide routine clinical practice has been slow and quite limited, likely due to workflow challenges and the perception of marginal clinical benefits, yet. However, emerging computerized image analysis and machine learning applications may help realize the full potential of DECT, potentially leading to greater interest and adoption of this technology in future.

1.2.3. Dynamic contrast-enhanced magnetic resonance imaging

Dynamic contrast-enhanced MRI (DCE-MRI) is a functional imaging modality that evaluates microvascular characteristics of tissues by analyzing signal intensity changes following the administration of gadolinium-based contrast agents [62]. The analysis can be approached at three levels: *qualitative*, *semi-quantitative*, and *quantitative*.

Qualitative analysis involves the visual assessment of enhancement patterns over time and descriptive evaluation of the shape of the TIC in voxels [62]. TICs are typically categorized into three types: type I (persistent), type II (plateau), and type III (wash-out). Malignant lesions frequently exhibit rapid enhancement followed by wash-out (type III), suggesting high vascular permeability [62, 63]. Citil et al. [22] in their study involving patients with laryngeal cancer discussed a different classification of curve patterns and reported that type A (showing peak enhancement within 120 s during the early phase and a decrease during the delayed phase) and type B

(demonstrating increasing enhancement in the early phase followed by a plateau in the delayed phase) curves were strongly associated with malignancy, whereas type C (showing no increasing peak and relatively stable enhancement throughout the examination) curves were linked to benign changes [22].

Semi-quantitative analysis uses TIC data to extract parameters such as maximum enhancement (MaxEn), time to peak (TTP), wash-in rate (WIR), wash-out rate (WOR), and area under the curve (AUC) without requiring pharmacokinetic modeling [62]. These parameters are easy to compute and provide insight into tumor vascularity. In a study involving patients with nasopharyngeal carcinoma, Huang et al. reported that the initial AUC and MaxEn were significantly higher in advanced-stage tumors, correlating with their aggressive angiogenic profile [64].

Quantitative analysis applies pharmacokinetic models such as the Tofts or the most commonly used "extended Tofts" model to derive biologically meaningful parameters, including K_{trans} (volume transfer constant) that reflects the rate of contrast agent movement from blood plasma to the extravascular extracellular space; K_{ep} (rate constant) that indicates reflux of contrast agent back into plasma; V_e (extracellular extravascular volume fraction), and V_p (plasma volume) [65–67].

In the field of head and neck pathologies, Yu et al. [67] demonstrated that malignant cartilage lesions had significantly high K_{trans} and V_e values, supporting DCE-MRI as an accurate and quantitative modality to evaluate neoplastic invasion of the laryngeal cartilage in a noninvasive way. However, other published studies showed inconsistent results [65, 68]. For this reason, standardized acquisition and analysis protocols should be regarded as an opportunity to harmonize clinical practice and ensure consistency in imaging methodology across studies and institutions [62]. To the best of our knowledge, no prior studies have specifically addressed the assessment of non-ossified thyroid cartilage invasion, highlighting a potential direction for future research.

1.3. Contrast-enhanced ultrasound

CEUS represents a significant advancement in medical imaging, offering enhanced diagnostic capabilities over conventional ultrasound. The term CEUS was formally introduced as an acronym by members of the European Federation of Societies for Ultrasound in Medicine and Biology (EFSUMB). Ultrasound contrast agents (UCAs) are used in this technique to enhance the visualization of blood flow and tissue perfusion, supporting more accurate assessment of different pathologies [25, 69, 70].

1.3.1. Basic principles and technique

A successful CEUS examination requires specific equipment and a standardized scanning protocol. The essential components include an ultrasound scanner equipped with contrast imaging software, UCAs, and 2 sets of hands available for intravenous injection and performance of CEUS imaging [70]. A CEUS capable ultrasound scanner is necessary, featuring a low mechanical index (MI) of 0.05–0.4 used for CEUS to minimize bubble disruption [71]. Most vendors of ultrasound devices offer systems with this capability. Additionally, it is important to have and choose the right probe. Linear probes operating at higher transmission frequencies can be beneficial for evaluating superficial lesions and in situations where greater spatial resolution is required [69, 70]. In such cases, administering higher doses of contrast may be advantageous for laryngeal imaging, as agents become less efficient nonlinear scatterers at higher frequencies [69]. A scanner must be able to record single images and multi-image cine clips of variable lengths, up to several minutes for quantitative analysis. Using a dual-screen option is recommended, displaying a gray-scale image on one screen for localization and the contrast-only image on the other. Moreover, a timer showing the time from the start of the injection is also essential [70].

It is suggested that CEUS should be carried out by practitioners who have acquired ample experience in both US and CEUS techniques [25,69,70,72].

Another important aspect of the quality of CEUS examination is a scanning protocol, which involves several key steps:

1. *Preparation*: initial gray-scale imaging is done to locate the area of interest. The patient is positioned to keep the lesion/tumor in the field of view and minimize its distance from the transducer. Intravenous access is established, preferably with an 18–20-G needle in an antecubital vein, and a 3-way stopcock is used to facilitate injection [70, 73].
2. *Contrast injection*: the UCA must be activated as required, and before each subsequent application, the container for contrast medium must be shaken [73]. Before injection, the gain on the contrast-only image is adjusted to be minimal (a nearly black screen). The UCA is injected at a rate of about 1 mL/s, immediately (a bolus) followed by a 5- to 10-mL saline flush [70].
3. *Imaging and recording*: the contrast-specific mode is activated. Depending on the application, image recording (cine clip) usually begins either with saline flush or when the first microbubble appears in the field of view. Continuous insonation of large areas should be avoided to prevent premature bubble destruction. A practical

approach is to perform continuous scanning and record a cine loop starting from the initial appearance of microbubbles, capturing the arterial enhancement peak and extending up to 60 s (based on the presence of early wash-out). Beyond this point, scanning should proceed intermittently, with single images or short cine loops stored every 30–60 s to document the onset of wash-out [69, 70].

4. *Repeat injections*: if the second dose is needed, it is best to wait about 5 min for the initial dose to dissipate or use a high-MI imaging mode (like a flash mode) to destroy the remaining bubbles before the next injection [69, 70].

After the cine clip is saved, the next step is postprocessing: (a) a detailed reassessment of the recorded cine loop in slow motion with qualitative and quantitative analysis; (b) discussion of the findings and preparation of a structured study summary; and (c) completion of the final report with recommendations for the patient [74]. The archived cine clip remains available for repeated analysis when necessary.

1.3.2. Contrast agents

UCAs are gas-filled tiny microbubbles that create an acoustic interface with the surrounding blood, enabling the visualization of blood flow and tissue perfusion. They are considered safe, lacking nephrotoxicity, and allow for repeated examinations in short intervals because their active components are quickly eliminated through exhalation [70, 75, 76]. To date, contrast agents can be divided into several generations: first-generation agents characterized by low stability, second-generation agents with improved stability, and third-generation agents composed of nanospheres. They can also be classified according to the type of shell: lipid-based or protein-based. Today in clinical practice, several UCAs with different compositions and approved indications shown in Table 1.3.2.1 are used [70, 76].

Table 1.3.2.1. *Clinically approved contrast agents in current use [76]*

Brand name	Manufacturer	Gas	Shell	Approved indications	Distribution compartments	First approval
Optison®	GE Healthcare	Perfluorpropane	Albumin	Cardio	Blood pool	1998
SonoVue® / Lumason®	Bracco	Sulphurhexafluorid	Phospholipids	Cardio, vascular, abdomen, breast, urinary tract	Blood pool	2001
Definity® / Luminity®	Lantheus Medical Imaging	Perfluorpropane	Phospholipids	Cardio	Blood pool	2001
Sonazoid®	GE Healthcare	Perfluorbutane	Phosphatidylserine	Abdomen (liver)	Blood pool, reticuloendothelial system uptake	2006

Adapted from the publication by Dietrich et al. [76].

1.3.2.1. Overview of the contrast agent SonoVue®

SonoVue is a second-generation UCA that is widely used in clinical settings. First approved in European countries in 2001, it is the most utilized contrast agent in clinical practice, and it is now registered in 44 countries including Lithuania [69, 75, 77, 78].

Physical characteristics. SonoVue is a stabilized aqueous suspension composed of microbubbles. These microbubbles contain sulfur hexafluoride (SF_6) gas and are enclosed by a phospholipid shell. Specifically, the shell is made of DSPC (1,2-distearoyl-sn-glycero-3-phosphocholine) and DPPG-Na (1,2-dipaloyl-sn-glycero-3-phospho-rac-glycerol sodium). The microbubbles range in size from 1.5 to 2.5 μm [77]. It is designed for real-time imaging using low MI modes, typically less than 0.1, and exhibits greater stability compared to first-generation UCAs. After injection, SonoVue is considered a pure blood pool agent, meaning it primarily circulates within the bloodstream. The gas is eventually exhaled through the lungs, while the shell is primarily metabolized by the liver [77].

Safety. SonoVue has a favorable safety profile [25, 77]. The microbubble phospholipid encapsulation lacks protein components, resulting in a relatively low incidence of allergic reactions. A large multi-center retrospective study involving 463,434 examinations reported adverse events in only 0.033% of cases, with just 0.001% classified as severe [79]. The most

common risk factors for intolerance to UCAs include a pronounced allergic predisposition to contrast media, cardiac insufficiency, and pulmonary hypertension. Furthermore, their use is contraindicated during pregnancy and lactation in some countries [73, 77].

1.3.3. Imaging data analysis of contrast-enhanced ultrasound

1.3.3.1. Qualitative analysis

Qualitative analysis in CEUS involves a different visual assessment of contrast uptake dynamics such as enhancement (intensity, homogeneity, margins, rims), perfusion pattern (centripetal, non-centripetal or a diffuse central pattern), wash-in and wash-out behavior, and comparison with adjacent tissues. These qualitative features can aid in distinguishing benign from malignant lesions and in characterizing vascular architecture in real time [24, 80].

The characteristics of qualitative analysis may vary, and their combinations depend on the specific region or organ under investigation as well as the underlying pathology [24, 25]. However, a minor pseudolimitation should be acknowledged, as qualitative analysis relies on the examiner's subjective assessment, which may introduce a degree of reduced objectivity.

So far, there are no officially approved CEUS algorithms for the diagnosis or staging of laryngeal cancer as just several small single-center studies have already been conducted [41, 81].

1.3.3.2. Quantitative analysis

The introduction of microbubble contrast agents has facilitated not only qualitative analysis but also the acquisition of essential quantitative data on tissue vascularity, perfusion, and even endothelial wall function [70,77]. Following the CEUS examination performed in accordance with the protocol outlined in section *1.3.1 Basic principles and techniques*, microvascular and perfusion dynamics can be evaluated using the TIC (Fig. 1.3.3.2.1) generated from contrast enhancement within a ROI. Quantitative parameters commonly derived from TIC analysis are shown in Tables 1.3.3.2.1 and 1.3.3.2.2, which provide objective measures of tissue perfusion and vascular behavior [82]. These parameters have been applied in studies on tumors, vascular diseases, and organ perfusion to discriminate benign versus malignant lesions, assess therapeutic response, or monitor microvascular changes [24, 25, 31, 83]. In certain cases, the diagnostic performance of CEUS can be enhanced through the combined use of qualitative and quantitative analysis methods.

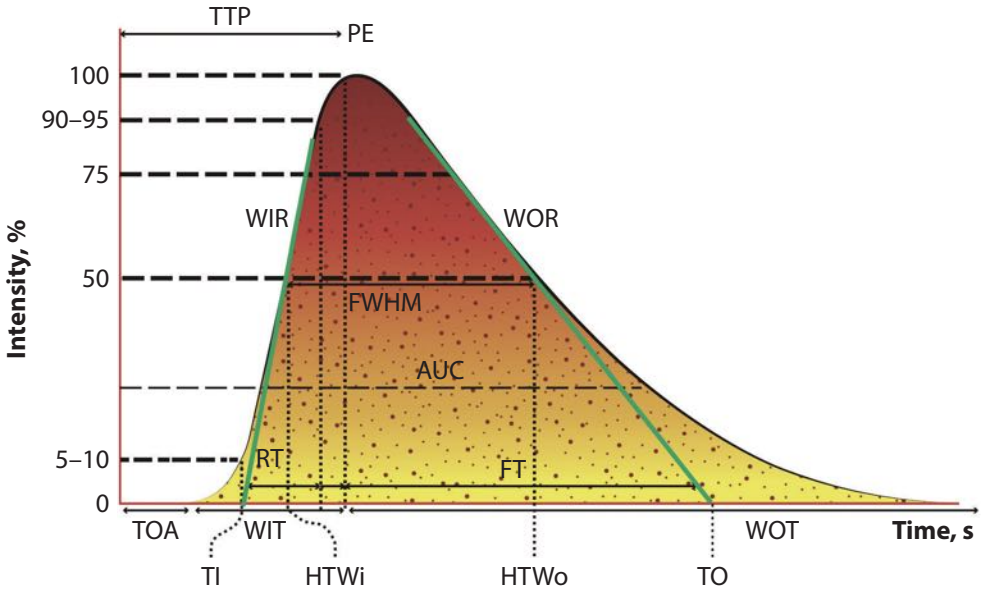

Fig. 1.3.3.2.1. *Time–intensity curve graph with common parameters*

TOA – time of arrival; RT – rise time; WIR – wash-in rate; TTP – time to peak; PE – peak enhancement; WOR – wash-out rate; AUC – area under the curve; FT – fall time; FWHM – full width at half maximum; WIT – wash-in time; WOT – wash-out time; TI – time of inflow; HTWi – half time wash-in; HTWo – half time wash-out; TO – time of outflow.
Reproduced from Peniaeva et al. [74] with permission.

Table 1.3.3.2.1. *Time–intensity curve parameters related to blood volume [28, 74]*

Parameter	Synonym	Definition
Peak intensity (PI)	Peak enhancement (PE), maximum intensity (IMAX)	The maximum value of the intensity in arbitrary units
Area under the curve (AUC)	Wash-in wash-out area under the curve (WiWoAUC)	The area under the time-intensity curve above baseline, which is calculated numerically between the starting time and a predefined end time
	Relative blood volume (RBV)	Allows to estimate the relative blood volume regardless of the time of arrival and flow velocity of the bubbles in ROI. Particularly important in lesions with irregular contrast enhancement

ROI – region of interest.

Table 1.3.3.2.2. *Time-related parameters in relation to blood flow [28, 74]*

Parameter name	Synonym	Definition
Time zero offset	Arrival time (AT) Time of arrival (ToA)	Time from the UCA injection to the first appearance of any UCA signal within the ROI, i.e. the point on the abscissa where the TIC curve starts the uprise
Time to peak (TTP)	TtoPk, tp, time to peak intensity (TPI)	Time to achieve the maximum intensity
Rise time (RT)	Wash-in time (WIT)	Time from UCA appearance / TI to maximum intensity time depending on the software used; RT can be described as time from 5% (10%) to 95% (90%)
Mean transit time (MTT)	Mean transit time (mTT)	The mean time taken by the bubbles to pass through the ROI
Wash-in rate – maximum slope (WiR)	Ascending slope (AS), rise slope (RS), wash-in slope (WIS)	Characterizes the rate of UCA accumulation in the ROI
Wash-out rate – minimum slope (WoR)	Descending slope (DS)	Characterizes the rate of UCA wash-out in the ROI
Fall time (FT)	Wash-out time (WOT)	Time from maximum intensity to TO, i.e. the point where the minimum slope tangent intersects the x-axis

UCA – ultrasound contrast agent; ROI – region of interest; TIC – time-intensity curve; TO – time of outflow.

The most commonly used parameters, which depend on the software, are arrival time (AT, ToA), time to peak (TTP), peak intensity (PI, PE), wash-in rate (WIR, AS, WIS), wash-out rate (WOR, DS), wash-out time (WOT), and area under the curve (AUC) [28, 84]. It is essential to know that many aspects can lead to variations in quantitative CEUS, some of them: the settings of the scanner, patient-related factors including physiological aspects, propagation/attenuation, and the types of bubbles and their management [74, 85]. In this context, the application of standardized protocols is considered an essential solution to ensure reproducibility and reliability. Notably, to our knowledge, there are no published studies providing the values of qualitative parameters of laryngeal cancer or laryngeal cartilages.

1.3.4. CEUS application in oncology

With a growing number of studies across various pathologies, CEUS has increasingly become a significant tool in oncology, offering numerous applications through its ability to provide real-time imaging without radiation

exposure or toxicity to the liver and the kidneys [24, 25, 30, 32, 36, 37, 68, 73, 80, 81, 83, 84, 86–109].

The EFSUMB, the leading European authority in ultrasound practice, regularly publishes consensus guidelines on CEUS, providing evidence-based recommendations that aim to standardize its clinical application across specialties rather than simply report research findings. The guidelines summarize current evidence evaluated by expert consensus, based on peer-reviewed publications and excluding abstracts or conference reports. Levels of evidence and grades of recommendation follow the Oxford Centre for Evidence-based Medicine criteria. In clinical practice, among the applications of CEUS in oncology listed in the EFSUMB guidelines (Table 1.3.4.1), laryngeal and hypopharyngeal cancers are not included, while the most widely used applications are those for the liver and the kidneys.

Table 1.3.4.1. *CEUS applications in oncology according to the EFSUMB guidelines in adults [24, 25]*

Organ/system	Applications in oncology
Liver	Hepatocelullar carcinoma, metastases, intrahepatic cholangiocarcinoma; lesion characterization (benign *vs.* malignant); detection of residual/recurrent tumor; monitoring treatment response
Kidney	Solid renal tumors, complex cystic lesions; differentiation of indeterminate masses; vascular assessment; monitoring after ablative therapy
Pancreas	Pancreatic adenocarcinoma, neuroendocrine tumors; differentiation malignant *vs.* benign; hypervascular tumor detection; biopsy guidance
Breast	Benign *vs.* malignant breast lesions; adjunct to BI-RADS; assessment of tumor vascularity
Thyroid	Thyroid carcinoma *vs.* benign nodules; vascularity analysis; evaluation of indeterminate nodules
Lymph nodes	Metastases, lymphoma, reactive nodes; differentiation malignant *vs.* benign; staging; therapy response assessment
Prostate	Prostate carcinoma; detection; biopsy targeting; focal therapy monitoring
Urinary bladder / urinary tract	Bladder tumors; differentiation from clots; evaluation of tumor extent with intravesical CEUS
Gynecologic organs	Ovarian carcinoma, endometrial carcinoma; differentiation benign *vs.* malignant; perfusion assessment
Soft tissue and musculoskeletal	Sarcomas, metastases; differentiation; biopsy guidance; vascular mapping

BIRADS – Breast Imaging Reporting and Data System; CEUS – contrast-enhanced ultrasound.

In summary, CEUS represents a safe, effective, and precise imaging technique that complements conventional approaches, boosting diagnostic assurance and procedural success rates in a range of cancer-related applications. However, the available literature on the application of CEUS in laryngeal cancer remains limited and insufficient.

1.4. Local staging of laryngeal cancer

Laryngeal squamous cell carcinoma (LSCC) represents more than 90% of malignant laryngeal tumors, with the vast majority being conventional SCC [4]. According to the latest WHO Classification of Head and Neck Tumours, additional histological subtypes include verrucous carcinoma, basaloid SCC, papillary SCC, spindle cell (sarcomatoid) SCC, adenosquamous carcinoma, and lymphoepithelial carcinoma, along with very rare forms such as NUT carcinoma, adenoid SCC, and carcinoma cuniculatum [4]. These subtypes are recognized clinicopathological entities with distinct morphology, differential diagnoses, and prognostic implications, which are integral to individualized treatment planning.

Precise tumor staging is crucial for planning optimal treatment strategies by prioritizing larynx preservation treatment whenever feasible. Only cross-sectional imaging can assess the submucosal extent of the tumor, cartilage invasion, and extralaryngeal spread, while the mucosal extent of the tumor and vocal cord mobility are optimally evaluated through endoscopic examination [110].

The American Joint Committee on Cancer (AJCC), in partnership with the Union for International Cancer Control (UICC), provides a leading staging classification system for all cancers based on their anatomical localization. Since its initial release in 1977, the AJCC staging manual has been updated approximately every 5 to 7 years, culminating in the last full 8th edition published in 2016. This latest classification system version has been applicable in manual since January 1, 2018 [111]. Despite the electronic release of AJCC Version 9 and subsequent updates through 2026, no modifications have been released to the T staging criteria for laryngeal cancer; thus, staging remains based on the 8th edition (Table 1.4.1) [111].

Table 1.4.1. *Definition of supraglottis, glottis, and subglottis primary tumor (T) for laryngeal cancer*

T category	T criteria
TX	Primary tumor cannot be assessed.
Tis	Carcinoma in situ.
Supraglottis	
T1	Tumor limited to one subsite of supraglottis with normal vocal cord mobility
T2	Tumor invades mucosa of more than one adjacent subsite of supraglottis or glottis or region outside the supraglottis (e.g., mucosa of the base of the tongue, vallecula, medial wall of pyriform sinus) without fixation of the larynx
T3	Tumor limited to larynx with vocal cord fixation and/or invades any of the following: postcricoid area, pre-epiglottic space, paraglottic space, and/or inner cortex of thyroid cartilage
T4	Moderately advanced or very advanced
– T4a	Moderately advanced local disease. Tumor invades through the outer cortex of the thyroid cartilage and/or invades tissues beyond the larynx (e.g., trachea, soft tissues of the neck including deep extrinsic muscle of the tongue, strap muscles, thyroid, or esophagus)
– T4b	Very advanced local disease. Tumor invades prevertebral space, encases carotid artery, or invades mediastinal structures
Glottis	
T1	Tumor limited to the vocal cord(s) (may involve anterior or posterior commissure) with normal mobility
– T1a	Tumor limited to one vocal cord
– T1b	Tumor involves both vocal cords
T2	Tumor extends to supraglottis and/or subglottis, and/or with impaired vocal cord mobility
T3	Tumor limited to the larynx with vocal cord fixation and/or invasion of paraglottic space and/or inner cortex of the thyroid cartilage
T4	Moderately advanced or very advanced
– T4a	Moderately advanced local disease. Tumor invades through the outer cortex of the thyroid cartilage and/or invades tissues beyond the larynx (e.g., trachea, cricoid cartilage, soft tissues of the neck including deep extrinsic muscle of the tongue, strap muscles, thyroid, or esophagus)
– T4b	Very advanced local disease. Tumor invades prevertebral space, encases carotid artery, or invades mediastinal structures

Table 1.4.1. *Continued*

T category	T criteria
Subglottis	
T1	Tumor limited to the subglottis
T2	Tumor extends to vocal cord(s) with normal or impaired mobility
T3	Tumor limited to the larynx with vocal cord fixation and/or invasion of paraglottic space and/or inner cortex of the thyroid cartilage
T4	Moderately advanced or very advanced
– T4a	Moderately advanced local disease. Tumor invades cricoid or thyroid cartilage and/or invades tissues beyond the larynx (e.g., trachea, soft tissues of the neck including deep extrinsic muscles of the tongue, strap muscles, thyroid, or esophagus)
– T4b	Very advanced local disease. Tumor invades prevertebral space, encases carotid artery, or invades mediastinal structures

Reproduced from: National Cancer Institute. PDQ® Adult Laryngeal Cancer Treatment. Bethesda, MD: National Cancer Institute. https://www.cancer.gov/types/head-and-neck/hp/adult/laryngeal-treatment-pdq. Accessed on 09/12/2025.

1.5. Thyroid cartilage

1.5.1. Histology and ossification

In non-ossified thyroid cartilage, the tissue maintains the characteristics of avascular hyaline cartilage, with chondrocytes embedded in a collagen-rich matrix and no mineralized bone present. Histological studies of laryngeal cartilage have shown that cartilage remains homogeneous and avascular until the onset of ossification, at which point cartilage canals and vascular channels appear [40, 112]. These canals are perichondral invaginations containing blood vessels and connective tissue, and their extracellular matrix exhibits immunoreactivity for collagens I, II, and pro-III, indicating fibroblastic and chondrogenic properties of the canal-associated cells. Adjacent hypertrophic chondrocytes show a strong expression of type X collagen, marking early sites of mineralization. Thus, the process involves not only the extracellular matrix but also specific cellular changes around cartilage canals that signal the initiation of ossification [112].

The ossification of thyroid cartilage generally starts at the posterior-inferior border of the lamina, subsequently extending into the inferior horn, and later progressing toward the superior horn and is generally completed in the fifth or sixth decade of life [113, 114]. In advanced stages, the ossification process may extend to the entire cartilage [39, 44, 113, 115]. With advancing age, the thyroid cartilage shows a progressive tendency toward ossification.

These changes are not uniform across sexes, as studies have demonstrated a lower degree of ossification in females compared with males [39, 114].

Considering the literature, the reduced incidence of cases observed in this doctoral research study, in which a laryngeal tumor reaches or invades the non-ossified thyroid cartilage can be reasonably explained.

1.5.2. The clinical role of thyroid cartilage invasion

The management of laryngeal cancer is multifaceted and should be individualized, with treatment strategies determined by tumor stage, anatomical localization, and patient condition [116]. Non-ossified thyroid cartilage invasion is perhaps the most challenging yet consequential pitfall of laryngeal cancer radiological staging. Unlike ossified cartilage, which is more easily detected on imaging due to its calcified structure, non-ossified cartilage presents diagnostic challenges because of its similarity in density to tumor tissue on contrast-enhanced CT. Meanwhile on MRI, peritumoral inflammation may mimic a tumor. The diagnostic accuracy of imaging modalities in such cases may remain suboptimal [9, 14, 117]. The assessment of thyroid cartilage involvement represents one of the most significant revisions in the contemporary staging of laryngeal carcinoma. According to the AJCC 8th edition, any degree of thyroid cartilage invasion warrants classification as T3 disease, while extension through the outer cortex qualifies as T4a, indicating moderately advanced local disease [9, 44].

From a therapeutic standpoint, precise radiological delineation of tumor boundaries – sometimes difference by only a few millimeters – represents a critical decision defining the indications for various surgical and therapeutic treatment tools. In early stage laryngeal cancer (T1–T2, N0, M0), the principal objective remains the preservation of laryngeal structure and function [116]. In contrast, according to Thurnher et al. [118], total laryngectomy remains the standard of advanced laryngeal tumors including cases with cartilage invasion. Despite the emergence of organ-preserving approaches such as open partial horizontal laryngectomy and TOLMS, these techniques are contraindicated when the tumor extends into the thyroid cartilage, due to their inability to ensure adequate oncological margins [118–120]. Open partial laryngectomy and TOLMS demonstrate excellent outcomes for early stage cancer, achieving comparable survival of patients after total laryngectomy in selected cases; however, their success depends on intact cartilage barriers and preserved laryngeal function [118]. In contrast, according to Thurnher et al. [118], total laryngectomy remains the standard of advanced laryngeal tumors including cases with cartilage invasion.

Currently, the standard treatment for locally advanced laryngeal cancer, when aiming at larynx preservation, is concurrent chemoradiation therapy (CRT). Consequently, underdiagnosis can lead to inappropriate CRT use in undetected T4a disease, often resulting in local treatment failure and need for salvage laryngectomy. A study by Mohamad et al. [23] perfectly illustrates this commonly encountered issue today. A significant discrepancy was observed between head and neck MRI-based clinical staging (cT) and pathological staging (pT) ($p < 0.05$), resulting in both radiological over- and understating [23]. Notably, approximately 12% of patients underwent unnecessary total laryngectomy due to overstaging by MRI, whereas some tumors initially classified as cT3 were later confirmed pathologically as lower-stage lesions amenable to functional preservation. Furthermore, tumors categorized as cT4a based on cartilage invasion demonstrated an increased risk of local recurrence following conservative treatment [23]. Nevertheless, research findings remain inconsistent when the outcomes of total laryngectomy and chemoradiotherapy are compared [118]. Importantly, thyroid cartilage invasion also complicates radiotherapy planning as it may require expanded target volumes and higher radiation doses and is often associated with poor response to radiotherapy [121, 122].

Overall, treatment selection should be guided by factors such as the patient's general condition, tumor characteristics, and the feasibility of organ preservation, keeping in mind that salvage total laryngectomy is associated with significantly poorer survival compared to primary total laryngectomy [8]. An additional essential factor is the availability of diagnostic modalities, along with appropriate and high-quality radiological evaluation.

To conclude, the invasion of thyroid cartilage is identified as one of the most significant factors, highlighting its complex influence on survival outcomes [123]. It continues to be one of the most important anatomical structures for local staging, treatment planning, and prognosis in laryngeal cancer. While emerging imaging techniques continue to enhance diagnostic accuracy, the therapeutic implications remain significant: most patients with confirmed cartilage invasion benefit more from primary surgical management than from CRT [124]. Moreover, the presence of cartilage invasion is a consistent marker of biologically aggressive disease, underscoring its critical role in contemporary oncological decision-making. Due to the extremely complicated locoregional staging and treatment response in these patients, it is essential that patients would be managed by a skilled multidisciplinary team with access to high-quality imaging and multiple radiological modalities complementing each other [124].

2. MATERIALS AND METHODS

We conducted a single-center prospective study at the Departments of Radiology as well as Ear, Nose, and Throat, Hospital of Lithuanian University of Health Sciences Kauno klinikos, from 2021 to 2025. The initiation of the study was challenged by the COVID-19 pandemic (2019–2020) because of contact restrictions and limited access to patients.

Artificial intelligence-assisted tools, including OpenAI's ChatGPT, were utilized in the preparation of this thesis to enhance clarity, coherence, and structural organization during the drafting process [125]. All ideas, interpretations, and original research contained in this work are solely those of the author. The use of AI tools was limited to linguistic refinement and assistance with organizing literature-related content. All AI-generated suggestions were thoroughly reviewed by the author to ensure compliance with academic standards and to preserve the integrity and originality of the work [126].

2.1. Ethics

The study was conducted in accordance with the guidelines of the Declaration of Helsinki. Ethical approval was obtained from Kaunas Regional Biomedical Research Ethics Committee (protocol No. 2021-BE-10-00016; dated December 17, 2021). All patients signed an informed consent form before inclusion into the study (Appendix 2).

2.2. Study population and design

The study involved 46 patients with histologically confirmed laryngeal carcinoma and suspected or radiologically diagnosed non-ossified thyroid cartilage invasion on CT, who were evaluated by a multidisciplinary head and neck oncology tumor board. Patients were included in the study following the board's decision to perform either total or partial laryngectomy. After informed consent was obtained, all eligible patients underwent CEUS and MRI. No patients underwent MRI as the first-choice radiological examination after inclusion in the study. Five patients did not undergo MRI because they either had metallic foreign bodies or did not consent to the examination. Fourteen patients were subsequently excluded because they refused surgical treatment or their treatment plan was changed; thus, the final study population comprised 32 patients. In the study, we analyzed cases of non-ossified thyroid

cartilage. Since six patients had two distinct areas of interest investigated, a total of 38 cases were analyzed. Fig. 2.2.1 depicts the study flow chart.

Prior to surgical treatment, the radiologically suspected area of local invasion identified on CT was delineated on the Assessment Scheme of Local Spread ("Lokalaus išplitimo ištyrimo schema", Appendix 1) to assist the pathologist in performing a more targeted and precise evaluation. Histopathological verification of local invasion was obtained from the surgical specimens and served as the gold standard for assessment.

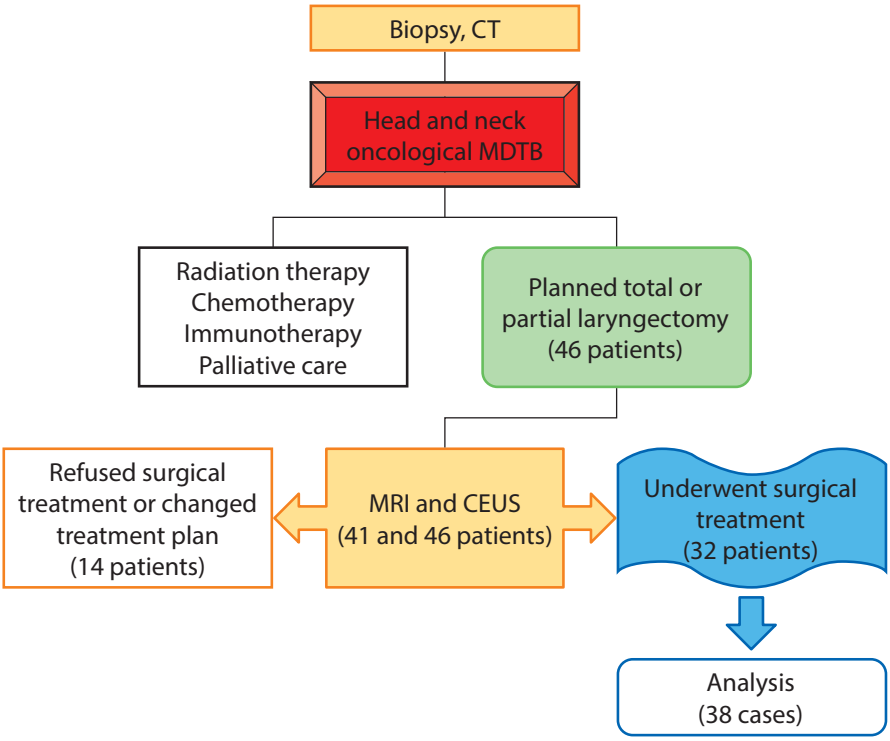

Fig. 2.2.1. *Study flow chart*

MDTB – multidisciplinary tumor board; MRI – magnetic resonance imaging; CEUS – contrast-enhanced ultrasonography.

2.3. Inclusion and exclusion criteria of the study population

The inclusion criteria were as follows:

1. Age of 18 years and more;
2. Diagnosis of laryngeal SCC;
3. CT scan demonstrating pathological infiltration adjacent to the non-ossified thyroid cartilage considering suspected invasion or definitive cartilage invasion;

4. No prior history of laryngeal–hypopharyngeal surgery or chemoradiation therapy;
5. Planned surgical treatment (total or partial laryngectomy);
6. Signed informed consent form.

The exclusion criteria were as follows:
1. Severe claustrophobia or the presence of metallic implants or foreign bodies incompatible with MRI and potentially posing a risk to the patient;
2. Previous allergic reaction to CEUS, MRI contrast agents;
3. History of an anaphylactic shock episode;
4. Concurrent patient illnesses that would render the patient unsuitable for this study or significantly interfere with the assessment of safety and toxicity.

2.4. Diagnostic methods

2.4.1. Computed tomography

2.4.1.1. Protocol

Multidetector CT scans were performed using an Aquilion ONE TSX-301 scanner (Toshiba, Japan) with the following settings: 120 kVp; effective mAs tailored to each patient based on patient's size and tissue thickness; collimation at 128 × 0.625 mm; a field of view measuring 260 mm; and a matrix of 512 × 512.

CT was performed following the head and neck soft tissue protocol; all patients underwent CT before inclusion into the study. Patients were positioned supine and instructed to breathe quietly while refraining from coughing and swallowing. The scanning range extended from the skull base to the aortic arch. Scans were performed both without and with intravenous contrast media (65–100 mL, using Ultravist®, Omnipaque®, Visipaque®), followed by a 50-mL saline flush to achieve contrast-enhanced images with a delay of 60–80 s after administration; the iodine concentration in the contrast agent was 320–370 mg/mL. All examination images were reconstructed according to the suprahyoid and infrahyoid neck regions in accordance with the established internal department protocol. For the infrahyoid region, images were reconstructed in axial (parallel to the plane of the true vocal cords), coronal and sagittal (perpendicular to the plane of the true vocal cords) planes using soft tissue (Table 2.4.1.1.1) and identical bone algorithms with a slice thickness of 2 mm. For the suprahyoid floor, images were also reconstructed in the axial plane, parallel to the plane of the hard palate.

Table 2.4.1.1.1. *Reconstructions of neck soft tissue images according to the protocol for laryngeal cancer*

Planes	Reconstructed image	Reconstruction plane lines
Suprahyoid neck region		
Axial	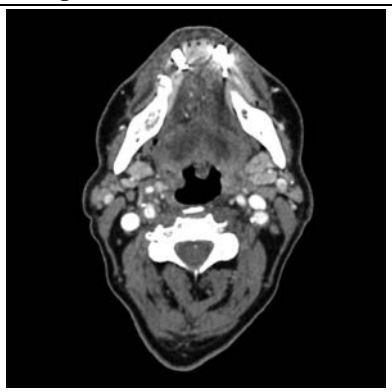	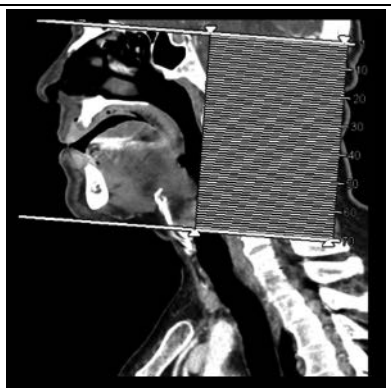
Infrahyoid neck region		
Axial		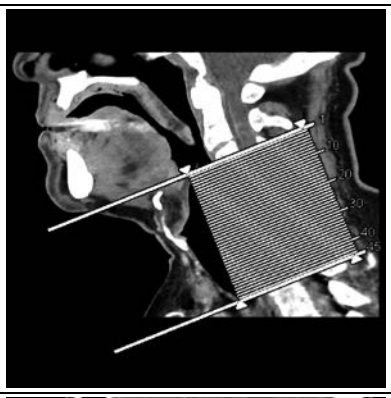
Coronal		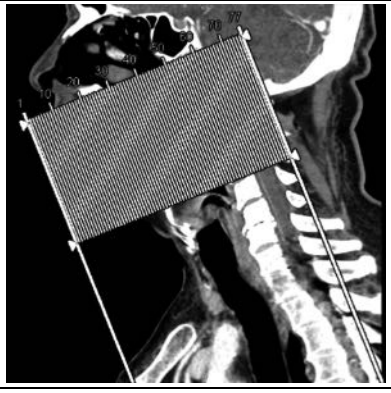

Table 2.4.1.1.1. *Continued*

Planes	Reconstructed image	Reconstruction plane lines
Sagittal		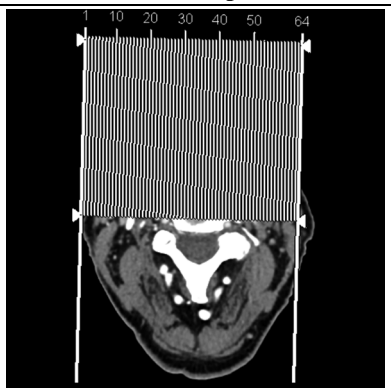

These CT images were selected from the PACS of the Hospital of Lithuanian University of Health Sciences Kauno klinikos by Milda Pucėtaitė.

2.4.1.2. Imaging evaluation

The results of CT scans were evaluated by one radiologist with more than 20 years of experience in head and neck imaging. The assessment of non-ossified thyroid cartilage invasion on contrast-enhanced CT images relies on specific criteria to determine positive findings. These criteria include the following: the presence of a focal cartilage defect (through the full thickness) adjacent to the tumor, replacement of cartilage by soft tissue with enhancement similar to adjacent tumor/structures, and direct contact between the lesion and thyroid cartilage with indistinguishable densities [81]. Fig. 2.4.1.2.1 illustrates these characteristics. Conversely, CT findings were considered negative when a clear distinction in density or a density pattern similar to edema was observed between the tumor (or pathologic infiltration) and the non-ossified cartilage.

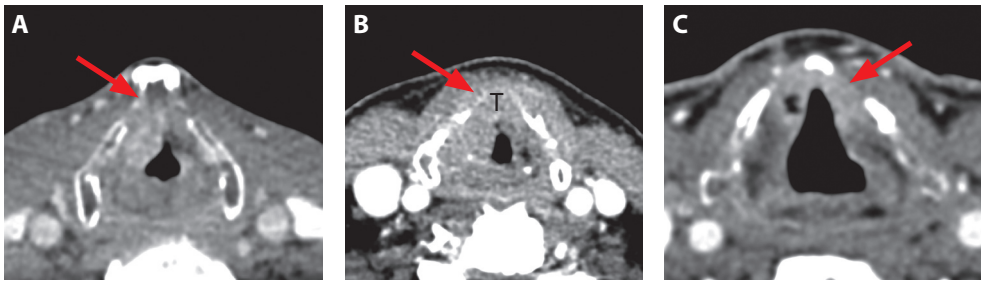

Fig. 2.4.1.2.1. *Positive criteria of non-ossified cartilage invasion (red arrow) on contrast-enhanced CT*

(A) focal defect adjacent to the similar density tumor; **(B)** replacement of cartilage by soft tissue with enhancement similar to tumor (T); **(C)** direct contact between the lesion and thyroid cartilage with indistinguishable densities.
These CT images were added from the PACS of the Hospital of Lithuanian University of Health Sciences Kauno klinikos by Milda Pucėtaitė.

2.4.2. Magnetic resonance imaging

2.4.2.1. Protocol

MRI examination was performed with a 3.0 Tesla Philips Ingenia scanner (Philips Healthcare, Best, the Netherlands) with dedicated head–neck 20-channel parallel imaging array coils. Upon inclusion into the study, the patient filled out a standard MRI consent form. A radiology technologist conducted the examination, and a radiologist (doctoral student) supervised the procedure. Patients were scanned in the supine position and were asked to breathe quietly and to refrain from swallowing and coughing during scanning. MRI was performed without and with IV contrast agent. A single intravenous dose of 0.1 mmol/kg (equivalent to 0.1 mL/kg) of gadolinium-based contrast agent (Gadovist®, Bayer Schering Pharma, Berlin, Germany) was administered via a left arm peripheral vein at an injection rate of 1.5–2 mL/s. Axial images were parallel to the plane of the true vocal cords; coronal images were perpendicular. The standard MRI protocol was slightly modified to reduce acquisition time and minimize motion artefacts associated with prolonged scanning by using a slightly smaller field of view, while thinner slices were used to improve the detection of small invasion. The current protocol is specified in Table 2.4.2.1.1.

Table 2.4.2.1.1. *MRI protocol for laryngeal cancer*

Sequence	Plane	Slice thickness, mm	Repetition time, ms	Time to echo, ms	Field of view, mm
High-resolution T2-weighted turbo spin echo Dixon	Axial, coronal, sagittal	2.5–3	2 888	80	190–210
High-resolution T1-weighted turbo spin echo Dixon	Axial	2.1–2.5	634	8	190–210
DWI and ADC	Axial	2	14 439; 220	66	250
Contrast-enhanced high-resolution T1-weighted turbo spin echo Dixon	Axial, coronal	2.1–2.5	634	8	190–210

DWI – diffusion-weighted imaging; ADC – apparent diffusion coefficient.

2.4.2.2. Imaging evaluation

One radiologist, specializing in head and neck imaging and having more than 20 years of experience, interpreted MRI scans. The radiologist was not blinded to the clinical information during image analysis. Cartilage invasion was considered positive on MRI when the non-ossified thyroid cartilage exhibited abnormal signal intensities as reassessed by Becker et al. [18]. The corresponding MRI criteria are specified in the Literature Review (Chapter 1.1.2). An example of thyroid cartilage invasion features is presented in Table 2.4.2.2.1. If the thyroid lamina exhibited T2-weighted signal intensity with contrast enhancement and the value of apparent diffusion coefficient (ADC) (when of sufficient quality) greater than those of the tumor, the abnormal signal was categorized as inflammatory.

Table 2.4.2.2.1. *MRI findings of non-ossified thyroid cartilage invasion (yellow arrow) in different sequences [18]*

Axial plane sequences	Image	Axial plane sequences	Image
T2WI Dixon	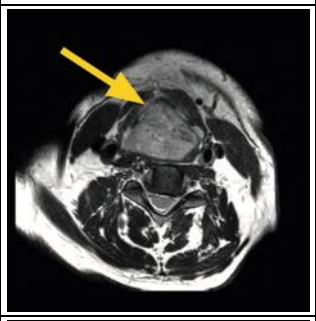	T2WI Dixon with fat saturation	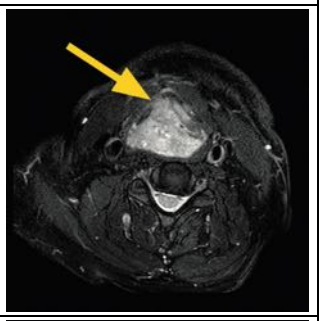
DWI	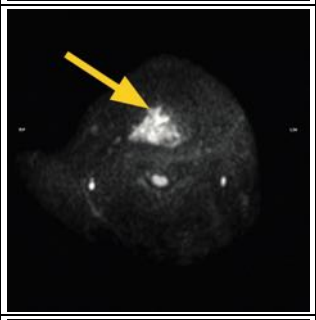	ADC	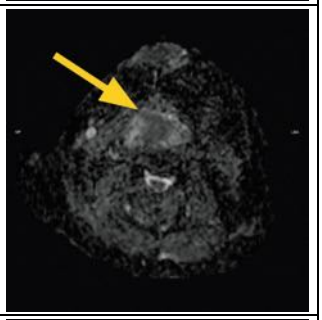
T1WI Dixon/ fat saturation	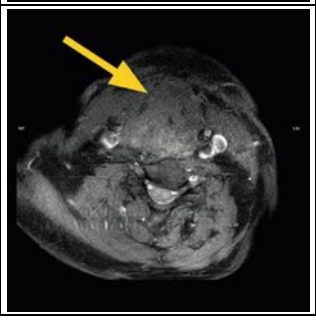	T1WI Dixon/ fat saturation with contrast	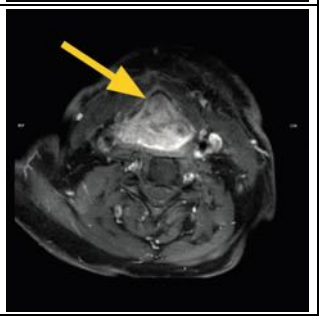

WI – weighted imaging; DWI – diffusion-weighted imaging; ADC – apparent diffusion coefficient. These MRI images were selected and added from the PACS of the Hospital of Lithuanian University of Health Sciences Kauno klinikos by Milda Pucėtaitė and Silvija Ryškienė.

2.4.3. Contrast-enhanced ultrasound

2.4.3.1. Protocol

Using a Philips Epiq 7 ultrasound system (Philips Healthcare, Best, the Netherlands) with a 5–12-MHz linear transducer and a mechanical index of ≤ 0.08, a CEUS examination was performed. Prior to the examination, a catheter (20 G) was inserted into a superficial vein in the left arm (antecubital fossa) by a medical nurse to prevent microsphere damage. The SonoVue contrast solution (5 mL of contrast agent) was then prepared and gently shaken by hand.

During the examination, a patient was placed in a supine position to optimize visualization; the neck was extended to the maximum comfortable degree to minimize the possibility of motion. Patients were instructed to refrain from swallowing or coughing during the procedure. First, the larynx and its surrounding structures were evaluated in both transverse and longitudinal sections. The distance from the lesion contact area to the non-ossified thyroid cartilage (as observed on CT) and to the upper border of the thyroid lamina was measured on CT and used as a reference to target the corresponding area on CEUS, where hypoechogenic pathological infiltration contacts non-ossified thyroid cartilage.

After identifying the ROI, a dual-screen mode was set on the device, displaying the CEUS image alongside the parallel B-mode ultrasound image in transverse section. Following the intravenous administration of a 5-mL bolus of SonoVue® (Bracco SpA, Milan, Italy) and a subsequent saline flush (10 mL of 0.9% NaCl), the timer and video recording were started.

The dynamic perfusion of the suspected non-ossified thyroid cartilage invasion area, along with the adjacent tumor and peritumoral tissues, was monitored and recorded on the device hard drive for approximately 60 s. If more than one suspected invasion site was investigated, the CEUS procedure was repeated after a 10-min interval. After recording, the images were reviewed by two radiologists for a qualitative evaluation of non-ossified thyroid cartilage invasion and quantitative analysis. The steps of CEUS examination procedure are summarized in Table 2.4.3.1.1.

Table 2.4.3.1.1. *The steps of CEUS examination*

Step	Action
1	Start the IV line
2	Perform a standard B-mode examination to locate the area of concern with a 5–12-MHz linear transducer
3	Set a dual window of CEUS (MI ≤ 0.08) and B-mode
4	Activate the contrast agent and inject into the catheter, start the timer and clip recording simultaneously
5	Inject the saline flush
6	Continue scanning and recording for approximately 60 s
7	If the second dose is required, use a high MI flash technique to destroy remaining bubbles
8	Repeat the injection process as needed
9	Select images/clips to send to PACS and Qlab®
10	Remove the IV catheter when the study is completed
11	Analyze the study

CEUS – contrast-enhanced ultrasound; MI – mechanical index; PACS – Picture Archiving and Communication System, Qlab® – Quantification Software; IV – intravenous; B – brightness.

2.4.3.2. Contrast-enhanced ultrasound analysis

The analysis of CEUS images for suspected non-ossified thyroid cartilage invasion involved a comprehensive approach combining both qualitative and quantitative methods. The recorded video loops were processed using advanced quantification software such as Qlab® 15 (Philips Medical Systems, Inc., Best, the Netherlands), which allowed for more detailed examination of blood perfusion patterns in the ROI or directly in the ultrasound machine software system. Analysis was conducted by two experienced radiologists: one with more than 4-year expertise in conventional US, and another, with more than 20-year expertise in conventional US and 8-year expertise in CEUS. The radiologists were not blinded to clinical information during the analysis of CEUS images.

2.4.3.2.1. Qualitative analysis

The qualitative analysis of CEUS images for evaluating tumor infiltration of non-ossified thyroid cartilage involves a detailed examination of contrast enhancement patterns. The consensus approach in interpreting CEUS images ensures a more reliable evaluation. Radiologists review the images together, discussing their observations and reaching a collective agreement on the presence or absence of tumor infiltration. This method helps minimize

individual bias and increases the accuracy of diagnosis. The main categories were defined as follows: when visual contrast enhancement was observed within the cartilage, tumor invasion was suggested; in the absence of enhancement, the cartilage was considered non-invaded (Fig. 2.4.3.2.1.1).

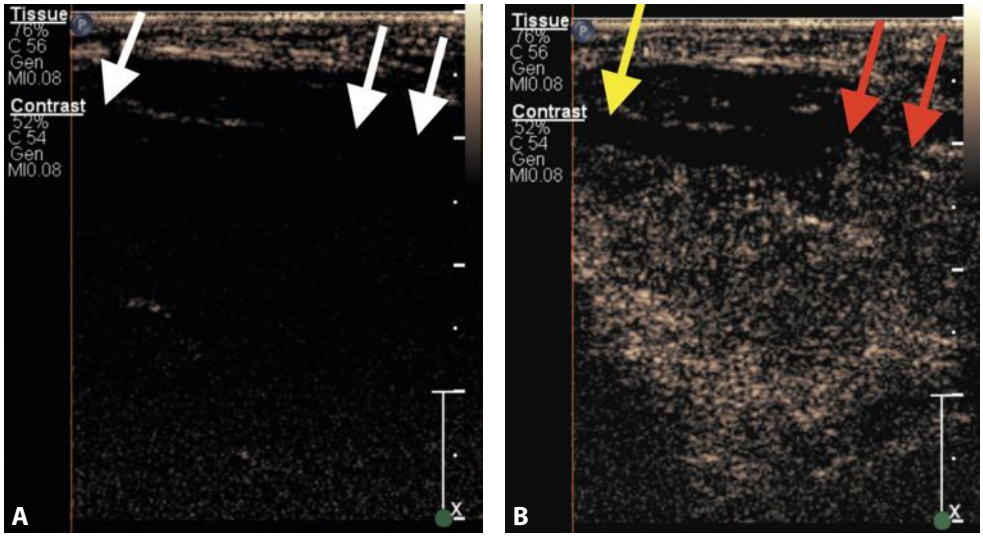

Fig. 2.4.3.2.1.1. *Positive and negative findings on CEUS of laryngeal cancer invasion on the left side of the thyroid cartilage*

(A) CEUS in the first seconds after IV UCA administration shows the non-ossified thyroid cartilage without enhancement (white arrows), which appears hypoechogenic; **(B)** CEUS after 32 s of IV UCA administration shows the cartilage enhancement (red arrows) corresponding as invasion (positive), and there are no enhancement on the other part of cartilage, specifically in the anterior part, where invasion was suspected (yellow arrow) on CT.
These CEUS images were taken from the Hospital of Lithuanian University of Health Sciences Kauno klinikos by Milda Pucėtaitė.

2.4.3.2.2. Quantitative analysis

The quantitative analysis process involved a meticulous approach to examining the tumor and non-ossified thyroid cartilage. Two distinct ROIs (Fig. 2.4.3.2.2.1) were carefully selected and manually delineated. The first ROI was positioned in the non-ossified area of the thyroid cartilage where invasion was suspected, while the second ROI was placed in the adjacent tumor tissue for comparative purposes. This strategic placement allowed for a direct comparison between the potentially invaded cartilage and the tumor itself, providing valuable insights into the extent of the invasion.

The size of ROIs was tailored to each patient's specific anatomy, ranging from 0.3 to 1.6 mm^2. This variation in size was necessary to accommodate

the differences in the thickness of non-ossified thyroid cartilage among different patients. Despite this variability, care was taken to ensure that for each individual patient, the ROI sizes were more comparable between the non-ossified cartilage and the adjacent tumor region. This consistency in ROI sizing within each patient's analysis was for maintaining the accuracy and reliability of quantitative measurements, allowing for meaningful comparisons between the two areas of interest.

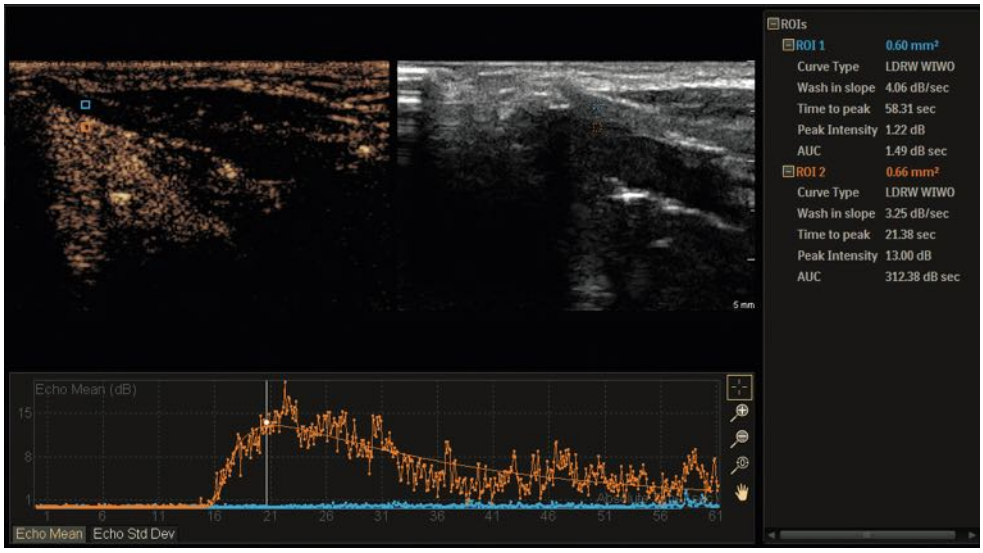

Fig. 2.4.3.2.2.1. *Qualitative ROI analysis of non-ossified thyroid cartilage (blue rectangle frame) and adjacent tumor (orange rectangle frame)*

This CEUS image was taken from the Hospital of Lithuanian University of Health Sciences Kauno klinikos by Milda Pucėtaitė.

TICs for the tumor and the non-ossified thyroid cartilage were generated from perfusion data and analyzed with a predefined software function Auto Curve Fit control model. Four TIC parameters values (Table 2.4.3.2.2.1) were analyzed using quantitative software. After quantitative analysis, the differences in TIC parameters (ΔTTP, ΔPI, ΔWIS, and ΔAUC) (Table 2.4.3.2.2.1) between the tumor (t) and the suspected site of thyroid cartilage (tc) invasion were also calculated, e.g., $\Delta PI = PI_t - PI_{tc}$ [127], and analyzed. The results were written as absolute values assuming that smaller differences should show similarity with vascular tumor tissue, which could be detected in invaded non-ossified thyroid cartilage.

Table 2.4.3.2.2.1. *TIC parameters and their differences for quantitative analysis*

Parameter	Description	Unit
TTP	Time to peak	seconds (s)
ΔTTP	Difference in time to peak (tumor−thyroid cartilage)	seconds (s)
PI	Peak intensity	decibels (dB)
ΔPI	Difference in peak intensity (tumor−thyroid cartilage)	decibels (dB)
WIS	Wash-in slope	decibels per second (dB/s)
ΔWIS	Difference in wash-in slope (tumor−thyroid cartilage)	decibels per second (dB/s)
AUC	Area under curve	decibels × seconds (dB × s)
ΔAUC	Difference in area under curve (tumor−thyroid cartilage)	decibels × seconds (dB × s)

2.5. Histopathology

Histopathological analysis was performed at the Department of Pathology, Medical Academy, Lithuanian University of Health Sciences, on a routine basis. Histopathological assessment was done by a pathologist with > 20-year experience. To ensure accurate correlation between radiological findings and pathological analysis, the radiologist marked the suspected area of non-ossified thyroid cartilage invasion on an anatomical sketch of the larynx (Appendix 1) in both axial and coronal planes for each case. The macroscopic and microscopic examination was performed for each specimen. The 8th edition of the TNM Classification of Malignant Tumours [128] was used for staging.

2.5.1. Examination of surgical laryngeal material

The surgical specimen was preserved in a 10% buffered formalin solution. During both macroscopic and microscopic evaluations, the type of laryngeal resection performed (partial, total, or another type) was specified, along with the organs and tissues included in the specimen. Tumor characteristics were detailed including its location (supraglottic, glottic, or subglottic), size, color, consistency, and its relationship with tissue fragment areas marked by special indelible dyes (applied by the surgeon in the operating room or by the pathologist in the macrodissection room). Tumor spread to other parts of the larynx and surrounding tissues was noted, based on the primary tumor location

according to the TNM criteria. The condition of the unaffected laryngeal mucosa, nearby structures, and lymph nodes was also described.

Macroscopically, the larynx was separated from the surrounding neck tissues (if they were present in the specimen). The larynx was opened longitudinally through the posterior surface, in cases of total laryngectomy. Soft tissues and ossified cartilages were cut longitudinally every 0.5 cm. According to the submitted Assessment Scheme of Local Spread ("Lokalaus išplitimo ištyrimo schema", Appendix 1), the additional material samples were prepared to evaluate tumor invasion at the targeted site. If indicated, photographs were taken of the tissues present in one fragment or already divided fragments.

For microscopic examination, at least 2 representative tumor fragments were taken (depending on the tumor size), as well as samples from the area of the thyroid cartilage suspected or identified as being invaded radiologically. Samples were taken from the vocal cords, epiglottis, and larynx fragments that reflect the greatest depth of tumor invasion into these structures, along with their relationship to the fragment margins marked with colors. Fragments from the thyroid gland and other adjacent organs were taken to reflect the greatest tumor invasion into them. All lymph nodes found and separately submitted were taken for examination; the lymph nodes were separated so that as many sections as possible could be examined, and larger nodes were embedded into several paraffin blocks.

The material underwent dehydration and then was embedded in paraffin blocks. Tissue samples were sliced into sections 4 μm in thickness using a microtome and stained following the standard hematoxylin/eosin technique. Hard tissues containing bone tissue required a decalcification process (TBD/EDTA).

When necessary for diagnosis, additional histochemical techniques (such as PAS, PAS diastase, mucicarmine, etc.) were employed to identify mucus, glycogen, basement membrane, and other characteristics. Immunohistochemical methods (including p63, p16, cytokeratins, lymphoid cell markers, melanoma markers, immunoproliferative marker Ki-67, PD-L1 expression assessment, etc.) and molecular diagnostic tests (such as BRAF gene mutation analysis) were frequently utilized to ascertain the histogenesis of tumors.

Under microscopic examination, the cellular composition and architecture of tumor tissue were detailed to identify the histological type and level of differentiation. Observations included the presence of mitoses, necrosis, vascular and lymphatic invasion, as well as the tumor extent, affected structures (such as parts of the larynx, nearby tissues, and the tumor relationship to the thyroid cartilage), and other findings. All submitted lymph nodes were scrutinized, including an evaluation of the number of tumor metastases, their

size, and their spread beyond the lymph node capsule. The results of immunohistochemical and other tests were documented.

The conclusion/diagnosis was made by indicating the histological type of the tumor, degree of differentiation, and extent of spread, in accordance with the latest WHO histological classification of neoplastic diseases and the TNM (8th edition) staging/spread criteria for neoplastic diseases [128].

2.6. Statistical analysis

All statistical analyses were performed using IBM SPSS Statistics 29.0 (IBM Corp., Armonk, NY, USA) and MedCalc 23.1.3 (MedCalc Software Ltd). Statistical procedures were conducted with consideration of overall available sample size meeting the inclusion criteria in our institution. The presence of statistically significant results using the proper tests indicates that the sample size was adequate for this study from statistical point of view.

Descriptive statistics were used to describe patients' characteristics.

The sensitivity, specificity, accuracy, positive predictive value (PPV), and negative predictive value (NPV) of CEUS, CT, and MRI in assessing non-ossified thyroid cartilage invasion were calculated using histopathological findings as the gold standard. Sensitivity and specificity were computed according to the following formulas:

$$\text{Sensitivity} = a / (a + c)$$
$$\text{Specificity} = d / (b + d),$$

where: a is the number of true-positive cases; b, number of false-positive cases; c, the number of false-negative cases; d, the number of true-negative cases.

Accuracy was defined as follows:

$$\text{Accuracy} = \frac{TP + TN}{TP + TN + FP + FN}$$

where: TP = true positive, TN = true negative, FP = false positive, and FN = false negative.

The McNemar test was used to compare the diagnostic value between CEUS and CT, and MRI. Combined sensitivity and specificity of CEUS with CT and MRI were calculated to find an added value of CEUS. Using "the OR rule", the invasion was positive when either test was positive. Using "the AND rule", the invasion was positive when only both tests were positive. The combined sensitivity formula using the OR rule is as follows: SECEUS + SECT/MRI – (SECEUS × SECT/MRI); the combined specificity formula is

as follows: SPCEUS × SPCT/MRI. The combined sensitivity formula using the AND rule is as follows: SECEUS × SECT/MRI; the combined specificity formula is as follows: SPCEUS + SPCT/MRI – (SPCEUS × SPCT/MRI), where SE is sensitivity, SP is specificity [129].

Due to the small sample size, non-parametric statistical methods were applied for analysis of TIC parameters. Continuous data were expressed as medians (range). Age was expressed as mean (SD). Comparisons of TIC parameters between the non-ossified thyroid cartilage with and without invasion and tumor tissue were conducted to evaluate perfusion and hemodynamic characteristics.

The Mann–Whitney U test was used to assess differences between independent groups, specifically comparing non-ossified thyroid cartilage with and without invasion. For paired or dependent samples – specifically, comparisons between tumor tissue and thyroid cartilage within the same patient – the Wilcoxon signed-rank test was employed. By treating these parameters as dependent variables, the analysis accounted for intraindividual variation, providing a more accurate assessment of perfusion differences between the thyroid cartilage and the tumor.

TIC parameters that showed statistically significant differences between invaded and non-invaded thyroid cartilage were included in logistic regression analysis (enter method) to calculate odds ratios (OR) and their 95% confidence intervals (CI). This approach enabled the quantification of the relationship between TIC parameters and the likelihood of thyroid cartilage invasion.

To assess the diagnostic performance of significant TIC parameters and their combinations, receiver operating characteristic (ROC) curve analysis was performed. The area under the ROC curve (AUCROC) was calculated to evaluate discriminative power, and sensitivity and specificity were determined for each parameter. The optimal cut-off values were defined as the points on the ROC curve with the greatest Youden index (sensitivity + specificity – 1). The McNemar test was again used to compare the diagnostic accuracy between significant parameters.

A p value < 0.05 was considered statistically significant for all analyses.

2.7. PhD candidate's contribution to the study

1. Development of research ideas and contribution to the study design and methodology;
2. Preparation and submission of documents required for obtaining bioethical approval;
3. Recruitment of the study population during multidisciplinary tumor board meetings;
4. Participation in the modification of the laryngeal MRI protocol for this study;
5. Collection and analysis of clinical and demographic data;
6. Monitoring and supervision of MRI examinations;
7. Performance of CEUS examinations and image assessment;
8. Development and implementation of the Assessment Scheme of Local Spread ("Lokalaus išplitimo ištyrimo schema");
9. Creation of the patient database and statistical analysis;
10. Preparation and submission of scientific abstracts and publications with co-authors.

3. RESULTS

3.1. Demographic analysis and distributions

A total of 32 patients were included in the study; all the patients were men. The age of the study population varied from 46 to 84 years, with a mean age of 63.25 years (SD, 8.37). The median time between diagnostic procedures and surgery were up to 30.5 days: 30.5 days (range, 5–85) from CT to surgery and 11.0 days (range, 0–42) from CEUS or MRI. The distribution of patients by the pathological tumor (pT) stage was relatively even; however, stage T3 and T1 tumors were most frequent (Fig. 3.1.1).

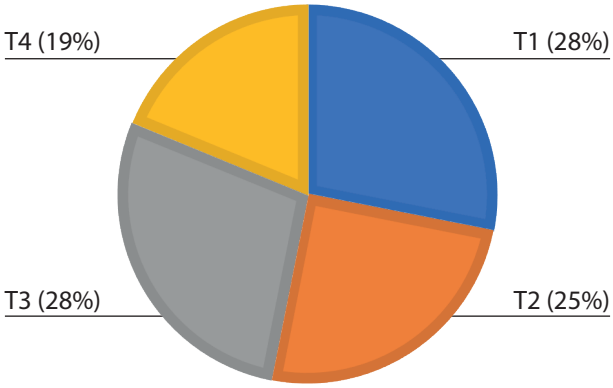

Fig. 3.1.1. *Distribution of 32 patients by pT*

According to tumor localization, 50.0% (n = 16) of the cases were glottic and 50.0% (n = 16) were transglottic laryngeal cancers. Bilateral involvement was slightly more common (40.6%, n = 13), followed by right-sided lesions (31.3%, n = 10) and left-sided lesions (28.1%, n = 9).

All patients had histologically confirmed laryngeal SCC. Based on the degree of laryngeal SCC differentiation, G2 carcinomas were most common (78.1%, n = 25), followed by G1 (15.6%, n = 5) and G3 (6.3%, n = 2) carcinomas.

3.2. Diagnostic performance of qualitative (visual) CEUS, CT, and MRI

Because 6 of the 32 patients had two distinct ROIs within the non-ossified thyroid cartilage, each region was considered a separate clinical case for analysis, resulting in a total of 38 cases (hereafter, *n* refers to the number of clinical cases, not individual patients). Histopathological examination after

surgery, used as the reference standard, confirmed tumor invasion of the non-ossified thyroid cartilage in 9 of the 38 cases.

CT and CEUS were analyzed in all 38 cases, whereas MRI was available in 32 cases (84.2%), as 5 patients did not undergo MRI examination.

The diagnostic performance of CEUS, CT, and MRI for detecting non-ossified thyroid cartilage invasion is summarized in Table 3.2.1. The results of each radiological examination were compared with those of postsurgical histopathology, and only CEUS as compared with postsurgical histopathology showed no statistically significant difference ($p = 0.375$). CEUS demonstrated the highest overall accuracy, with a high sensitivity of 88.9% (95% CI: 51.8–99.7) and a specificity of 86.2% (95% CI: 68.3–96.1), yielding an overall accuracy of 86.8% (95% CI: 71.9–95.6). The PPV was higher compared to those of CT (66.7% *vs.* 35.0%) and MRI (66.7% *vs.* 46.2%); however, the NPV for CEUS was better than that for CT (96.2% *vs.* 88.9%), but slightly worse than that of MRI (96.2% *vs.* 100.0%). Moreover, CT showed lower diagnostic performance, but a moderate specificity of 73.1% (95% CI: 52.2–88.4) and accuracy of 78.1% (95% CI: 60.0–90.1). Overall, CEUS provided the most balanced diagnostic accuracy and specificity, whereas MRI achieved a perfect sensitivity but a lower PPV, likely due to the diagnostic overestimation of invasion.

Table 3.2.1. *Diagnostic performance of CEUS, CT, and MRI comparing with postsurgical histopathology as the gold standard*

Imaging modality	TP, n	TN, n	FP, n	FN, n	Sensitivity, % (95% CI)	Specificity, % (95% CI)	Accuracy, % (95% CI)	PPV, %	NPV, %	p value*
CEUS (n = 38)	8	25	4	1	88.9 (51.8–99.7)	86.2 (68.3–96.1)	86.8 (71.9–95.6)	66.7	96.2	0.375
CT (n = 38)	7	16	13	2	77.8 (40.0–97.2)	55.2 (35.7–73.6)	60.5 (43.4–76.0)	35.0	88.9	0.007
MRI (n = 32)	6	19	7	0	100.0 (54.1–100.0)	73.1 (52.2–88.4)	78.1 (60.0–90.1)	46.2	100.0	0.016

CEUS – contrast-enhanced ultrasound; CT – computed tomography; MRI – magnetic resonance tomography; TP – true positive; TN – true negative; FP – false positive; FN – false negative; PPV – positive predictive value; NPV – negative predictive value; * – comparisons with postsurgical histopathology were done using the McNemar test.

Moreover, a statistically significant difference in diagnostic performance was observed between CEUS and CT (McNemar test, $p = 0.039$). However, no statistically significant difference was found between MRI and CEUS ($p = 0.109$).

3.3. Added values of qualitative (visual) CEUS

The diagnostic performance of the combined use of CEUS with CT and MRI was evaluated using two decision rules: OR and AND rules.

The OR rule is primarily intended to maximize sensitivity and is most appropriate in settings where the main clinical objective is to avoid false-negative results. In the present study, the application of the OR rule did not result in a meaningful improvement in diagnostic performance. Sensitivity reached 88.9% for the combination of CEUS and CT and 100% for the combination of CEUS and MRI, which was comparable to the performance of CEUS (88.9%) and MRI alone (100%). Therefore, the OR rule was not selected as the primary approach for evaluating the added diagnostic value of combining CEUS with CT and MRI, and subsequent analysis focused on the AND rule, which provided more clinically relevant confirmation of invasion.

When CEUS and CT as well as CEUS and MRI were combined using the AND rule, non-ossified thyroid cartilage invasion was diagnosed only when the signs of invasion were present on both imaging modalities, thereby reducing FP results. Using this approach, the CEUS and CT combined method achieved a higher specificity (89.7%) than CEUS or CT alone, an overall diagnostic accuracy of 86.8%, and a sensitivity of 77.8%. The CEUS and MRI combination demonstrated even a higher specificity, reaching 100%, but very slightly reduced sensitivity to 83.3%. The application of the AND rule reduced the number of false-positive findings and enabled more reliable confirmation of thyroid cartilage invasion.

The detailed results of diagnostic performance analysis are presented in Tables 3.3.1 and 3.3.2.

Table 3.3.1. *Diagnostic performance of CEUS, CT, and their combination using the AND rule for the assessment of non-ossified thyroid cartilage invasion*

Imaging modality	TP, n	TN, n	FP, n	FN, n	Sensitivity, % (95% CI)	Specificity, % (95% CI)	Accuracy, % (95% CI)	PPV, %	NPV, %
CEUS (n = 38)	8	25	4	1	88.9 (51.8–99.7)	86.2 (68.3–96.1)	86.8 (71.9–95.6)	66.7	96.2
CT (n = 38)	7	16	13	2	77.8 (40.0–97.2)	55.2 (35.7–73.6)	60.5 (43.4–76.0)	35.0	88.9
CEUS + CT (n = 38; AND rule)	7	26	3	2	77.8 (40.0–97.2)	89.7 (72.7–97.8)	86.8 (71.9–95.6)	70.0	92.9

CEUS – contrast-enhanced ultrasound; CT – computed tomography; TP – true positive; TN – true negative; FP – false positive; FN – false negative; PPV – positive predictive value; NPV – negative predictive value. CEUS and CT are presented for direct comparison to illustrate the added diagnostic value of their combination.

Table 3.3.2. *Diagnostic performance of CEUS, MRI, and their combination using the AND rule for the assessment of non-ossified thyroid cartilage invasion*

Imaging modality	TP, n	TN, n	FP, N	FN, n	Sensitivity, % (95% CI)	Specificity, % (95% CI)	Accuracy, % (95% CI)	PPV, %	NPV, %
CEUS (n = 38)	8	25	4	1	88.9 (51.8–99.7)	86.2 (68.3–96.1)	86.8 (71.9–95.6)	66.7	96.2
MRI (n = 32)	6	19	7	0	100.0 (54.1–100.0)	73.1 (52.2–88.4)	78.1 (60.0–90.1)	46.2	100.0
CEUS + MRI (n = 32; AND rule)	5	26	0	1	83.3 (35.9–99.6)	100.0 (86.8–100.0)	96.9 (83.8–99.9)	100.0	96.3

CEUS – contrast-enhanced ultrasound; MRI – magnetic resonance tomography; TP – true positive; TN – true negative; FP – false positive; FN – false negative; PPV – positive predictive value; NPV – negative predictive value. CEUS and MRI are presented for direct comparison to illustrate the added diagnostic value of their combination.

3.4. Analysis of time–intensity curve parameters

For quantitative analysis, of 38 cases, 4 were excluded due to severe motion artefacts, leaving 34 cases for the statistical analysis of TIC parameters. Of 34 cases, only 8 (23.5%) were histologically confirmed to have tumor invasion into the non-ossified thyroid cartilage.

3.4.1. TTP, PI, AUC, WIS analysis of non-ossified thyroid cartilage and laryngeal tumor

TIC parameters were analyzed and compared among the groups: non-ossified thyroid cartilage without invasion and non-ossified thyroid cartilage with invasion (Table 3.4.1.1), non-ossified thyroid cartilage without invasion and tumor tissue (Table 3.4.1.2), and non-ossified thyroid cartilage with invasion and tumor tissue (Table 3.4.1.3). The comparison revealed statistically significant differences in TTP and PI among all these groups ($p < 0.05$). The AUC values of thyroid cartilage with and without invasion also differed significantly ($p = 0.002$), whereas no significant difference was observed in WIS ($p = 0.002$). Both AUC and WIS values differed significantly between thyroid cartilage without invasion and tumor tissue ($p < 0.001$ and $p = 0.016$, respectively). In contrast, no significant differences were observed between tumor tissue and thyroid cartilage with invasion ($p = 0.093$ and $p = 0.208$), indicating comparable median values between these tissues.

Table 3.4.1.1. *Comparison of TIC parameters between the thyroid cartilage with and without invasion groups*

Parameter	Thyroid cartilage without invasion (n = 26)	Thyroid cartilage with invasion (n = 8)	p value*
TTP, s	45.21 (39.44–51.73)	31.12 (28.26–35.72)	0.002
PI, dB	2.16 (1.18–3.32)	8.46 (6.00–20.56)	0.001
AUC, dB × s	7.62 (1.33–16.97)	109.97 (13.45–282.05)	0.002
WIS, dB/s	3.92 (2.61–8.38)	4.62 (1.14–24.56)	0.872

Values are medians (IQR). TTP – time to peak; PI – peak intensity; AUC – area under curve; WIS – wash-in slope; * – comparisons made using the Mann-Whitney U test.

Table 3.4.1.2. *Comparison of TIC parameters between the tumor and the thyroid cartilage without invasion groups*

Parameter	Thyroid cartilage without invasion (n = 26)	Tumor (n = 26)	p value*
TTP, s	45.21 (39.44–51.73)	28.44 (26.39–32.09)	< 0.001
PI, dB	2.16 (1.18–3.32)	13.09 (10.46–18.07)	< 0.001
AUC, dB × s	7.62 (1.33–16.97)	305.63 (191.71–419.03)	< 0.001
WIS, dB/s	3.92 (2.61–8.38)	1.74 (1.21–2.84)	0.016

Values are medians (IQR). TTP – time to peak; PI – peak intensity; AUC – area under curve; WIS – wash-in slope; * – comparisons made using the Wilcoxon test.

Table 3.4.1.3. *Comparison of TIC parameters between the tumor and the thyroid cartilage with invasion groups*

Parameter	Thyroid cartilage with invasion (n = 8)	Tumor (n = 8)	p value*
TTP, s	31.12 (28.26–35.72)	27.15 (25.65–29.09)	0.017
PI, dB	8.46 (6.00–20.56)	12.07 (8.78–24.90)	0.012
AUC, dB × s	109.97 (13.45–282.05)	257.94 (191.65–320.60)	0.093
WIS, dB/s	4.62 (1.14–24.56)	1.22 (0.88–7.61)	0.208

Values are medians (IQR). TTP – time to peak; PI – peak intensity; AUC – area under curve; WIS – wash-in slope; * – comparisons made using the Wilcoxon test.

Given the nearly identical median values of TIC parameters in the tumor tissue, which did not differ significantly between the groups with and without thyroid cartilage invasion ($p > 0.05$), we calculated pooled median TIC parameter values for the tumor tissue of all patients and used them as the main reference values. Accordingly, medians were calculated for the entire cohort (n = 34) and are presented in Table 3.4.1.4. When we compared these

medians with the medians of thyroid cartilage with invasion and without invasion, we obtained the same p values as in Table 3.4.1.2 and Table 3.4.1.3.

Table 3.4.1.4. *TIC parameters of the tumor in the entire cohort*

Parameter	Value
TTP, s	28.44 (26.38–31.56)
PI, dB	13.09 (9.86–19.49)
AUC, dB × s	300.87 (191.88–413.58)
WIS, dB/s	1.67 (1.10–3.24)

Values are medians (IQR). TTP – time to peak; PI – peak intensity; AUC – area under curve; WIS – wash-in slope.

3.4.2. ΔTTP, ΔPI, ΔAUC, ΔWIS analysis of non-ossified thyroid cartilage

Quantitative differences in TIC parameters (ΔTTP, ΔPI, ΔWIS, and ΔAUC) between the tumor (t) and the suspected site of non-ossified thyroid cartilage (tc) invasion were calculated, e.g., $\Delta PI = PI_t - PI_{tc}$ [127].

A detailed comparison of ΔTTP, ΔPI, ΔWIS, and ΔAUC between with and without non-ossified thyroid cartilage invasion is presented in Table 3.4.2.1. The analysis demonstrated that the median values of ΔTTP, ΔPI, and ΔAUC in cases with thyroid cartilage invasion were significantly lower than in cases without thyroid cartilage invasion ($p < 0.05$) (Fig. 3.4.2.1–3.4.2.3). These findings suggest that hemodynamic changes observed in invaded thyroid cartilage share similarities with those seen in the adjacent tumor tissue and may reflect increased vascularity and disrupted microcirculation resulting from tumor infiltration.

Table 3.4.2.1. *Comparison of differences of TIC parameters (ΔTTP, ΔPI, ΔWIS, ΔAUC) between the groups of thyroid cartilage without and with invasion*

Parameters	Thyroid cartilage without invasion (n = 8)	Thyroid cartilage with invasion (n = 26)	p value
ΔTTP, s	15.19 (8.74–26.21)	4.81 (1.14–6.87)	< 0.001
ΔPI, dB	11.60 (7.88–16.98)	3.10 (0.93–11.34)	0.013
ΔAUC, dB × s	333.75 (201.71–407.33)	94.96 (50.17–297.73)	0.018
ΔWIS, dB/s	5.11 (1.33–7.26)	3.39 (0.11–17.65)	0.842

Values are medians (IQR). ΔTTP – difference in time to peak between non-ossified thyroid cartilage and tumor; ΔPI – difference in peak intensity between non-ossified thyroid cartilage and tumor; ΔAUC – difference in the area under the curve between non-ossified thyroid cartilage and tumor; ΔWIS – difference in the wash-in slope between non-ossified thyroid cartilage and tumor.

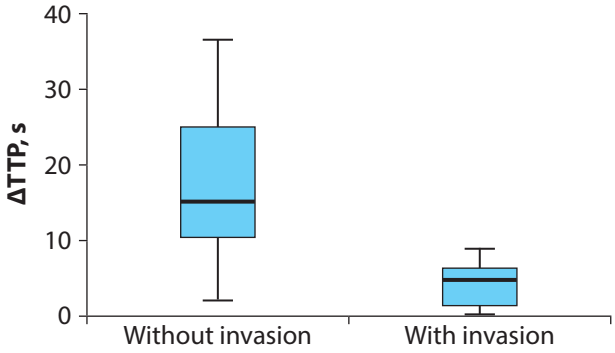

Fig. 3.4.2.1. *Boxplots for ΔTTP values of non-ossified thyroid cartilage without and with invasion*

Error bars indicate the range of distribution; the box, the interquartile range; the horizontal line, median value.

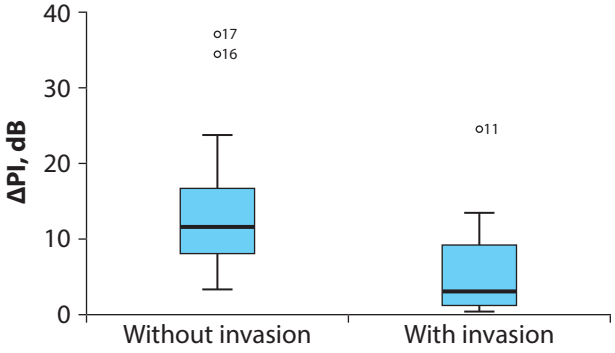

Fig. 3.4.2.2. *Boxplots for ΔPI values of non-ossified thyroid cartilage without and with invasion*

Error bars indicate the range of distribution; the box, the interquartile range; the horizontal line, median value.

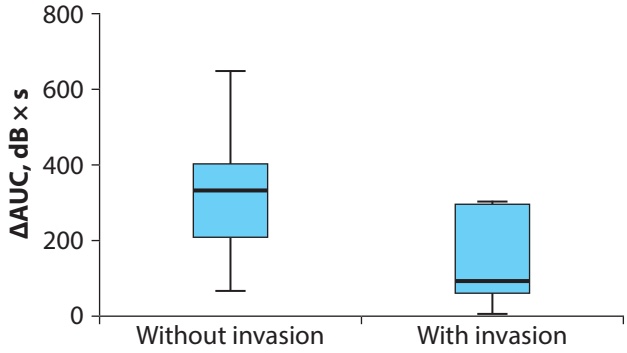

Fig. 3.4.2.3. *Boxplots for ΔAUC values of non-ossified thyroid cartilage without and with invasion*

Error bars indicate the range of distribution; the box, the interquartile range; the horizontal line, median value.

3.4.3. Logistic regression analysis for prediction of non-ossified thyroid cartilage invasion

The results of logistic regression analysis of TIC parameters for diagnosing non-ossified thyroid cartilage invasion are presented in Table 3.4.3.1. In the univariate logistic regression, all TIC parameters, except ΔPI, demonstrated statistically significant associations with cartilage invasion. Longer TTP time (OR = 0.84, 95% CI: 0.73–0.97) and greater ΔTTP (OR = 0.76, 95% CI: 0.60–0.96) were associated with a decreased likelihood of invasion, indicating that increased time to peak enhancement was related to the absence of tumor infiltration. ΔAUC also showed a significant association (OR = 0.99, 95% CI: 0.98–1.00). Conversely, higher PI (OR = 1.81, 95% CI: 1.14–2.92) and AUC (OR = 1.04, 95% CI: 1.00–1.08) values were positively associated with cartilage invasion.

Table 3.4.3.1. *Logistic regression for the prediction of non-ossified thyroid cartilage invasion*

Univariate logistic regression	β	Odds ratio	95% CI	TP, %	TN, %	p value
TTP, 1 s	–0.173	0.84	0.73–0.97	62.5	96.2	0.015
PI, 1 dB	0.599	1.82	1.14–2.92	75.0	96.0	0.013
AUC, 1 dB × s	0.038	1.04	1.00–1.08	62.5	100.0	0.030
ΔTTP, 1 s	–0.281	0.76	0.60–0.96	37.5	88.5	0.020
ΔPI, 1 dB	–0.163	0.85	0.72–1.01	37.5	100.0	0.057
ΔAUC, 1 dB × s	–0.009	0.99	0.98–1.00	62.5	91.3	0.025

Table 3.4.3.1. *Continued*

Univariate logistic regression		β	Odds ratio	95% CI	TP, %	TN, %	p value
Multivariate logistic regression models							
Model 1	PI, 1 dB	0.553	1.74	1.01–2.99	75.0	100.0	0.046
	ΔAUC, 1 dB × s	–0.007	0.99	0.98–1.00			0.139
Model 2	PI, 1 dB	0.437	1.55	1.06–2.27	87.5	100.0	0.026
	ΔPI, 1 dB	–0.182	0.83	0.65–1.07			0.155
Model 3	TTP, 1 s	–0.139	0.87	0.76–1.00	62.5	92.0	0.048
	ΔPI, 1 dB	–0.071	0.93	0.81–1.08			0.330
Model 4	ΔTTP, 1 s	–0.252	0.78	0.61–0.99	62.5	92.0	0.038
	ΔPI, 1 dB	–0.072	0.931	0.83–1.05			0.233

TTP – time to peak; PI – peak intensity; AUC – area under curve. ΔTTP – difference in time to peak between non-ossified thyroid cartilage and tumor; ΔPI – difference in peak intensity between non-ossified thyroid cartilage and tumor; ΔAUC – difference in the area under the curve between non-ossified thyroid cartilage and tumor.

In multivariable binary logistic regression, four models were tested to evaluate combined parameter performance. By pairing TIC parameters and their derived values, four models with one statistically significant parameter were obtained. Model 1, which included PI and ΔAUC, revealed that PI remained a significant independent predictor of invasion (OR = 1.74, 95% CI: 1.01–2.99). Similarly, Model 2 (PI + ΔPI) confirmed PI as a significant predictor (OR = 1.55, 95% CI: 1.06–2.27). In Model 3 (TTP + ΔPI), TTP retained marginal significance (OR = 0.87, 95% CI: 0.76–1.00), while in Model 4 (ΔTTP + ΔPI), ΔTTP remained a significant negative predictor (OR = 0.78, 95% CI: 0.61–0.99). However, no statistically significant associations were found in combining other parameters in pairs. To sum up, no one of these models statistically significantly increased its predicting ability of non-ossified thyroid cartilage invasion.

3.4.4. ROC analysis of time–intensity curve parameters and their combinations

Based on the analysis of TIC perfusion parameters, even several quantitative indicators demonstrated a significant diagnostic value in differentiating invaded from non-invaded non-ossified thyroid cartilage. According to the greatest Youden index, the optimal cut-off values for distinguishing non-invaded from invaded non-ossified thyroid cartilage are presented in Table 3.4.4.1. Lower values of TTP (≤ 36.6 s), ΔTTP (≤ 9.6 s), ΔPI (≤ 5.15 dB), and ΔAUC (≤ 116.29 dB × s) and higher PI (≥ 5.51 dB) and

AUC (≥ 82.78 dB × s) values were linked to non-ossified thyroid cartilage invasion.

Table 3.4.4.1. *Diagnostic performance of TIC parameters in predicting non-ossified thyroid cartilage invasion*

Parameter	AUROC, (95% CI)	Sensitivity, % (95% CI)	Specificity, % (95% CI)	Accuracy, % (95% CI)	Cut-off value	p value
Univariate models						
TTP	0.86 (0.63–1.09)	87.5 (47.4–99.7)	92.3 (74.9–99.1)	91.2 (76.3–98.1)	36.6 s	0.002
PI	0.87 (0.66–1.08)	87.5 (47.4–99.7)	92.0 (74.0–99.0)	90.9 (75.7 –98.1)	5.51 dB	0.001
AUC	0.85 (0.68–1.02)	62.5 (24.5–91.5)	100.0 (86.3–100.0)	90.9 (75.7–98.1)	82.78 dB × s	< 0.001
ΔTTP	0.91 (0.81–1.01)	100.0 (63.1–100.0)	76.9 (56.4–91.0)	82.3 (65.5–93.2)	9.6 s	< 0.001
ΔPI	0.79 (0.55–1.03)	75.0 (34.9–96.8)	92.0 (74.0–99.0)	87.9 (71.8–96.6)	5.15 dB	0.018
ΔAUC	0.78 (0.60–0.97)	62.5 (24.5–91.5)	91.3 (72.0–98.9)	83.9 (66.3–94.6)	116.29 dB × s	0.002
Multivariate models						
Model 1 (PI + ΔAUC)	0.88 (0.69–1.06)	75.0 (34.9–96.8)	100.0 (85.2–100.0)	93.6 (78.6–99.2)	–	< 0.001
Model 2 (PI + ΔPI)	0.94 (0.80–1.07)	87.5 (47.4–99.7)	100.0 (86.3–100.0)	97.0 (84.2–99.9)	–	< 0.001
Model 3 (TTP + ΔPI)	0.79 (0.57–1.01)	62.5 (24.5–91.5)	92.0 (74.0–99.0)	84.9 (68.1–94.9)	–	0.009
Model 4 (ΔTTP + ΔPI)	0.79 (0.57–1.01)	62.5 (24.5–91.5)	92.0 (74.0–99.0)	84.9 (68.1–94.9)	–	0.009

TTP – time to peak; PI – peak intensity; AUC – area under curve; ΔTTP – difference in time to peak between non-ossified thyroid cartilage and tumor; ΔPI – difference in peak intensity between non-ossified thyroid cartilage and tumor; ΔAUC – difference in the area under the curve between non-ossified thyroid cartilage and tumor; AUCROC – area under the receiver operating characteristic curve.

Among the univariate models, ΔTTP showed the highest AUROC = 0.91 ($p < 0.001$), achieving 100.0% sensitivity, 76.9% specificity, and 82.3% accuracy. The PI parameter also demonstrated good diagnostic performance (AUROC = 0.87, $p = 0.001$), with 87.5% sensitivity, 92.0% specificity, and 90.9% accuracy. The AUC achieved high AUROC = 0.85 ($p < 0.001$) with 100% specificity at the identified threshold. The ΔAUC (AUROC = 0.78, $p = 0.002$) and ΔPI (AUROC = 0.79, $p = 0.018$) parameters also provided

significant diagnostic information, although their overall performance was slightly lower.

In the multivariate models, the combination of PI and ΔPI (Model 2) yielded the highest diagnostic performance (AUROC = 0.94, $p < 0.001$), demonstrating 87.5% sensitivity, 100% specificity, and an overall accuracy of 97.0%. Model 1 (PI + ΔAUC) also performed well (AUROC = 0.88, $p < 0.001$), achieving 100% specificity and 93.6% accuracy. Models 3 (TTP + ΔPI) and 4 (ΔTTP + ΔPI) demonstrated a lowest discriminative ability (AUROC = 0.79, $p = 0.009$).

The diagnostic performance of TIC parameters (AUC, PI, ΔAUC, TTP, ΔPI, and ΔTTP) was statistically significant for the detection of thyroid cartilage invasion ($p < 0.05$). Fig. 3.4.4.1 demonstrates the ROC curves with the diagnostic performances of PI and AUC. Fig. 3.4.4.2 illustrates the ROC curves with the diagnostic performances of TTP, ΔTTP, ΔPI, and ΔAUC.

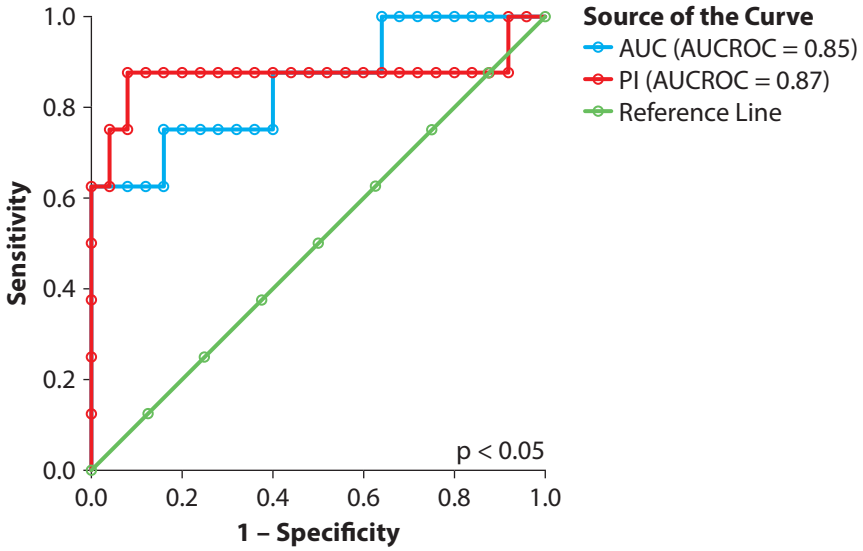

Fig. 3.4.4.1. *Receiver operating characteristic (ROC) analysis of the time–intensity curve parameters (PI and AUC) of non-ossified thyroid cartilage with suspected tumor invasion*

PI – peak intensity; AUC – area under the curve.

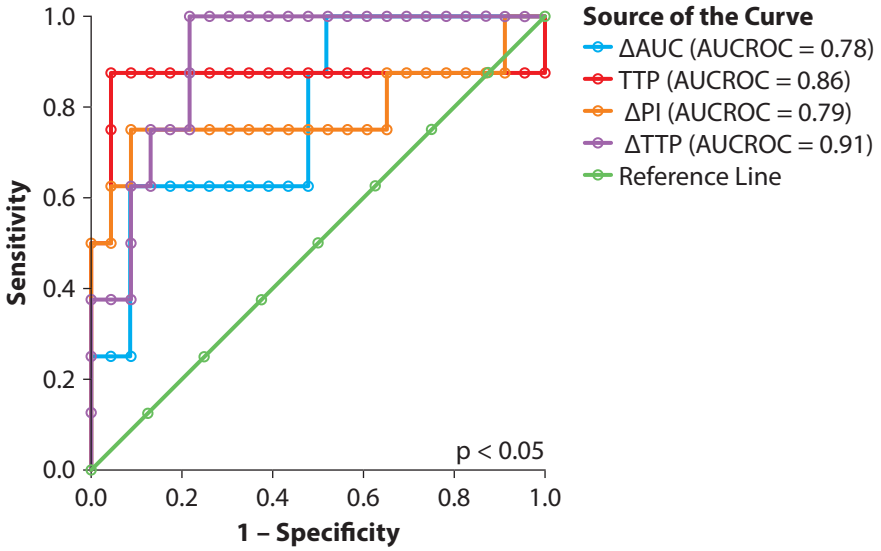

Fig. 3.4.4.2. *Receiver operating characteristic (ROC) analysis of the time–intensity curve parameters (ΔAUC, TTP, ΔPI, and ΔTTP) of non-ossified thyroid cartilage with suspected tumor invasion*

TTP – time to peak; ΔTTP – difference in time to peak between non-ossified thyroid cartilage and tumor; ΔPI – difference in peak intensity between non-ossified thyroid cartilage and tumor; ΔAUC – difference in the area under the curve between non-ossified thyroid cartilage and tumor.

4. DISCUSSION

The optimal treatment strategy continues to be a topic of considerable debate. When thyroid cartilage invasion is confirmed or even suspected, TOLMS is generally contraindicated due to the risk of incomplete tumor excision. In such cases, alternative options such as partial laryngectomy, total laryngectomy, or non-surgical modalities should be considered [6, 7, 130–132]. Furthermore, extensive tumor infiltration into the thyroid cartilage is associated with poor outcomes following radiotherapy [131].

In recent years, CEUS has been extensively investigated, and its clinical applications have significantly expanded, particularly for the diagnosis and differentiation of tumor types and inflammatory diseases, owing to its ability to assess vascularity and perfusion characteristics [24, 25, 69]. Nonetheless, despite its recognized advantages, a standardized CEUS protocol for laryngeal cancer staging has not been endorsed by the EFSUMB yet [24]. Considering the limited literature and lack of standardized guidelines, our research aimed to assess the diagnostic value of qualitative and quantitative CEUS for detecting non-ossified thyroid cartilage invasion in patients with laryngeal cancer. Qualitative findings, based on visual assessment (i.e., detection of enhancement), were compared with the widely used CT and then with MRI for detecting non-ossified thyroid cartilage tumor invasion, using postsurgical histopathological examination as the reference standard. The absence of a statistically significant difference between CEUS and postsurgical histopathology suggests that CEUS may represent a valuable diagnostic tool for assessing non-ossified thyroid cartilage invasion. The diagnostic accuracy of CEUS, CT, and MRI was 86.8%, 60.5%, and 78.1%, respectively, showing slight variations among the modalities with variations of PPV (66,7%, 35.0%, and 46.2%, respectively) and with high NPV (96.2%, 88.9%, and 100.0%, respectively). It is important that the added value of CEUS increased specificity and accuracy in combination with CT and MRI. Moreover, in qualitative analysis exploring microvascular changes we found statistically significant differences with marginally higher accuracy for CEUS when using TIC parameters such as TTP, PI, AUC, and ΔTTP, ΔPI, ΔAUC achieving accuracies of 91.2%, 90.9%, 90.9%, and 82.3%, 87.9%, 83.9%, respectively, in detecting non-ossified thyroid cartilage invasion. Based on our results, CEUS may improve the preoperative staging of the tumor “T” component in the TNM classification of laryngeal cancers, particularly in cases with equivocal CT and/or MRI findings.

4.1. Qualitative (visual) radiologic assessment of thyroid cartilage invasion

As mentioned before, an accurate detection of laryngeal cartilage invasion plays a crucial role in determining the most appropriate treatment strategy and influences the prognosis of SCC. Therefore, a precise radiological evaluation of local tumor extension – particularly the assessment of cartilage involvement – is essential for minimizing complications, ensuring complete resection, and improving overall disease control and survival outcomes.

Cross-sectional imaging using multi-slice CT or MRI is primarily aimed at delineating the deep extension of the tumor into submucosal soft tissues and laryngeal cartilages. CT is fast, widely accessible, and enables volumetric data acquisition with submillimetric voxel resolution. The short acquisition time reduces the likelihood of motion artifacts, while the high spatial resolution enhances the visualization of subtle tumor invasion within soft tissue planes and bony or ossified structures [14, 45, 49]. MRI provides superior contrast resolution, which can be further enhanced using various pulse sequence combinations. These advantages have been extensively applied in evaluating laryngeal cartilage invasion [9,18]. Several studies have demonstrated that MRI exhibits a markedly higher sensitivity for detecting laryngeal cartilages invasion compared with CT [45]. According to a recent meta-analysis of studies on laryngo-hypopharyngeal cancer by Cho et al. [45], the pooled sensitivity values to detect cartilage invasion were 88% for MRI and 66% for CT, while the corresponding specificities were 81% and 90%. As expected, CT performance appeared to be more variable, depending on the specific cartilage assessed. When the analysis was restricted to thyroid cartilage invasion, the reported sensitivity reached 69%, which is comparable to that observed in our study (77.8%), whereas specificity was higher (86% *vs.* 55.2%).

When compared with the study by Mohamad et al. [23], evaluating the diagnostic performance of head and neck MRI in predicting laryngeal subsite invasion (2008–2021 cohort), our results demonstrated a notably higher diagnostic accuracy for thyroid cartilage invasion. Mohamad et al. [23] reported sensitivity, specificity, and accuracy for full-thickness thyroid cartilage invasion to be 74%, 61%, and 69%, respectively, while our study showed 100.0%, 73.1%, and 78.1%, respectively. Similarly, the NNP and PPV in our study (100.0% and 46.2%, respectively) also differed substantially from those previously reported by Mohamad et al. (58% and 76%) [23]. These discrepancies may be attributed to differences in imaging protocols, MRI sequence optimization, and characteristics of study populations, including cartilage ossification status.

Furthermore, ongoing advancements in imaging technology continue to enhance the potential for acquiring high-quality images of the entire larynx with isotropic 1-mm resolution sequence, free of artifacts, within only a few minutes [23, 133, 134]. Recent improvements in MRI sequence design, such as contrast-enhanced three-dimensional (3D) T1-weighted radial gradient-recalled echo (GRE) imaging, have demonstrated high diagnostic accuracy in detecting neoplastic thyroid cartilage invasion. Park et al. [133] reported that this 3D technique achieved a significantly higher sensitivity (75.0%), specificity (96.4%), and overall accuracy (86.5%) than conventional two-dimensional (2D) spin-echo T1-weighted imaging, with superior diagnostic performance (AUC = 0.963 *vs.* 0.862). In comparison, the specificity and accuracy obtained in our study using 2D spin-echo T1-weighted MRI were 73.1% and 78.1%, respectively. Moreover, in our study, the accuracy of CEUS (86.8%) in assessing non-ossified thyroid cartilage was very similar to that of MRI reported by Park et al., suggesting that CEUS may provide a reliable alternative for evaluating cartilage invasion. It worth noting, however, that our study specifically investigated the invasion of non-ossified thyroid cartilage, whereas the study by Park et al. included patients with varying degrees of cartilage ossification. These findings reflect a degree of heterogeneity, but also collectively underscore the potential of advanced MRI protocols to further enhance the precision of preoperative staging in patients with laryngeal and hypopharyngeal cancer. Nevertheless, the evaluation of thyroid cartilage invasion remains diagnostically challenging, but is generally more accurately assessed with MRI than with CT.

Nevertheless, most studies assessing the diagnostic accuracy of imaging modalities in detecting cartilage invasion have predominantly concentrated – either intentionally or unintentionally – on ossified cartilage or did not specify cartilage ossification. This may be explained by several aspects. First, in most clinical cases, tumor infiltration primarily involves the ossified portions of cartilage. Second, both CT and MRI are effective in visualizing these areas, as invasion typically shows characteristic features on CT, such as sclerosis, cortical erosion, or destruction accompanied by replacement of cartilage with tumor tissue, while MRI may provide a more accurate evaluation in many cases [17]. The evaluation of non-ossified cartilage, however, remains more challenging. On CT, the similar attenuation values between tumor tissue and non-ossified thyroid cartilage often obscure invasion, while on MRI, overlapping signal characteristics caused by reactive inflammation, edema, or fibrosis further complicate interpretation and cause overdiagnosis [9, 45]. Additionally, peritumoral inflammation at the tumor–cartilage interface may act as a confounding factor; nevertheless, the application of multiple MRI

sequences improves tissue differentiation and diagnostic accuracy, if the acquired images are of high quality [23].

Recently, DECT has emerged as a promising technique for improving tissue characterization in head and neck imaging. Forghani and colleagues [59] investigated the potential of DECT in differentiating between tumor tissue and non-ossified thyroid cartilage by analyzing their spectral attenuation profiles. VMIs reconstructed at different energy levels demonstrated a decrease in tumor tissue attenuation at higher keV settings, whereas non-ossified cartilage retained consistently high attenuation, thereby enabling clearer differentiation between the two tissue types [59]. However, it is important to note that this study did not directly assess the cases of tumor infiltration into non-ossified cartilage, limiting the conclusions regarding its diagnostic performance, but supported the findings of earlier study by Kuno et al. [60]. Kuno et al. [60] reported that non-ossified cartilage infiltrated by tumor tissue, which exhibits iodine distribution, can be more readily distinguished from normal cartilage on DECT iodine overlay images than on conventional weighted-average images. This advantage arises because iodine is selectively color-coded and enhanced on iodine overlay images, thereby improving visual differentiation. The combined evaluation of weighted-average and iodine overlay images obtained with DECT was shown to increase the specificity from 70% to 96% for detecting thyroid cartilage invasion ($p = 0.031$) without compromising sensitivity (86%) [60]. A few years later, Kuno et al. [61] conducted another study that compared DECT with MRI. The study demonstrated that DECT achieved higher specificity than MRI for detecting thyroid cartilage invasion (100% *vs.* 64%, $p < 0.001$), with comparable diagnostic performance (AUC = 0.95 *vs.* 0.94, $p = 0.70$). Although the sensitivity did not differ significantly between the two modalities for all cartilage types (81% *vs.* 97%, $p = 0.16$) or for the thyroid cartilage (89% *vs.* 100%, $p = 0.50$), there was a tendency toward higher sensitivity with MRI [61]. These studies suggest that relying solely on currently applied radiological methods may be insufficient and highlight the considerable potential of developing and implementing alternative, more accurate imaging techniques for the evaluation of laryngeal cartilage invasion.

US has also been investigated for its potential role in addressing the diagnostic challenge of thyroid cartilage invasion. Given the superficial location of the larynx, US occupies a surprisingly unique position among cross-sectional imaging modalities, particularly in the evaluation of non-ossified cartilage invasion. This advantage arises from its superior ability to visualize non-ossified cartilage, which often presents the greatest diagnostic difficulty when using CT [41, 135, 136]. In one study involving 62 patients with laryngeal or hypopharyngeal cancer, US and CT demonstrated the sensitivity

of 98% and 91%, respectively, with the equal specificity of 75% in detecting thyroid cartilage invasion [135]. However, this study did not evaluate the different groups of ossified and non-ossified thyroid cartilage but mentioned that a better acoustic window was in cases with non-ossified cartilage.

The promising findings from previous studies encouraged further exploration of ultrasound by integrating CEUS techniques. Our findings for identifying thyroid cartilage invasion, particularly in demonstrating that CEUS provides a higher diagnostic accuracy than CT (86.8% and 60.5%, respectively), are consistent with those reported by Hu et al. [41] (CEUS 90.0%, CT 83.3%). Several methodological differences set our study apart from the study above. In our study, the exact area of suspected non-ossified cartilage invasion on CT was subsequently evaluated with both CEUS and MRI, followed by postoperative histopathological confirmation. In addition, the radiologists who performed and analyzed CEUS and MRI examinations and the pathologist who did histopathological assessment were not blinded to the results of CT. To our knowledge, this is the first investigation directly comparing CEUS with CT and MRI specifically for the assessment of non-ossified thyroid cartilage involvement. We found a statistically significant difference in diagnostic performance between CEUS and CT ($p = 0.039$), while no significant differences emerged when comparing MRI with CEUS ($p = 0.109$). Differences in diagnostic performance between imaging modalities were largely driven by variability in false-positive rates. CT demonstrated a relatively low specificity (55.2%), corresponding to a high proportion of false-positive findings, indicating a greater likelihood of overestimating non-ossified thyroid cartilage invasion. In contrast, CEUS showed a substantially higher specificity (86.2%), suggesting a lower likelihood of false-positive classification compared with CT. MRI demonstrated an intermediate specificity (73.1%), with a still notable rate of false-positive results, potentially leading to overdiagnosis in agreement with observations reported by other investigators [18, 133].

To address this issue, we conducted an analysis of the added diagnostic value of CEUS when combined with CT and MRI for the assessment of non-ossified thyroid cartilage invasion. When CEUS was combined with cross-sectional imaging using the AND rule, false-positive findings were markedly reduced. The combination of CEUS and CT increased specificity to 89.7%, which was comparable to the specificity reported for CT (86%) by Cho et al. [45]. However, it should be noted that the study Cho et al. evaluated thyroid cartilage invasion without distinguishing between ossified and non-ossified cartilage, which may have affected specificity, given that the ossified parts of the thyroid cartilage are more accurately assessed on CT.

In the present study, the combination of CEUS and MRI achieved a very high specificity of 100%, effectively eliminating FP cases in this cohort. In addition, the specificity achieved in our study was higher than that reported in previous studies evaluating CT and MRI alone for thyroid cartilage invasion [23, 45, 133]. Notably, Park et al. [133] reported a very high specificity of 96.4% while using an advanced contrast-enhanced 3D T1W GRE sequence on MRI; however, specificity was higher in our study when CEUS was combined with MRI, despite the use of contrast-enhanced 2D T1W MRI with slightly thicker slices. In contrast, Kuno et al. [61] reported the same specificity of 100% when an advanced modality as DECT was used to assess thyroid cartilage invasion, comparable to the specificity achieved with the CEUS and MRI combination in our study.

Overall, the use of CEUS in combination with CT or MRI substantially reduces the risk of overdiagnosis. From a clinical perspective, minimizing false-positive findings is crucial, as overestimation of cartilage invasion may lead to tumor overstaging and unnecessarily aggressive treatment.

4.2. Quantitative time–intensity curve analysis in CEUS assessment of thyroid cartilage invasion

In the second part of our study analysis, we focused on quantitative perfusion parameters namely TTP, PI, AUC, and WIS derived from TIC analysis to explore microcirculatory changes in laryngeal SCC and non-ossified thyroid cartilage. This approach represents an early step in extending CEUS to the evaluation of laryngeal tumors and underscores its potential for detailed perfusion assessment in non-ossified cartilage, providing a platform for further research in this area. In line with our expectations, we found statistically significant differences in the TIC parameters of thyroid cartilage invasion with high sensitivity and specificity, as follows: TTP (87.5% and 92.3%), PI (87.5% and 92.0%), AUC (62.5% and 100.0%), ΔTTP (100% and 76.9%), ΔPI (75.0% and 92.0%), and ΔAUC (62.5% and 91.3%). Moreover, combining PI and ΔPI increased the specificity to 100% for excluding non-ossified thyroid cartilage invasion and achieved an overall accuracy of 97%, outperforming any single TIC parameter. Taken together, these findings indicate that CEUS may facilitate more accurate preoperative T-staging within the TNM classification of laryngeal tumors, particularly when CT or MRI yield inconclusive results.

Given that tissue perfusion differs substantially between malignant and normal structures, the study was designed to include not only qualitative CEUS assessment but also quantitative TIC-based analysis. The quantitative

approach provides objective measurements of perfusion dynamics and enables a more precise characterization of non-ossified thyroid cartilage involvement, whereas qualitative evaluation offers only an initial visual impression of enhancement patterns [24,73]. The vascular network of tumors is fundamentally unlike that of healthy tissue: instead of a well-organized and efficient system, tumor vessels tend to be irregular, tortuous, and permeable, leading to uneven blood flow and increased permeability. Tumor angiogenesis, stimulated by various growth factors, promotes rapid endothelial proliferation and the formation of new, often fragile capillaries in response to tumor-derived signals. While this aberrant vascular architecture sustains tumor progression by improving access to nutrients and facilitating the removal of metabolic waste, it also contributes to the highly heterogeneous microenvironment characteristic of malignant lesions [137].

The principle described above has served as the foundation for studies assessing laryngeal cartilage invasion in patients with laryngeal carcinoma across multiple radiological imaging modalities [19, 22, 41, 53, 67, 81, 127, 138].

DCECT, which evaluates tissue perfusion, has been explored in head and neck imaging with the expectation of improving diagnostic accuracy. The technique relies on repeated acquisitions after contrast administration to derive perfusion-related parameters, but these may be influenced by motion artefacts due to the longer acquisition time compared with contrast-enhanced CT [19]. However, Dankbaar et al. [19] have shown that DCE-CT parameter maps offer no clear advantage in detecting thyroid cartilage invasion. In fact, conventional CECT demonstrated a higher sensitivity than DCE-CT (85% *vs.* 75%) [19]. Similar findings were reported by Trojanowska et al. [53] who observed that CECT outperformed DCE-CT in identifying malignant involvement of the thyroid cartilage, with superior sensitivity (66.6% *vs.* 33.3%), identical specificity (96.5%), and higher PPV and NPV (80.0% *vs.* 66.6%, and 93.33% *vs.* 87.5%, respectively). The evaluation relied on placing ROIs on contrast-enhanced CT images within various neck structures to distinguish tumor tissue from healthy tissue. Variations in DCE-CT-derived quantitative parameters (perfusion CT) between these ROIs were then used to assess the presence of tumoral infiltration. Collectively, these results indicate that DCE-CT does not provide the diagnostic benefit initially anticipated for evaluating laryngeal cartilage invasion.

Interest in advanced MRI techniques has grown steadily, including the use of DCE-MRI, a noninvasive method, or evaluating microvascular perfusion by monitoring contrast agent dynamics within specific tissues. Because malignant tumors typically demonstrate disordered and abnormal vascular architecture, DCE-MRI has been widely explored for its potential in cancer

detection, prognostic assessment, and treatment monitoring [22, 64, 66, 68, 139–141]. Within the laryngeal region, Citil et al. [22] reported that DCE-MRI achieved 100% sensitivity, specificity, and accuracy in identifying cartilage invasion, with 15 true negative and 5 true positive cases. Another study, which included three groups namely 16 patients with benign laryngopharyngeal lesions, 17 with malignant lesions, and 23 healthy controls demonstrated that DCE-MRI can distinguish benign from malignant cartilage abnormalities and can accurately and quantitatively detect neoplastic infiltration of the laryngeal cartilage in a noninvasive manner [67]. Although these findings are encouraging, studies with larger patients' groups and a more detailed assessment of thyroid cartilage involvement are still needed, highlighting the importance of continued research.

Returning to a modality that is receiving growing scientific attention and practical application, this study is, to the best of our knowledge, the first to use CEUS for the quantitative evaluation of laryngeal SCC and non-ossified thyroid cartilage. Our findings allowed us to establish TIC parameter values for these structures for the first time, providing a valuable reference point for future investigations. As no comparable data have been published to date, direct comparison with previous research is not possible. Nevertheless, our statistical analysis revealed several TIC parameters that demonstrated significant differences in distinguishing thyroid cartilage invasion.

Our analysis of the hemodynamic parameters in the tumor group showed pronounced perfusion alterations that clearly differentiated tumor tissue from non-invaded non-ossified thyroid cartilage. The tumor exhibited the shortest TTP values (median 28.44 s), indicating substantially faster contrast arrival compared with non-invaded cartilage (median 45.21 s), while the TTP values of invaded non-ossified thyroid cartilage (median 31.12 s) were more similar to those of the tumor. These differences were statistically significant ($p < 0.05$), and this reflects the rapid and disorganized vascular filling characteristic of malignant lesions. Using a TTP cutoff of 36.6 s, lower TTP values enabled discrimination between invaded and non-invaded non-ossified thyroid cartilage with an accuracy of 91.2%, yielding a sensitivity of 87.5% and a specificity of 92.3%.

Similarly, PI values were markedly higher in the tumor group (13.09 dB) and in the invaded thyroid cartilage (8.46 dB) than in non-invaded cartilage (2.16 dB), consistent with stronger contrast enhancement due to increased microvascular density within the tumor. These differences also reached a strong statistical significance ($p < 0.001$; 0.012). A PI cut-off of 5.51 dB yielded 90.9% accuracy, with 87.5% sensitivity and 92.0% specificity. More-

over, PI remained an independent predictor in multivariate models, suggesting that enhancement intensity retains diagnostic strength even when other perfusion parameters are considered.

AUC values in the tumor were the highest (300.87 dB × s), exceeding those of both non-invaded and invaded cartilage. As the AUC reflects the overall amount of contrast uptake over time, these elevated values correspond to the increased vascular volume and permeability typical of malignant tissue [24]. Although the AUC differed significantly between the tumor and non-invaded cartilage ($p < 0.001$), no significant difference was observed between the tumor and invaded cartilage ($p > 0.05$), suggesting that cartilage infiltration results in perfusion characteristics that resemble those of the tumor itself. An AUC cut-off of 82.78 dB × s provided 90.9% accuracy, with 62.5% sensitivity and 100.0% specificity. Higher AUC and PI values correspond to a greater likelihood of invasion, suggesting increased vascularity and perfusion in the affected tissue; notably, each 1-dB increase in PI and each 1-dB × s increase in the AUC raised the likelihood of thyroid cartilage invasion by 1.81 and 1.04 times, respectively.

We confirmed our hypothesis: the analysis of the derived TIC parameters showed clear differences between non-invaded and invaded non-ossified thyroid cartilage. As in the main results, the perfusion pattern of invaded cartilage tended to shift toward the values observed in the tumor, which prompted us to calculate the absolute differences between tumor and cartilage measurements. These findings show that the derived TIC parameters – most notably ΔTTP – provide the strongest evidence of non-ossified thyroid cartilage infiltration. ΔTTP not only demonstrated the largest separation between invaded and non-invaded cartilage but also achieved excellent diagnostic performance. ΔTTP offered the best overall performance (AUROC 0.91) with a cut-off value of 9.6 s, yielding an accuracy of 82.3%, a sensitivity of 100%, and a specificity of 76.9%. Its predictive value was further supported by logistic regression, where lower ΔTTP values significantly increased the probability of invasion. For example, for every 1-s increase in ΔTTP, the likelihood of thyroid cartilage invasion decreased by approximately 24%. Although ΔPI and ΔAUC showed consistent trends, their ability to discriminate invasion was more modest. Overall, the robust cut-off values, high specificity, and favorable AUROC profiles indicate that time-dependent parameters such as ΔTTP, especially when supported by intensity-based measures like PI and AUC, can meaningfully enhance diagnostic performance when evaluating the potential invasion of non-ossified thyroid cartilage.

After these promising results, we decided to construct models combining two parameters to determine whether their pairing could improve diagnostic prediction. When these parameters were combined into multivariate models,

two of the combinations showed clear improvement according to ROC analysis. The combination of PI + ΔAUC (Model 1) increased the AUROC to 0.88 and achieved a specificity of 100%, with an overall accuracy of 93.6%. However, Model 2 (PI + ΔPI) performed even better, with an AUROC of 0.94 and an accuracy of 97.0%; its sensitivity and specificity were 87.5% and 100%, respectively, making it the most predictive combination. In comparison, the remaining models that paired either TTP or ΔTTP with ΔPI showed weaker performance (AUROC of 0.79, accuracy of 84.9%) and offered no clear advantage over the single-parameter measures.

Taken together, these TIC findings underscore how strongly the microcirculatory pattern of laryngeal SCC differs from that of normal non-ossified thyroid cartilage, clearly separating non-invaded cartilage from the tissue already affected by tumor infiltration. The results further suggest that once invasion occurs, the perfusion behavior of the non-ossified thyroid cartilage begins to resemble that of the tumor.

LIMITATIONS

This research has several limitations that should be acknowledged. The most important limitation is a small sample size as the study was conducted at a single center and included a small group of patients due to fewer common cases of the adjacent tissues of non-ossified thyroid cartilage and tumor, who underwent surgery. Another limitation is that CT and MRI images were interpreted by a single reader, which may introduce observer bias; however, this can be viewed as a controversial point. Moreover, the CEUS technique is also highly operator-dependent and requires experience in both CEUS and cross-sectional laryngeal imaging to accurately identify the area of interest. In our study, matching the suspected invasion site on CT with the corresponding area on CEUS was not always straightforward due to the small ROI, especially in locally advanced cancer cases. This limitation may be addressed in future studies by using CT–CEUS image fusion. Additional limitation – anatomical variations such as thin, non-ossified thyroid cartilage – may have influenced TIC parameters values because it is more difficult to keep a small ROI from slight movement errors. Moreover, some cases were excluded from quantitative CEUS evaluation due to motion artifacts in patients who had difficulty maintaining shallow breathing. The final limitation is that only one ROI can be assessed at a time during CEUS, requiring repeated contrast injections when multiple areas need evaluation, which lengthens the examination.

CONCLUSIONS

1. Qualitative (visual) CEUS yielded high specificity (86.2%) and sensitivity (88.9%) in the assessment of laryngeal carcinoma invasion into non-ossified thyroid cartilage, showing no significant difference from post-operative histopathological findings ($p > 0.05$).
2. The combination of CEUS with CT and particularly with MRI enhanced diagnostic performance in evaluating laryngeal carcinoma invasion into non-ossified thyroid cartilage by improving diagnostic specificity and overall accuracy.
3. Quantitative CEUS parameters (TTP, PI, and AUC) and their derived differences between cartilage and tumor (ΔPI, ΔAUC, and especially ΔTTP) allowed reliable ($p < 0.05$) confirmation or exclusion of laryngeal carcinoma invasion into non-ossified thyroid cartilage.
4. The combination of PI and ΔPI demonstrated the highest diagnostic performance (AUROC = 0.94) among single parameters and their combinations in assessing laryngeal carcinoma invasion into non-ossified thyroid cartilage.

PRACTICAL RECOMMENDATIONS

The results of our study highlight CEUS as an informative and easily accessible imaging modality in assessing laryngeal cancer invasion into the non-ossified thyroid cartilage.

In clinical practice, CEUS is recommended as a complementary imaging modality to CT and/or MRI in cases where non-ossified thyroid cartilage invasion remains unclear. To achieve higher diagnostic accuracy and reliability, which are crucial in determining the optimal treatment method and its extent, it is recommended to apply both qualitative and quantitative CEUS assessment.

From **a scientific perspective**, further research on this topic is warranted. We recommend, where feasible, considering the use of CT and CEUS image fusion to ensure accurate and more standardized identification of the ROI in CEUS examinations.

SANTRAUKA

SUTRUMPINIMAI

ADC	–	tariamas difuzijos koeficientas (angl. *apparent diffusion coefficient*)
AJCC	–	Amerikos jungtinis vėžio komitetas (angl. *American Joint Committee on Cancer*)
AUC	–	plotas po kreive (LIK parametras-angl. *area under the curve*)
AUCROC	–	kreivės plotas po ROC kreive (angl. *area under the curve*)
DDKK	–	daugiadalykės komandos konsiliumas
DEKT	–	dvigubos energijos kompiuterinė tomografija
DWI	–	difuzijos svertinis vaizdavimas (angl. *diffusion-weighted imaging*)
KT	–	kompiuterinė tomografija
KUT	–	kontrastinis ultragarsinis tyrimas
LIK	–	laiko–intensyvumo kreivė
MRT	–	magnetinio rezonanso tomografija
PI	–	pikinis intensyvumas
PLK	–	plokščiųjų ląstelių karcinoma
Qlab®	–	kiekybinės analizės programinė įranga
T	–	naviko T stadija
TNM	–	naviko, limfmazgių ir atokiųjų metastazių klasifikavimo sistema
TTP	–	laikas iki piko (angl. *time to peak*)
WIS	–	įtekėjimo greitis (angl. *wash-in slope*)
ΔAUC	–	ploto po kreive skirtumas
ΔPI	–	pikinio intensyvumo skirtumas
ΔTTP	–	laiko iki piko skirtumas
ΔWIS	–	įtekėjimo greičio skirtumas

ĮVADAS

Per pastarąjį dešimtmetį gerklų vėžio atvejų skaičius pasaulyje padidėjo maždaug 23 proc. [1], o ši liga ir toliau reikšmingai dažniau nustatoma vyrams [1, 2]. Be to, daugumą (apie 90-95 proc.) piktybinių gerklų navikų atvejų sudaro plokščiųjų ląstelių karcinomos histologinis tipas [3,4].

Tikslus vaizdiniais tyrimais nustatomas naviko (T) išplitimo, ypač į skydinę ir žiedinę kremzles, vertinimas yra vienas esminių veiksnių nustatant ligos stadiją ir parenkant tinkamiausią gydymo taktiką konkrečiu atveju. Kremzlių pažeidimo vertinimas tiesiogiai lemia chirurginio gydymo apimties pasirinkimą – ar bus atliekama visiška laringektomija, atvira dalinė laringektomija, transoralinė lazerinė mikrochirurgija, ar pasirenkamas konservatyvus gydymas taikant spindulinę terapiją ir (arba) chemoterapiją [5–9]. Šie sprendimai daro tiesioginę įtaką gydymo veiksmingumui, prognozei po spindulinės terapijos ir paciento gyvenimo kokybei.

Šiuo aspektu radiologiniai vaizdiniai tyrimai yra ypač svarbūs diferencijuojant T stadijas pagal naviko, limfmazgių ir atokiųjų metastazių (TNM) klasifikavimo sistemą [10]. Kompiuterinė tomografija (KT) ir magnetinio rezonanso tomografija (MRT) jau daugelį metų yra pagrindiniai gerklų karcinomos stadijavimo metodai [7, 11–16]. Nors pagal galiojančias rekomendacijas taikomi tiek KT, tiek MRT tyrimai, kiekvienas metodas pasižymi savitais privalumais ir ribotumais, o pasirinkimą dažnai lemia vietiniai diagnostikos protokolai bei įrangos prieinamumas. KT yra efektyvi vertinant naviko išplitimą į gerklų kremzles, ypač tose srityse, kur kremzlės yra sukaulėjusios. Be to, dėl trumpos tyrimo trukmės šis metodas yra palankus pacientams, kuriems pasireiškia kvėpavimo sutrikimai. Vis dėlto reikšminga diagnostinė problema – navikinis audinys ir nesukaulėjusi skydinė kremzlė dažnai pasižymi panašiu tankiu, todėl sudėtinga patikimai įvertinti naviko išplitimą ir jo mastą [17]. Tokiais atvejais pirmenybė teikiama MRT tyrimui, taikant 2008 m. Becker ir bendraautorių pasiūlytus atnaujintus MRT vertinimo kriterijus [18]. Vis dėlto, nepaisant ilgalaikio MRT taikymo ir patikimumo, išlieka nemažas klaidingai teigiamų rezultatų skaičius. Nors MRT ir dvigubos energijos kompiuterinė tomografija (DEKT) pagerino diagnostinį tikslumą, nė vienas skerspjūvio vaizdinimo metodas iki šiol nuosekliai neįrodė vienareikšmio pranašumo vertinant naviko išplitimą į nesukaulėjusią skydinę kremzlę [14, 16–23]. Dėl šios priežasties ir toliau ieškoma naujų vaizdinimo parametrų galimybių ir technologijų, galinčių pagerinti gerklų vėžio radiologinio stadijavimo tikslumą. Kontrastinis ultragarsinis tyrimas (KUT) pastaraisiais metais sulaukė didelio susidomėjimo onkologinės diagnostikos srityje dėl aukštos erdvinės raiškos, gero akustinio lango ir galimybės realiuoju laiku vertinti bei kiekybiškai analizuoti mikrovaskulinę perfuziją [24, 25]. Vienas iš šio metodo pranašumų – galimybė atlikti ne tik kokybinę, bet ir kiekybinę vaizdų analizę, taip didinant vertinimo objektyvumą [24, 26–37].

Atsižvelgiant į tai, kad nesukaulėjusi skydinė kremzlė sudaryta iš avaskulinės hialininės kremzlės, galima kelti hipotezę, kad ją galima diferencijuoti nuo vaskuliarizuoto navikinio audinio, remiantis skirtingais perfuzijos požymiais, nustatomais atliekant KUT tyrimą [38–40]. Šia tema rastas tik vienas publikuotas tyrimas: Hu ir bendraautoriai [41] parodė KUT potencialą nustatant gerklų naviko išplitimą į gerklų kremzles pacientams, sergantiems gerklų vėžiu. Vis dėlto šiame tyrime vertintos visos gerklų kremzlės ir taikyta tik kokybinė (vizualinė) KUT analizė. Apibendrinant galima teigti, kad KUT diagnostinė reikšmė vertinant naviko išplitimą į nesukaulėjusią skydinę kremzlę išlieka nepakankamai ištirta. Iki šiol nėra tyrimų, kuriuose būtų taikyta kiekybinė analizė, todėl ši tyrimų kryptis laikytina moksliškai pagrįsta ir perspektyvia tolesniems tyrimams atlikti.

1. TIKSLAS IR UŽDAVINIAI

1.1. Tikslas

Nustatyti kontrastinio ultragarsinio tyrimo (KUT) kokybinio ir kiekybinio vertinimo diagnostinę vertę tiriant gerklų plokščiųjų ląstelių karcinomos išplitimą į nesukaulėjusią skydinę kremzlę, lyginant su pooperaciniu histopatologiniu tyrimu.

1.2. Uždaviniai

1. Nustatyti kokybinio (vizualinio) KUT specifiškumą ir jautrumą vertinant gerklų karcinomos išplitimą į nesukaulėjusią skydinę kremzlę.
2. Įvertinti pridėtinę KUT diagnostinę vertę, derinant su KT ir MRT tyrimais, tiriant gerklų karcinomos išplitimą į nesukaulėjusią skydinę kremzlę.
3. Išanalizuoti ir nustatyti KUT kiekybinių laiko–intensyvumo kreivės (LIK) parametrų diagnostinę vertę tiriant gerklų karcinomos išplitimą į nesukaulėjusią skydinę kremzlę.
4. Nustatyti, kurių LIK parametrų derinys turi didžiausią diagnostinę gebą, vertinant gerklų karcinomos išplitimą į nesukaulėjusią skydinę kremzlę.

1.3. Darbo naujumas

Naviko išplitimo į nesukaulėjusią skydinę kremzlę diagnostika iki šiol išlieka reikšmingu radiologinės diagnostikos iššūkiu, dažnai lemiančiu klaidingą vaizdų interpretaciją. Šiame tyrime siekta rasti papildomą diagnostinį sprendimą šiai problemai spręsti. Mūsų žiniomis, tai pirmasis mokslinis tyrimas, kuriame KUT taikomas specifiškai analizuojant naviko išplitimą į nesukaulėjusią skydinę kremzlę pacientams, sergantiems gerklų plokščiųjų ląstelių karcinoma. Nors prieš kelerius metus publikuotas panašaus pobūdžio tyrimas [41], jame vertintas gerklų vėžio išplitimas į visas gerklų kremzles, atskirai neišskiriant nesukaulėjusios skydinės kremzlės. Be to, minėtame tyrime atlikta tik kokybinė (vizualinė) KUT vaizdų analizė [41].

Remiantis šiuo metu publikuotais literatūros duomenimis, šis tyrimas yra pirmasis, kuriame minėta tema analizuojama keliomis svarbiomis kryptimis. Pirma, pagrindinis dėmesys skirtas būtent nesukaulėjusios skydinės kremzlės vertinimui. Antra, atlikta ne tik kokybinė, bet ir kiekybinė KUT vaizdų analizė. Trečia, pirmą kartą nustatyta LIK parametrų diagnostinė vertė vertinant nesukaulėjusią skydinę kremzlę tais atvejais, kai nustatytas gerklų vėžio išplitimas, ir tais atvejais, kai jo nenustatyta, taip pat šie parametrai palyginti su navikinio audinio rodikliais. Ketvirta, palyginimui pacientams buvo atliktas

ne tik KT, bet ir MRT tyrimas. Penkta, įvertinta KUT pridėtinė diagnostinė vertė, derinant su KT ir MRT duomenimis.

Tyrimo naujumą dar labiau išryškina tai, kad visais atvejais aukso standartu laikytas pooperacinis histopatologinis ištyrimas, prieš tai pateikus specialiai šiam tyrimui kurtą „Lokalaus išplitimo ištyrimo schemą“ (1 priedas), kurioje, remiantis KT vaizdais, tiksliai pažymėta tiriama sritis.

Šis tyrimas pateikia naujų mokslinių įrodymų, pagrindžiančių KUT, kaip papildomo neinvazinio vaizdinimo metodo, potencialą prieš operaciją vertinant gerklų vėžio išplitimą į nesukaulėjusią skydinę kremzlę greta KT ir/arba MRT. Gauti rezultatai gali prisidėti prie diagnostinių algoritmų tobulinimo, stadijavimo tikslumo gerinimo ir diagnostinių klaidų mažinimo, taip sudarant prielaidas parinkti optimalesnį ir galbūt mažiau traumuojantį gydymą pacientams, sergantiems gerklų plokščiųjų ląstelių karcinoma.

2. METODIKA

2.1. Tyrimo eiga

Perspektyvusis vieno centro mokslinis tyrimas atliktas Lietuvos sveikatos mokslų universiteto ligoninės Kauno klinikų Radiologijos ir Ausų, nosies ir gerklės ligų klinikose 2021–2025 metais. Dėl COVID-19 apribojimų, pandemijos laikotarpiu (2019–2020 m.) tyrimas negalėjo būti vykdomas pagal pradinį planą. Pagrindinis tyrimo tikslas buvo nustatyti kontrastinio ultragarsinio tyrimo diagnostinę vertę tiriant gerklų karcinomos išplitimą į nesukaulėjusią skydinę kremzlę. Tyrimo protokolą patvirtino Kauno regioninis biomedicininių tyrimų etikos komitetas (protokolo Nr. 2021-BE-10-00016; 2021 m.). Visi pacientai prieš įtraukimą į tyrimą pasirašė informuoto asmens sutikimo formą (2 priedas), laikantis Helsinkio deklaracijos principų.

Pacientai į tyrimą įtraukti po jų atvejų aptarimo galvos ir kaklo onkologinių ligų daugiadalykės komandos konsiliume. Į tyrimą įtraukti 46 pacientai, kuriems:

a) daugiau nei 18 metų;
b) pirmą kartą histologiškai patvirtinta gerklų karcinoma;
c) anksčiau nebuvo atlikta gerklų ir gerklaryklės operacija, nebuvo taikytas chemospindulinis gydymas;
d) KT tyrimu su intraveniniu kontrastavimu įtartas arba nustatytas naviko išplitimas į nesukaulėjusią skydinę kremzlę;
e) konsiliumo sprendimas – atlikti visišką arba dalinę laringektomiją;
f) gauta pasirašyta informuoto asmens sutikimo forma.

Visiems įtraukimo kriterijus atitikusiems pacientams atlikti KUT ir MRT tyrimas be ir su intraveniniu kontrastavimu. Penkiems pacientams MRT

neatliktas dėl metalinių svetimkūnių arba nesutikus atlikti tyrimą. Vėliau 14 pacientų iš tyrimo pašalinti, nes atsisakė chirurginio gydymo ar buvo pakeistas gydymo planas, todėl galutinė imtis – 32 pacientai. Vis dėlto tyrime analizuoti 38 nesukaulėjusios skydinės kremzlės galimo išplitimo atvejai, nes šešiems iš 32 pacientų tirtos dvi atskiros dominančios kremzlės sritys. Tyrimo eigos schema pateikiama 2.1.1 pav.

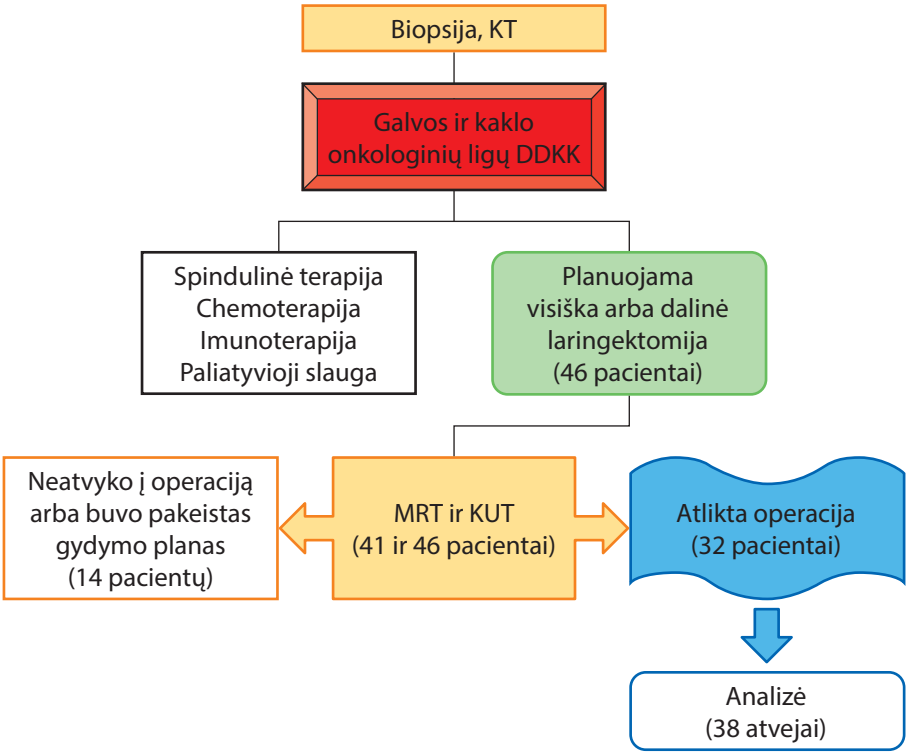

2.2.1 pav. *Tyrimo eigos schema*

DDKK – daugiadalykės komandos konsiliumas; MRT – magnetinio rezonanso tomografija; KUT – kontrastinis ultragarsinis tyrimas.

2.2. Metodai

KT tyrimas su intraveniniu kontrastavimu atliktas taikant standartinį kaklo minkštųjų audinių-gerklų tyrimo protokolą, atliekant privalomas rekonstrukcijas (ašine, koronarine ir sagitaline plokštuma), orientuotas pagal tikrąsias balso klostes. Remiantis KT vaizdais, į tyrimą įtraukti pacientai, kuriems nustatytas bent vienas iš šių požymių: a) lokalus skydinės kremzlės defektas (per visą storį) greta gerklų naviko; b) skydinės kremzlės srityje

matomas aiškus minkštųjų audinių tankio kontrasto sustiprėjimas, analogiškas gretimam navikiniam audiniui; c) gerklų naviko sąlytis su nesukaulėjusia skydine kremzle, kai jų tankis tampa neatskiriamas.

Į tyrimą įtrauktiems pacientams taip pat atliktas gerklų MRT tyrimas su intraveniniu kontrastavimu, siekiant palyginti ir įvertinti pridėtinę diagnostinę vertę, derinant su KUT. Tyrimas atliktas tuo pačiu 3T magnetinio rezonanso aparatu („Phillips Insegnia“). Tyrimą atliko radiologijos technologas, prižiūrint gydytojui radiologui (doktorantui). Tyrimas atliekamas pacientui gulint ant nugaros, ramiai kvėpuojant ir susilaikant nuo rijimo bei kosėjimo. MRT atlikta be intraveninio kontrastavimo ir su juo; sušvirkšta vienkartinė 0,1 mmol/kg (0,1 ml/kg) gadolinio pagrindo kontrastinės medžiagos dozė („Gadovist®“, „Bayer Schering Pharma“, Berlynas, Vokietija) per kairės rankos periferinę veną, 1,5–2 ml/s greičiu. MRT protokolą sudarė didelės skiriamosios gebos T2 sekos be riebalų supresijos ir su ja („Dixon“), atliktos ašinėje, koronarinėje ir sagitalinėje plokštumose; T1 seka be riebalų supresijos ir su ja („Dixon“), taip pat DWI (su ADC žemėlapiu) seka, atliktos ašinėje plokštumoje. Su intraveniniu kontrastavimu atliktos T1 „Dixon“ sekos ašinėje ir koronarinėje plokštumoje. Ašinės sekos orientuotos lygiagrečiai tikrųjų balso klosčių plokštumai, sagitalinės ir koronarinės – statmenai. Išplitimas į skydinę kremzlę vertintas pagal Becker ir bendraautorių pateiktus kriterijus [18].

Visiems dalyviams KUT tyrimas atliktas pagal nustatytą protokolą, naudojant „Philips“ ultragarso aparatą su 5–12 MHz linijiniu davikliu, taikant mechaninį indeksą ≤ 0,08. Prieš tyrimą slaugytoja į kairės rankos paviršinę veną (alkūninėje duobėje) įvedė 20 G kateterį, kad būtų išvengta mikrosferų pažeidimo. Iš pradžių atliktas įprastas B režimo ultragarsinis tyrimas, siekiant identifikuoti dominančią sritį. Ją nustačius, įjungtas dvigubo vaizdo režimas, vienu metu vaizduojant KUT (mechaninis indeksas ≤ 0,08) ir B režimo vaizdus. Tuo metu paruoštas „SonoVue“ kontrastinės medžiagos tirpalas (5 ml), kuris pagal gamintojo instrukcijas švelniai suplaktas rankomis ir sušvirkštas per intraveninį kateterį, tuo pačiu metu paleidžiant laikmatį ir pradedant vaizdo įrašymą. Po kontrastinės medžiagos suleidimo atliktas praplovimas fiziologiniu tirpalu. KUT vaizdo įrašymas tęstas apie 60 sekundžių. Jei reikėjo pakartotinės kontrastinės medžiagos dozės, likę mikroburbuliukai sunaikinti taikant didelio mechaninio indekso impulsą (angl. *high mechanical index flash*), po kurio kontrastinė medžiaga suleista pakartotinai ir tyrimas atliktas ta pačia eiga. Atrinkti vaizdai ir vaizdo įrašai išsaugoti vaizdų archyvavimo sistemoje ir persiųsti į „Qlab®“ programinę sistemą. Atlikta tiek kokybinė tiek kiekybinė vaizdų analizė. Analizuoti keturi kokybiniai LIK parametrai: TTP – laikas iki piko; PI – pikinis intensyvumas; AUC – plotas po kreive; WIS – įtekėjimo greitis.

Prieš chirurginį gydymą radiologiškai įtarta arba nustatyta išplitimo į kremzlę sritis pažymėta „Lokalaus išplitimo ištyrimo schemoje“ (1 priedas), remiantis KT vaizdais, siekiant tiksliau paruošti dominančios srities pooperacinę medžiagą atlikti išsamesniam histopatologiniam vertinimui, kuris šiame tyrime laikytas aukso standartu.

Statistinė analizė atlikta naudojant „IBM SPSS Statistics 29.0“ („IBM Corp.“, Niujorkas, JAV) ir „MedCalc 23.1.3“ („MedCalc Software Ltd“) programas. Statistiškai reikšmingų rezultatų nustatymas taikant tinkamus testus patvirtino imties pakankamumą statistiniu požiūriu. KUT, KT ir MRT jautrumas, specifiškumas, teigiama ir neigiama prognostinė vertės (TPV ir NPV), nustatant gerklų vėžio išplitimą į nesukaulėjusią skydinę kremzlę, apskaičiuoti naudojant histopatologinius duomenis kaip aukso standartą. KUT ir KT, KUT ir MRT poriniam tarpusavio palyginimui, taip pat jų palyginimui su histopatologinio tyrimo rezultatais atlikti taikytas McNemaro testas. KUT pridėtinė diagnostinė vertė vertinta apskaičiuojant KUT derinių su KT ir MRT jautrumą ir specifiškumą, taikant OR ir AND taisykles. Dėl mažos imties taikyti neparametriniai statistiniai metodai: Mano-Vitnio U testas nepriklausomoms grupėms ir Vilkoksono rangų testas priklausomoms imtims vertinti. LIK parametrų ryšiui su gerklų naviko išplitimu į skydinę kremzlę vertinti taikyta logistinė regresija, apskaičiuojant šansų santykius (ŠS) ir 95 proc. pasikliautinuosius intervalus (PI). Reikšmingų LIK parametrų diagnostinė vertė vertinta ROC kreivių analize, nustatant AUC ir optimalius ribinius dydžius pagal Judeno indeksą. Statistiškai reikšmingais laikyti rezultatai, kai $p < 0,05$.

2.2.1. Doktorantės indėlis į tyrimą

1. Idėjos sukūrimas ir dalyvavimas tyrimo dizaino bei metodikos kūrimo procese.
2. Dokumentų, reikalingų bioetikos leidimui gauti, rengimas ir pateikimas.
3. Dalyvavimas modifikuojant gerklų MRT tyrimo protokolą šiam moksliam tyrimui.
4. Pacientų atranka į tiriamąją grupę dalyvaujant DDKK.
5. Klinikinių ir demografinių duomenų rinkimas bei analizė.
6. MRT tyrimų atlikimo stebėsena ir priežiūra.
7. KUT atlikimas ir vertinimas.
8. „Lokalaus išplitimo ištyrimo schemos“ kūrimas ir pritaikymas moksliniame tyrime.
9. Pacientų duomenų bazės kūrimas ir statistinė duomenų analizė.
10. Mokslinių tezių ir publikacijų rengimas ir pateikimas kartu su bendraautoriais.

3. REZULTATAI

3.1. Demografinė analizė ir pasiskirstymas

Į tyrimą įtraukti 32 pacientai, visi – vyrai. Tiriamųjų amžius svyravo nuo 46 iki 84 metų, vidutinis amžius – 63,25 ± 8,37 metų. Laiko mediana nuo diagnostinių tyrimų atlikimo iki chirurginio gydymo: nuo KT iki operacijos – 30,5 d. (ribos 5–85 d.), o nuo KUT arba MRT – 11,0 d. (ribos 0–42 d.).

Patologinė naviko (pT) stadija pasiskirstė gana tolygiai, tačiau dažniausiai nustatytos T3 ir T1 stadijos. Pagal naviko lokalizaciją 50,0 proc. (n = 16) atvejų sudarė vidurinės dalies (angl. *glottic*), o 50,0 proc. (n = 16) – visų gerklų dalių (angl. *transglottic*) karcinomos. Dvipusė pažaida nustatyta šiek tiek dažniau – 40,6 proc. (n = 13) atvejų, dešiniosios pusės pažeidimai sudarė 31,3 proc. (n = 10), o kairiosios pusės – 28,1 proc. (n = 9). Visiems pacientams histologiškai patvirtinta gerklų PLK. Pagal diferenciacijos laipsnį dažniausiai nustatyta vidutinio diferencijavimo laipsnio (G2) karcinoma – 78,1 proc. (n = 25), rečiau – gerai diferencijuota (G1) – 15,6 proc. (n = 5) ir blogai diferencijuota (G3) – 6,3 proc. (n = 2).

3.2. Kokybinio (vizualinio) KUT, KT ir MRT diagnostinis efektyvumas

Šešiems iš 32 pacientų nustatyta po dvi atskiras analizuojamas sritis nesukaulėjusioje skydinėje kremzlėje, kiekviena sritis laikyta atskiru klinikiniu atveju, todėl iš viso analizuoti 38 klinikiniai atvejai (toliau n žymi klinikinių atvejų, o ne individualių pacientų skaičių). Pooperaciniu histopatologiniu tyrimu, laikytu aukso standartu, iš 38 atvejų patvirtinti devyni naviko išplitimo į nesukaulėjusią skydinę kremzlę atvejai.

KT ir KUT tyrimais įvertinti visi 38 atvejai, o MRT atliktas ir įvertintas 32 atvejais (84,2 proc.), nes penkiems pacientams šis tyrimas neatliktas.

Kiekvieno vaizdinio tyrimo rezultatai lyginti su pooperacinio histopatologinio tyrimo duomenimis (3.2.1 lentelė). Statistiškai reikšmingo skirtumo nenustatyta tik KUT atveju (p = 0,375), kas rodo šio tyrimo aukštą diagnostinę vertę.

KUT pasižymėjo didžiausiu bendru diagnostiniu tikslumu, palyginti su KT ir MRT: jautrumas siekė 88,9 proc. (95 proc. PI – 51,8–99,7), specifiškumas – 86,2 proc. (95 proc. PI – 68,3–96,1), o bendras tikslumas – 86,8 proc. (95 proc. PI – 71,9–95,6). Teigiamos prognostinės vertės (PPV) buvo didesnės nei KT (66,7 proc., palyginti su 35,0 proc.) ir MRT (66,7 proc., palyginti su 46,2 proc.). Neigiama prognostinė vertė (NPV) KUT atveju buvo didesnė nei KT (96,2 proc., palyginti su 88,9 proc.), tačiau šiek tiek mažesnė nei MRT (96,2 proc., palyginti su 100,0 proc.).

Nors KT pasižymėjo mažesniu bendru diagnostiniu efektyvumu nei KUT, nustatytas vidutinis specifiškumas – 73,1 proc. (95 proc. PI – 52,2–88,4), o bendras tikslumas – 78,1 proc. (95 proc. PI – 60,0–90,1).

Apibendrinant, KUT užtikrino labiausiai subalansuotą jautrumo, specifiškumo ir bendro tikslumo derinį, o MRT pasižymėjo 100 proc. jautrumu, tačiau mažesne teigiama prognostine verte.

Nustatytas statistiškai reikšmingas skirtumas tarp KUT ir KT (p = 0,039), vertinant gerklų naviko išplitimą į nesukaulėjusią skydinę kremzlę. Tarp MRT ir KUT statistiškai reikšmingo skirtumo nenustatyta (p = 0,109).

3.2.1 lentelė. *KUT, KT ir MRT diagnostiniai rodikliai, palyginti su pooperaciniu histopatologiniu tyrimu (aukso standartas)*

Tyrimas	**TT, n**	**TN, n**	**KT*, n**	**KN, n**	**Jautrumas, proc. (95 proc. PI)**	**Specifiškumas, proc. (95 proc. PI)**	**Tikslumas, proc. (95 proc. PI)**	**TPV, proc.**	**NPV, proc.**	**p****
KUT (n = 38)	8	25	4	1	88,9 (51,8–99,7)	86,2 (68,3–96,1)	86,8 (71,9–95,6)	66,7	96,2	0,375
KT (n = 38)	7	16	13	2	77,8 (40,0–97,2)	55,2 (35,7–73,6)	60,5 (43,4–76,0)	35,0	88,9	0,007
MRT (n = 32)	6	19	7	0	100,0 (54,1–100,0)	73,1 (52,2–88,4)	78,1 (60,0–90,1)	46,2	100,0	0,016

KUT – kontrastinis ultragarsinis tyrimas; KT – kompiuterinė tomografija; KT*– klaidingai teigiamas; TT – tikrasis teigiamas atvejis; TN – tikrasis neigiamas atvejis; KN – klaidingai neigiamas atvejis; TPV – teigiama prognostinė vertė; NPV – neigiama prognostinė vertė; PI – pasikliautinasis intervalas. ** – palyginimai su pooperaciniu histopatologiniu tyrimu atlikti, taikant McNemaro testą.

3.3. Kokybinio (vizualinio) KUT pridėtinė diagnostinė vertė

KUT derinių su KT ir MRT diagnostinė vertė vertinta taikant dvi sprendimo taisykles – OR ir AND.

OR taisyklė pirmiausia taikoma jautrumui padidinti ir yra tinkamiausia tais atvejais, kai pagrindinis klinikinis tikslas – išvengti klaidingai neigiamų rezultatų. Šiame tyrime OR taisyklės taikymas reikšmingo diagnostinių rodiklių pagerėjimo neparodė. Derinant KUT su KT, jautrumas siekė 88,9 proc., o derinant KUT su MRT – 100 proc., t. y. šie rodikliai buvo panašūs į KUT (88,9 proc.) ir MRT (100 proc.) taikant atskirai. Atsižvelgiant į tai, OR taisyklė nebuvo pasirinkta kaip pagrindinis metodas vertinant KUT pridėtinę diagnostinę vertę, derinant su KT ir MRT. Toliau taikyta AND taisyklė, kuri leido patikimiau patvirtinti kliniškai reikšmingą naviko išplitimą į skydinę kremzlę.

Taikant AND taisyklę, išplitimas į nesukaulėjusią skydinę kremzlę diagnozuotas tik tais atvejais, kai išplitimo požymiai nustatyti abiem vaizdinimo metodais, taip sumažinant klaidingai teigiamų atvejų skaičių. Derinant KUT su KT pagal AND taisyklę, nustatytas didesnis specifiškumas (89,7 proc.), nei taikant KUT arba KT atskirai, bendras diagnostinis tikslumas siekė 86,8 proc., o jautrumas – 77,8 proc. KUT ir MRT derinys pasižymėjo dar didesniu specifiškumu (100 proc.), tačiau jautrumas nežymiai sumažėjo iki 83,3 proc.

Taigi, AND taisyklės taikymas sumažino klaidingai teigiamų rezultatų skaičių ir leido patikimiau patvirtinti išplitimą į skydinę kremzlę.

Išsami diagnostinių rodiklių analizė pateikiama 3.3.1 ir 3.3.2 lentelėse.

3.3.1 lentelė. *KUT, KT ir jų derinio taikant AND taisyklę diagnostinės vertės rodikliai vertinant išplitimą į nesukaulėjusią skydinę kremzlę*

Tyrimas	**TT, n**	**TN, N**	**KT*, n**	**KN, n**	**Jautrumas, proc. (95 proc. PI)**	**Specifiškumas, proc. (95 proc. PI)**	**Tikslumas, proc. (95 proc. PI)**	**TPV, proc.**	**NPV, proc.**
KUT (n = 38)	8	25	4	1	88,9 (51,8–99,7)	86,2 (68,3–96,1)	86,8 (71,9–95,6)	66,7	96,2
KT (n = 38)	7	16	13	2	77,8 (40,0–97,2)	55,2 (35,7–73,6)	60,5 (43,4–76,0)	35,0	88,9
KUT + KT (n = 38)	7	26	3	2	77,8 (40,0–97,2)	89,7 (72,7–97,8)	86,8 (71,9–95,6)	70,0	92,9

KUT – kontrastinis ultragarsinis tyrimas; KT – kompiuterinė tomografija; KT*– klaidingai teigiamas; TT – tikrasis teigiamas atvejis; TN – tikrasis neigiamas atvejis; KN – klaidingai neigiamas atvejis; TPV – teigiama prognostinė vertė; NPV – neigiama prognostinė vertė; PI – pasikliautinasis intervalas. KUT ir KT vertės pateikiamos tiesioginiam palyginimui atlikti, siekiant iliustruoti jų derinio pridėtinę diagnostinę vertę.

3.3.2 lentelė. *KUT, MRT ir jų derinio taikant AND taisyklę diagnostinės vertės rodikliai vertinant išplitimą į nesukaulėjusią skydinę kremzlę*

Tyrimas	TT, n	TK, N	KT*, n	KN, n	Jautrumas, proc. (95 proc. PI)	Specifiškumas, proc. (95 proc. PI)	Tikslumas, proc. (95 proc. PI)	TPV, proc.	NPV, proc.
KUT (n = 38)	8	25	4	1	88,9 (51,8–99,7)	86,2 (68,3–96,1)	86,8 (71,9–95,6)	66,7	96,2
MRT (n = 32)	6	19	7	0	100,0 (54,1–100,0)	73,1 (52,2–88,4)	78,1 (60,0–90,1)	46,2	100,0
KUT + MRT (n = 32)	5	26	0	1	83,3 (35,9–99,6)	100,0 (86,8–100,0)	96,9 (83,8–99,9)	100,0	96,3

KUT – kontrastinis ultragarsinis tyrimas; MRT – magnetinio rezonanso tomografija; KT*– klaidingai teigiamas; TT – tikrasis teigiamas atvejis; TN – tikrasis neigiamas atvejis; KN – klaidingai neigiamas atvejis; TPV – teigiama prognostinė vertė; NPV – neigiama prognostinė vertė; PI – pasikliautinasis intervalas.
KUT ir MRT vertės pateikiamos tiesioginiam palyginimui atlikti, siekiant iliustruoti jų derinio pridėtinę diagnostinę vertę.

3.4. Laiko–intensyvumo kreivės parametrų analizė

Kiekybinių parametrų statistinės analizės imtį sudarė 34 atvejai, nes keturi iš 38 atvejų atmesti dėl ryškių judesio artefaktų, galinčių lemti nepatikimas LIK parametrų kiekybines reikšmes. Iš 32 atvejų aštuoniems (23,5 proc.) histologiškai patvirtintas naviko išplitimas į nesukaulėjusią skydinę kremzlę.

3.4.1. TTP, PI, AUC ir WIS analizė nesukaulėjusioje skydinėje kremzlėje ir gerklų naviko audinyje

Kiekybiniai LIK parametrai analizuoti ir lyginti tarp šių grupių: nesukaulėjusi skydinė kremzlė be naviko išplitimo ir nesukaulėjusi skydinė kremzlė su naviko išplitimu (3.4.1.1 lentelė), nesukaulėjusi skydinė kremzlė be naviko išplitimo ir gerklų naviko audinys (3.4.1.2 lentelė), taip pat nesukaulėjusi skydinė kremzlė su naviko išplitimu ir gerklų naviko audinys (3.4.1.3 lentelė).

Lyginamoji analizė parodė, kad TTP ir PI parametrų reikšmės statistiškai reikšmingai skyrėsi visose grupėse ($p < 0,05$). AUC parametro reikšmės tarp nesukaulėjusios skydinės kremzlės su naviko išplitimu ir be jo taip pat statistiškai reikšmingai skyrėsi ($p = 0,002$), o WIS parametro skirtumas nebuvo statistiškai reikšmingas ($p = 0,002$).

AUC ir WIS parametrų reikšmės statistiškai reikšmingai skyrėsi tarp grupių, lyginant skydinę kremzlę be naviko išplitimo ir gerklų naviko audinį (atitinkamai $p < 0,001$ ir $p = 0,016$). Lyginant gerklų naviko audinio ir skydinės kremzlės su naviko išplitimu grupes, statistiškai reikšmingų skirtumų

nenustatyta (atitinkamai p = 0,093 ir p = 0,208), o tai rodo panašias šių audinių medianų reikšmes.

3.4.1.1 lentelė. *LIK parametrų palyginimas tarp nesukaulėjusios skydinės kremzlės su naviko išplitimu ir be jo grupių*

Parametras	Skydinė kremzlė be naviko išplitimo (n = 26)	Skydinė kremzlė su naviko išplitimu (n = 8)	p*
TTP, s	45,21 (39,44–51,73)	31,12 (28,26–35,72)	0,002
PI, dB	2,16 (1,18–3,32)	8,46 (6,00–20,56)	0,001
AUC, dB × s	7,62 (1,33–16,97)	109,97 (13,45–282,05)	0,002
WIS, dB/s	3,92 (2,61–8,38)	4,62 (1,14–24,56)	0,872

Reikšmės pateikiamos kaip medianos (tarpkvartiliniai pločiai). TTP – laikas iki piko; PI – pikinis intensyvumas; AUC – plotas po kreive; WIS – įtekėjimo greitis. * Palyginimai atlikti taikant Mano-Vitnio U kriterijų.

3.4.1.2 lentelė. *LIK parametrų palyginimas tarp nesukaulėjusios skydinės kremzlės be naviko išplitimo ir gerklų naviko grupių*

Parametras	Skydinė kremzlė be naviko išplitimo (n = 26)	Gerklų navikas (n = 26)	p*
TTP, s	45,21 (39,44–51,73)	28,44 (26,39–32,09)	< 0,001
PI, dB	2,16 (1,18–3,32)	13,09 (10,46–18,07)	< 0,001
AUC, dB × s	7,62 (1,33–16,97)	305,63 (191,71–419,03)	< 0,001
WIS, dB/s	3,92 (2,61–8,38)	1,74 (1,21–2,84)	0,016

Reikšmės pateikiamos kaip medianos (tarpkvartiliniai pločiai). TTP – laikas iki piko; PI – pikinis intensyvumas; AUC – plotas po kreive; WIS – įtekėjimo greitis. * Palyginimai atlikti taikant Vilkoksono testą.

3.4.1.3 lentelė. *LIK parametrų palyginimas tarp nesukaulėjusios skydinės kremzlės su naviko išplitimu ir gerklų naviko grupių*

Parametras	Skydinė kremzlė su naviko išplitimu (n = 8)	Gerklų navikas (n = 8)	p*
TTP, s	31,12 (28,26–35,72)	27,15 (25,65–29,09)	0,017
PI, dB	8,46 (6,00–20,56)	12,07 (8,78–24,90)	0,012
AUC, dB × s	109,97 (13,45–282,05)	257,94 (191,65–320,60)	0,093
WIS, dB/s	4,62 (1,14–24,56)	1,22 (0,88–7,61)	0,208

Reikšmės pateikiamos kaip medianos (tarpkvartiliniai pločiai). TTP – laikas iki piko; PI – pikinis intensyvumas; AUC – plotas po kreive; WIS – įtekėjimo greitis. * Palyginimai atlikti taikant Vilkoksono testą.

Atsižvelgiant į tai, kad gerklų naviko audinio LIK parametrų medianos buvo panašios ir statistiškai reikšmingai nesiskyrė priklausomai nuo to, ar navikas išplito į skydinę kremzlę, ar ne ($p > 0,05$), visai tiriamajai imčiai apskaičiuotos bendros naviko audinio kiekybinių parametrų medianos. Bendrosios medianos reikšmės buvo šios: TTP – 28,44 s (tarpkvartilinis plotis: 26,38–31,56), PI – 13,09 dB (9,86–19,49), AUC – 300,87 dB × s (191,88–413,58) ir WIS – 1,67 dB/s (1,10–3,24).

3.4.2. ΔTTP, ΔPI, ΔAUC ir ΔWIS analizė vertinant naviko išplitimą į nesukaulėjusią skydinę kremzlę

Apskaičiuoti kiekybinių LIK parametrų skirtumai (ΔTTP, ΔPI, ΔWIS ir ΔAUC) tarp naviko (t) ir įtariamo naviko išplitimo į nesukaulėjusią skydinę kremzlę (tc) vietos, pvz., $\Delta PI = PI_t - PI_{tc}$.

Išsami ΔTTP, ΔPI, ΔWIS ir ΔAUC parametrų palyginamoji analizė tarp atvejų su patvirtintu ir nepatvirtintu naviko išplitimu į nesukaulėjusią skydinę kremzlę pateikiama 3.4.2.1 lentelėje. ΔTTP, ΔPI ir ΔAUC medianos atvejais, kai nustatytas naviko išplitimas į nesukaulėjusią skydinę kremzlę, buvo statistiškai reikšmingai mažesnės, palyginti su atvejais, kai naviko išplitimas nenustatytas ($p < 0,05$).

Šie rezultatai rodo, kad hemodinaminiai pokyčiai nesukaulėjusioje skydinėje kremzlėje, esant naviko išplitimui, artėja prie gretimo navikinio audinio charakteristikų.

3.4.2.1 lentelė. *LIK parametrų (ΔTTP, ΔPI, ΔWIS, ΔAUC) skirtumų palyginimas tarp nesukaulėjusios skydinės kremzlės su naviko išplitimu ir be jo grupių*

Parametras	Skydinė kremzlė su naviko išplitimu (n = 8)	Skydinė kremzlė be naviko išplitimo (n = 26)	p
ΔTTP, s	15,19 (8,74–26,21)	4,81 (1,14–6,87)	< 0,001
ΔPI, dB	11,60 (7,88–16,98)	3,10 (0,93–11,34)	0,013
ΔAUC, dB × s	333,75 (201,71–407,33)	94,96 (50,17–297,73)	0,018
ΔWIS, dB/s	5,11 (1,33–7,26)	3,39 (0,11–17,65)	0,842

Reikšmės pateikiamos kaip medianos (tarpkvartiliniai pločiai). ΔTTP – laiko iki piko skirtumas tarp nesukaulėjusios skydinės kremzlės ir naviko; ΔPI – pikinio intensyvumo skirtumas tarp nesukaulėjusios skydinės kremzlės ir naviko; ΔAUC – ploto po kreive skirtumas tarp nesukaulėjusios skydinės kremzlės ir naviko; ΔWIS – įtekėjimo greičio skirtumas tarp nesukaulėjusios skydinės kremzlės ir naviko.

3.4.3. Naviko išplitimo į nesukaulėjusią skydinę kremzlę logistinės regresijos analizė

Statistiškai reikšmingų LIK parametrų logistinės regresijos analizės rezultatai, vertinant naviko išplitimą į nesukaulėjusios skydinę kremzlę, pateikiami 3.4.3.1 lentelėje.

Atliekant vienmatę logistinės regresijos analizę nustatyta, kad visi LIK parametrai, išskyrus ΔPI, statistiškai reikšmingai susiję su naviko išplitimu į nesukaulėjusią skydinę kremzlę. Ilgesnis TTP (ŠS = 0,84; 95 proc. PI – 0,73–0,97) ir ΔTTP (ŠS = 0,76; 95 proc. PI – 0,60–0,96) laikas buvo susiję su mažesne išplitimo tikimybe, t. y. ilgesnis laikas iki pikinio kontrasto sustiprėjimo susijęs su naviko išplitimo nebuvimu. ΔAUC taip pat buvo statistiškai reikšmingai susijęs su naviko išplitimu (ŠS = 0,99; 95 proc. PI – 0,98–1,00). Didesnės PI (ŠS = 1,81; 95 proc. PI – 1,14–2,92) ir AUC (ŠS = 1,04; 95 proc. PI – 1,00–1,08) reikšmės buvo statistiškai reikšmingai susijusios su naviko išplitimu į nesukaulėjusią skydinę kremzlę.

Atliekant daugiamatę dvejetainę logistinės regresijos analizę sudaryti keturi modeliai, siekiant įvertinti dviejų kombinuotų parametrų prognostinę vertę. Sujungus LIK parametrus ir jų išvestinius skirtumus (Δ), nebuvo nei vieno modelio, kurio abu parametrai būtų statistiškai reikšmingi. Keturiuose modeliuose nustatytas tik vienas statistiškai reikšmingas kiekybinis parametras:

- **1 modelis (PI + ΔAUC)**: PI išliko nepriklausomu naviko išplitimo prognostiniu rodikliu (ŠS = 1,74; 95 proc. PI – 1,01–2,99; p = 0,046).
- **2 modelis (PI + ΔPI)**: PI išliko statistiškai reikšmingu prognostiniu rodikliu (ŠS = 1,55; 95 proc. PI – 1,06–2,27; p = 0,026).
- **3 modelis (TTP + ΔPI)**: TTP išlaikė ribinį statistinį reikšmingumą (ŠS = 0,87; 95 proc. PI – 0,76–1,00; p = 0,048).
- **4 modelis (ΔTTP + ΔPI)**: ΔTTP išliko reikšmingu neigiamu prognostiniu rodikliu (ŠS = 0,78; 95 proc. PI – 0,61–0,99; p = 0,038).

3.4.4. LIK parametrų ir jų derinių ROC analizė

Remiantis LIK kiekybinių parametrų analize, net keli kiekybiniai parametrai parodė reikšmingai aukštą diagnostinę vertę diferencijuojant tarp nesukaulėjusios skydinės kremzlės su naviko išplitimu ir be jo. Pagal didžiausią Judeno indeksą nustatytos parametrų optimalios ribinės vertės, prognozuojant naviko išplitimą į nesukaulėjusią skydinę kremzlę, pateikiamos 3.4.4.1 lentelėje. Mažesnės TTP (≤ 36,6 s), ΔTTP (≤ 9,6 s), ΔPI (≤ 5,15 dB) ir ΔAUC (≤ 116,29 dB × s) reikšmės bei didesnės PI (≥ 5,51 dB) ir AUC (≥ 82,78 dB × s) reikšmės buvo susijusios su naviko išplitimu į nesikaulėjusią skydinę kremzlę.

3.4.4.1 lentelė. *LIK parametrų diagnostinis efektyvumas, prognozuojant naviko išplitimą į nesukaulėjusią skydinę kremzlę*

Parametras	AUROC, (95 proc. PI)	Jautrumas, proc. (95 proc. PI)	Specifiš-kumas, proc. (95 proc. PI)	Tikslumas, proc. (95 proc. PI)	Ribinė reikšmė	p
Vienmačiai modeliai						
TTP	0,86 (0,63–1,09)	87,5 (47,4–99,7)	92,3 (74,9–99,1)	91,2 (76,3–98,1)	36,6 s	0,002
PI	0,87 (0,66–1,08)	87,5 (47,4–99,7)	92,0 (74,0–99,0)	90,9 (75,7–98,1)	5,51 dB	0,001
AUC	0,85 (0,68–1,02)	62,5 (24,5–91,5)	100,0 (86,3–100,0)	90,9 (75,7–98,1)	82,78 dB × s	< 0,001
ΔTTP	0,91 (0,81–1,01)	100,0 (63,1–100,0)	76,9 (56,4–91,0)	82,3 (65,5–93,2)	9,6 s	< 0,001
ΔPI	0,79 (0,55–1,03)	75,0 (34,9–96,8)	92,0 (74,0–99,0)	87,9 (71,8–96,6)	5,15 dB	0,018
ΔAUC	0,78 (0,60–0,97)	62,5 (24,5–91,5)	91,3 (72,0–98,9)	83,9 (66,3–94,6)	116,29 dB × s	0,002
Daugiamačiai modeliai						
1 modelis (PI + ΔAUC)	0,88 (0,69–1,06)	75,0 (34,9–96,8)	100,0 (85,2–100,0)	93,6 (78,6–99,2)	–	< 0,001
2 modelis (PI + ΔPI)	0,94 (0,80–1,07)	87,5 (47,4–99,7)	100,0 (86,3–100,0)	97,0 (84,2–99,9)	–	< 0,001
3 modelis (TTP + ΔPI)	0,79 (0,57–1,01)	62,5 (24,5–91,5)	92,0 (74,0–99,0)	84,9 (68,1–94,9)	–	0,009
4 modelis (ΔTTP + ΔPI)	0,79 (0,57–1,01)	62,5 (24,5–91,5)	92,0 (74,0–99,0)	84,9 (68,1–94,9)	–	0,009

TTP – laikas iki piko; PI – pikinis intensyvumas AUC – plotas po kreive; ΔTTP – laiko iki piko skirtumas tarp nesukaulėjusios skydinės kremzlės ir naviko; ΔPI – pikinio intensyvumo skirtumas tarp nesukaulėjusios skydinės kremzlės ir naviko; ΔAUC – ploto po kreive skirtumas tarp nesukaulėjusios skydinės kremzlės ir naviko; AUROC – plotas po ROC kreive.

Atliekant vienmatę analizę, ΔTTP pasižymėjo didžiausia diskriminacine geba (AUROC = 0,91; p < 0,001) – 100,0 proc. jautrumas, 76,9 proc. specifiškumas ir 82,3 proc. bendras tikslumas. PI parametras taip pat pasižymėjo aukštu diagnostiniu efektyvumu (AUROC = 0,87; p = 0,001) – 87,5 proc. jautrumas, 92,0 proc. specifiškumas, 90,9 proc. bendras tikslumas. AUC parametras taip pat pasiekė gana aukštą diagnostinę vertę (AUROC = 0,85; p < 0,001) – 100 proc. specifiškumas, esant nustatytai ribinei vertei. ΔAUC (AUROC = 0,78; p = 0,002) ir ΔPI (AUROC = 0,79; p = 0,018) taip pat suteikė statistiškai reikšmingos diagnostinės informacijos, nors jų diagnostinė geba buvo šiek tiek mažesnė.

Daugiamačiuose modeliuose PI ir ΔPI derinys (2 modelis) parodė didžiausią diskriminacinę gebą (AUROC = 0,94; p < 0,001), pasiekdamas 87,5 proc. jautrumą, 100 proc. specifiškumą ir 97,0 proc. bendrą tikslumą. 1 modelis (PI + ΔAUC) taip pat pasižymėjo gera, tačiau mažesne nei 2 modelio diskriminacine geba (AUROC = 0,88; p < 0,001), pasiekdamas 100 proc. specifiškumą ir 93,6 proc. tikslumą. 3 (TTP + ΔPI) ir 4 (ΔTTP + ΔPI) modeliai rodė mažesnę diagnostinę gebą (AUROC = 0,79; p = 0,009).

Visų analizuotų parametrų diagnostinė vertė, nustatant naviko išplitimą į nesukaulėjusią skydinę kremzlę, buvo statistiškai reikšminga (p < 0,05). 3.4.4.1 pav. ir 3.4.4.2 pav. rodo LIK parametrų ROC kreivių analizę, vertinant naviko išplitimą į nesukaulėjusią skydinę kremzlę.

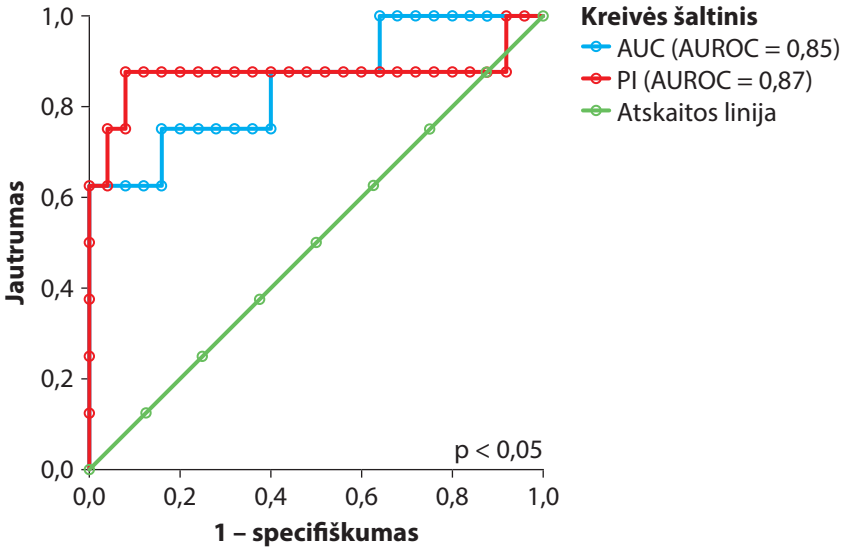

3.4.4.1 pav. *LIK parametrų (AUC ir PI) ROC (angl. receiver operating characteristic) kreivių analizė, vertinant naviko išplitimą į nesukaulėjusią skydinę kremzlę*

PI – pikinis intensyvumas; AUC – plotas po kreive.

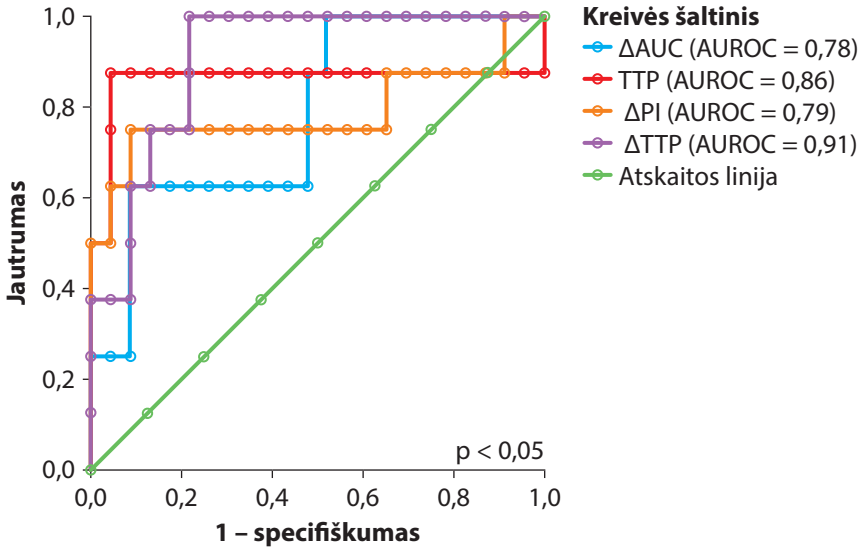

3.4.4.2 pav. *LIK parametrų (ΔAUC, TTP, ΔPI ir ΔTTP) ROC (angl. receiver operating characteristic) kreivių analizė, vertinant naviko išplitimą į nesukaulėjusią skydinę kremzlę*

TTP – laikas iki piko; ΔTTP – laiko iki piko skirtumas tarp nesukaulėjusios skydinės kremzlės ir naviko; ΔPI – pikinio intensyvumo skirtumas tarp nesukaulėjusios skydinės kremzlės ir naviko; ΔAUC – ploto po kreive skirtumas tarp nesukaulėjusios skydinės kremzlės ir naviko.

IŠVADOS

1. Kokybinis (vizualinis) KUT, vertinant gerklų karcinomos išplitimą į nesukaulėjusią skydinę kremzlę, pasižymėjo aukštu specifiškumu (86,2 proc.) ir jautrumu (88,9 proc.) bei reikšmingai nesiskyrė nuo pooperacinio histopatologinio tyrimo duomenų ($p > 0,05$).
2. KUT derinimas su KT ir ypač su MRT didina diagnostinę vertę, nustatant gerklų karcinomos išplitimą į nesukaulėjusią skydinę kremzlę, gerinant diagnostinį specifiškumą bei tikslumą.
3. KUT kiekybiniai parametrai (TTP, PI, AUC) ir jų skirtumo parametrai tarp kremzlės ir naviko (ΔPI, ΔAUC ir ypač ΔTTP) leidžia patikimai ($p < 0,05$) patvirtinti arba paneigti gerklų karcinomos išplitimą į nesukaulėjusią skydinę kremzlę.
4. Didžiausia diagnostine geba tarp atskirų parametrų ir jų derinių, vertinant gerklų karcinomos išplitimą į nesukaulėjusią skydinę kremzlę, pasižymėjo PI ir ΔPI parametrų derinys (AUROC = 0,94).

PRAKTIKINĖS REKOMENDACIJOS

Šio tyrimo rezultatai rodo, kad KUT yra informatyvus ir lengvai prieinamas vaizdinimo metodas vertinant naviko išplitimą į nesukaulėjusią skydinę kremzlę pacientams, sergantiems gerklų plokščiųjų ląstelių karcinoma.

Klinikinėje praktikoje KUT rekomenduojama taikyti kaip papildomą radiologinį tyrimą kartu su KT ir (arba) MRT tais atvejais, kai po rutininio radiologinio tyrimo naviko išplitimas į nesukaulėjusią skydinę kremzlę išlieka abejotinas. Siekiant didesnio diagnostinio tikslumo ir patikimumo, nuo kurių priklauso optimalaus gydymo metodo ir apimties pasirinkimas, rekomenduojama taikyti tiek kokybinį, tiek kiekybinį KUT vertinimą.

Mokslinės perspektyvos atžvilgiu reikalingi tolesni šios srities tyrimai. Ateityje rekomenduojame apsvarstyti KT ir KUT vaizdų suliejimo galimybes, siekiant užtikrinti tikslesnį ir labiau standartizuotą dominančios srities nustatymą KUT tyrimuose.

REFERENCES

1. Gormley M, Creaney G, Schache A, Ingarfield K, Conway DI. Reviewing the epidemiology of head and neck cancer: definitions, trends and risk factors. Br Dent J. 2022 Nov;233(9):780–6. doi: 10.1038/s41415-022-5166-x. Epub 2022 Nov 11.
2. Park JO, Nam IC, Kim CS, Park SJ, Lee DH, Kim HB, Han KD, Joo YH. Sex Differences in the Prevalence of Head and Neck Cancers: A 10-Year Follow-Up Study of 10 Million Healthy People. Cancers (Basel). 2022 May 20;14(10):2521. doi: 10.3390/cancers14102521.
3. Doğan S, Vural A, Kahriman G, İmamoğlu H, Abdülrezzak Ü, Öztürk M. Non-squamous cell carcinoma diseases of the larynx: clinical and imaging findings. Braz J Otorhinolaryngol. 2020 Jul-Aug;86(4):468–82. doi: 10.1016/j.bjorl.2019.02.003. Epub 2019 Mar 16.
4. Zidar N, Thompson LDR, Agaimy A, Stenman G, Hellquist H, Nadal A, Mäkitie AA, López F, Strojan P, Ferlito A. The impact of histopathology on prognosis of squamous cell carcinoma of the larynx: can we do better? Virchows Arch. 2025 Jul;487(1):13-32. doi: 10.1007/s00428-025-04082-w. Epub 2025 Mar 27. Erratum in: Virchows Arch. 2025 Aug;487(2):483. doi: 10.1007/s00428-025-04186-3.
5. Choi YS, Park SG, Song EK, Cho SH, Park MR, Park KU, Lee KH, Song IC, Lee HJ, Jo DY, Kim S, Yun HJ; Korean South West Oncology Group (KSWOG) Investigators. Comparison of the therapeutic effects of total laryngectomy and a larynx-preservation approach in patients with T4a laryngeal cancer and thyroid cartilage invasion: A multicenter retrospective review. Head Neck. 2016 Aug;38(8):1271–7. doi: 10.1002/hed.24438. Epub 2016 Apr 4.
6. Connor S. Laryngeal cancer: how does the radiologist help? Cancer Imaging. 2007 May 28;7(1):93–103. doi: 10.1102/1470-7330.2007.0010.
7. Hermans R. Staging of laryngeal and hypopharyngeal cancer: value of imaging studies. Eur Radiol. 2006 Nov;16(11):2386–400. doi: 10.1007/s00330-006-0301-7. Epub 2006 May 30.
8. Shoushtari ST, Gal J, Chamorey E, Schiappa R, Dassonville O, Poissonnet G, et al. Salvage vs. Primary Total Laryngectomy in Patients with Locally Advanced Laryngeal or Hypopharyngeal Carcinoma: Oncologic Outcomes and Their Predictive Factors. J Clin Med. 2023;12(4):1305. DOI: 10.3390/jcm12041305.
9. Becker M, Monnier Y, de Vito C. MR Imaging of Laryngeal and Hypopharyngeal Cancer. Magn Reson Imaging Clin N Am. 2022 Feb;30(1):53–72. doi: 10.1016/j.mric.2021.08.002.
10. Deganello A, Ruaro A, Gualtieri T, Berretti G, Rampinelli V, Borsetto D, Russo S, Boscolo-Rizzo P, Ferrari M, Bussu F. Central Compartment Neck Dissection in Laryngeal and Hypopharyngeal Squamous Cell Carcinoma: Clinical Considerations. Cancers (Basel). 2023 Jan 28;15(3):804. doi: 10.3390/cancers15030804.
11. Junn JC, Soderlund KA, Glastonbury CM. Imaging of Head and Neck Cancer With CT, MRI, and US. Semin Nucl Med. 2021 Jan;51(1):3–12. doi: 10.1053/j.semnuclmed.2020.07.005.
12. Allegra E, Ferrise P, Trapasso S, Trapuzzano O, Barca A, Tamburrini S, et al. Early glottic cancer: Role of MRI in the preoperative staging. Biomed Res Int. 2014; 2014:890385. doi: 10.1155/2014/890385. Epub 2014 Aug 14

13. Elkholy SF, Kandeel MA, Hamela MAA, Asaad REI. Comparative Study between CT and MRI in Assessment of Laryngeal Cartilage Invasion in Laryngeal Carcinoma. Med. J. Cairo Univ. 2021 Jun; 89(3):873–880. Available from: https://www.medicaljournal-ofcairouniversity.net/images/pdf/2021/June/a03.pdf
14. Kuno H, Onaya H, Fujii S, Ojiri H, Otani K, Satake M. Primary staging of laryngeal and hypopharyngeal cancer: CT, MR imaging and dual-energy CT. Eur J Radiol. 2014 Jan;83(1):e23–35. doi: 10.1016/j.ejrad.2013.10.022. Epub 2013 Oct 27.
15. Castelijns JA, Hermans R, van den Brekel MW, Mukherji SK. Imaging of laryngeal cancer. Semin Ultrasound CT MR. 1998 Dec;19(6):492–504.
16. Becker M, Burkhardt K, Dulguerov P, Allal A. Imaging of the larynx and hypopharynx. Eur J Radiol. 2008 Jun;66(3):460–79. doi: 10.1016/j.ejrad.2008.03.027. Epub 2008 May 20.
17. Dadfar N, Seyyedi M, Forghani R, Curtin HD. Computed tomography appearance of normal nonossified thyroid cartilage: implication for tumor invasion diagnosis. J Comput Assist Tomogr. 2015 Mar-Apr;39(2):240–3. doi: 10.1097/RCT.0000000000000196.
18. Becker M, Zbären P, Casselman JW, Kohler R, Dulguerov P, Becker CD. Neoplastic invasion of laryngeal cartilage: reassessment of criteria for diagnosis at MR imaging. Radiology. 2008 Nov;249(2):551–9. doi: 10.1148/radiol.2492072183.
19. Dankbaar JW, Oosterbroek J, Jager EA, de Jong HW, Raaijmakers CP, Willems SM, Terhaard CH, Philippens ME, Pameijer FA. Detection of cartilage invasion in laryngeal carcinoma with dynamic contrast-enhanced CT. Laryngoscope Investig Otolaryngol. 2017 Oct 31;2(6):373–9. doi: 10.1002/lio2.114.
20. Li B, Bobinski M, Gandour-Edwards R, Farwell DG, Chen AM. Overstaging of cartilage invasion by multidetector CT scan for laryngeal cancer and its potential effect on the use of organ preservation with chemoradiation. Br J Radiol. 2011 Jan;84(997):64–9. doi: 10.1259/bjr/66700901.
21. Wegner I, Hooft L, Reitsma JB, Pameijer FA, de Bree R, Stegeman I. MRI versus CT for detecting cartilage invasion in patients with laryngeal and hypopharyngeal squamous cell carcinoma. Cochrane Database of Systematic Reviews. 2016;2016(4): CD012115. doi: 10.1002/14651858.CD012115.
22. Citil S, Dogan S, Atilgan HI, Menzilcioglu MS, Sahin T, Abdulrezzak U, Duymus M, Ozturk M. Comparison of Dynamic Contrast-Enhanced MRI and PET/CT in the Evaluation of Laryngeal Cancer After Inadequate CT Results. Pol J Radiol. 2015 Sep 13;80:428–32. doi: 10.12659/PJR.895041.
23. Mohamad I, Hejleh TA, Qandeel M, Al-Hussaini M, Koro S, Taqash A, Almousa A, Abuhijla F, Abuhijlih R, Ajlouni F, Al-Ibraheem A, Laban DA, Hussein T, Mayta E, Al-Gargaz W, Hosni A. Concordance between head and neck MRI and histopathology in detecting laryngeal subsite invasion among patients with laryngeal cancer. Cancer Imaging. 2023 Oct 19;23(1):99. doi: 10.1186/s40644-023-00618-y.
24. Sidhu PS, Cantisani V, Dietrich CF, Gilja OH, Saftoiu A, Bartels E, Bertolotto M, Calliada F, Clevert DA, Cosgrove D, Deganello A, D'Onofrio M, Drudi FM, Freeman S, Harvey C, Jenssen C, Jung EM, Klauser AS, Lassau N, Meloni MF, Leen E, Nicolau C, Nolsoe C, Piscaglia F, Prada F, Prosch H, Radzina M, Savelli L, Weskott HP, Wijkstra H. The EFSUMB Guidelines and Recommendations for the Clinical Practice of Contrast-Enhanced Ultrasound (CEUS) in Non-Hepatic Applications: Update 2017 (Long Version). Ultraschall Med. 2018 Apr;39(2):e2–e44. English. doi: 10.1055/a-0586-1107. Epub 2018 Mar 6.

25. Dietrich CF, Nolsøe CP, Barr RG, Berzigotti A, Burns PN, Cantisani V, Chammas MC, Chaubal N, Choi BI, Clevert DA, Cui X, Dong Y, D'Onofrio M, Fowlkes JB, Gilja OH, Huang P, Ignee A, Jenssen C, Kono Y, Kudo M, Lassau N, Lee WJ, Lee JY, Liang P, Lim A, Lyshchik A, Meloni MF, Correas JM, Minami Y, Moriyasu F, Nicolau C, Piscaglia F, Saftoiu A, Sidhu PS, Sporea I, Torzilli G, Xie X, Zheng R. Guidelines and Good Clinical Practice Recommendations for Contrast-Enhanced Ultrasound (CEUS) in the Liver-Update 2020 WFUMB in Cooperation with EFSUMB, AFSUMB, AIUM, and FLAUS. Ultrasound Med Biol. 2020 Oct;46(10):2579–604. doi: 10.1016/j.ultrasmedbio.2020.04.030.
26. Petrasova H, Slaisova R, Rohan T, Stary K, Kyclova J, Pavlik T, Kovalcikova P, Kazda T, Valek V. Contrast-Enhanced Ultrasonography for Differential Diagnosis of Benign and Malignant Thyroid Lesions: Single-Institutional Prospective Study of Qualitative and Quantitative CEUS Characteristics. Contrast Media Mol Imaging. 2022 Apr 23;2022:8229445. doi: 10.1155/2022/8229445.
27. Wu M, Hu Y, Hang J, Peng X, Mao C, Ye X, et al. Qualitative and Quantitative Contrast-Enhanced Ultrasound Combined with Conventional Ultrasound for Predicting the Malignancy of Soft Tissue Tumors. Ultrasound Med Biol. 2022 Feb 1;48(2):237–47.
28. Badiu SM, Gheorghe EC, Nicolau C, Săftoiu A. Quantitative time intensity curve analysis of contrast-enhanced ultrasound (CEUS) examinations for the assessment of focal liver lesions. Med Ultrason. 2024 Mar 27;26(1):63–71. doi: 10.11152/mu-4108. Epub 2023 Nov 6.
29. Schwarz S, Clevert DA, Ingrisch M, Geyer T, Schwarze V, Rübenthaler J, Armbruster M. Quantitative Analysis of the Time-Intensity Curve of Contrast-Enhanced Ultrasound of the Liver: Differentiation of Benign and Malignant Liver Lesions. Diagnostics (Basel). 2021 Jul 12;11(7):1244. doi: 10.3390/diagnostics11071244.
30. Jokisch F, Buchner A, Schulz GB, Grimm T, Weinhold P, Pfitzinger PL, Chaloupka M, Stief CG, Schlenker B, Clevert DA. Prospective evaluation of 4-D contrast-enhanced-ultrasound (CEUS) imaging in bladder tumors. Clin Hemorheol Microcirc. 2020;74(1):1–12. doi: 10.3233/CH-199231.
31. Strobel D, Jung EM, Ziesch M, Praktiknjo M, Link A, Dietrich CF, et al. Real-life assessment of standardized contrast-enhanced ultrasound (CEUS) and CEUS algorithms (CEUS LI-RADS®/ESCULAP) in hepatic nodules in cirrhotic patients – a prospective multicenter study. Eur Radiol. 2021 Oct 1;31(10):7614–25. doi: 10.1007/s00330-021-07872-3. Epub 2021 Apr 15.
32. Chen L, Chen L, Liu J, Wang B, Zhang H. Value of Qualitative and Quantitative Contrast-Enhanced Ultrasound Analysis in Preoperative Diagnosis of Cervical Lymph Node Metastasis From Papillary Thyroid Carcinoma. J Ultrasound Med. 2020 Jan;39(1):73–81. doi: 10.1002/jum.15074. Epub 2019 Jun 20.
33. Li QL, Ma T, Wang ZJ, Huang L, Liu W, Chen M, Sang T, Ren XG, Tong J, Cao CL, Dong J, Li J. The value of contrast-enhanced ultrasound for the diagnosis of metastatic cervical lymph nodes of papillary thyroid carcinoma: A systematic review and meta-analysis. J Clin Ultrasound. 2022 Jan;50(1):60–9. doi: 10.1002/jcu.23073. Epub 2021 Oct 8.
34. Bartolotta TV, Terranova MC, Gagliardo C, Taibbi A. CEUS LI-RADS: a pictorial review. Insights Imaging. 2020 Feb 4;11(1):9. doi: 10.1186/s13244-019-0819-2.
35. Sorrenti S, Dolcetti V, Fresilli D, Del Gaudio G, Pacini P, Huang P, Camponovo C, Leoncini A, D'Andrea V, Pironi D, Frattaroli F, Trimboli P, Radzina M, Cantisani V. The Role of CEUS in the Evaluation of Thyroid Cancer: From Diagnosis to Local Staging. J Clin Med. 2021 Sep 30;10(19):4559. doi: 10.3390/jcm10194559.

36. Tufano A, Rosati D, Moriconi M, Santarelli V, Canale V, Salciccia S, Sciarra A, Franco G, Cantisani V, Di Pierro GB. Diagnostic Accuracy of Contrast-Enhanced Ultrasound (CEUS) in the Detection of Muscle-Invasive Bladder Cancer: A Systematic Review and Diagnostic Meta-Analysis. Curr Oncol. 2024 Feb 1;31(2):818–27. doi: 10.3390/curroncol31020060.
37. Sultan SR, AlKharaiji M, Rajab SH. Diagnosis of parotid gland tumours with Contrast-Enhanced Ultrasound: a systematic review and meta-analysis. Med Ultrason. 2022 May 25;24(2):211–8. doi: 10.11152/mu-3119. Epub 2021 Jul 21.
38. Umlauf D, Frank S, Pap T, Bertrand J. Cartilage biology, pathology, and repair. Cell Mol Life Sci. 2010 Dec;67(24):4197–211. doi: 10.1007/s00018-010-0498-0. Epub 2010 Aug 25.
39. Claassen H, Schicht M, Sel S, Paulsen F. Special pattern of endochondral ossification in human laryngeal cartilages: X-ray and light-microscopic studies on thyroid cartilage. Clin Anat. 2014 Apr;27(3):423–30. doi: 10.1002/ca.22309. Epub 2014 Feb 4.
40. Nossin Y, Farrell E, Koevoet WJLM, Datema F, Somoza RA, Caplan AI, van Osch GJVM. The Releasate of Avascular Cartilage Demonstrates Inherent Pro-Angiogenic Properties In Vitro and In Vivo. Cartilage. 2021 Dec;13(2_suppl):559S–570S. doi: 10.1177/19476035211047628. Epub 2021 Sep 30.
41. Hu Q, Zhu SY, Liu RC, Zheng HY, Lun HM, Wei HM, Weng JJ. Contrast-enhanced ultrasound for the preoperative assessment of laryngeal carcinoma: a preliminary study. Acta Radiol. 2021 Aug;62(8):1016–24. doi: 10.1177/0284185120950108. Epub 2020 Aug 18.
42. Agnello F, Cupido F, Sparacia G, Midiri F, Miroddi M, Grassedonio E, Galia M. Computerised tomography and magnetic resonance imaging of laryngeal squamous cell carcinoma: A practical approach. Neuroradiol J. 2017 Jun;30(3):197–204. doi: 10.1177/1971400916689373. Epub 2017 Feb 20.
43. Vishwanath V, Jafarieh S, Rembielak A. The role of imaging in head and neck cancer: An overview of different imaging modalities in primary diagnosis and staging of the disease. J Contemp Brachytherapy. 2020 Oct;12(5):512–8. doi: 10.5114/jcb.2020.100386. Epub 2020 Oct 30.
44. Itamura K, Hsue VB, Barbu AM, Chen MM. Diagnostic Assessment (Imaging) and Staging of Laryngeal Cancer. Otolaryngol Clin North Am. 2023 Apr;56(2):215–31. doi: 10.1016/j.otc.2022.12.006.
45. Cho SJ, Lee JH, Suh CH, Kim JY, Kim D, Lee JB, Lee MK, Chung SR, Choi YJ, Baek JH. Comparison of diagnostic performance between CT and MRI for detection of cartilage invasion for primary tumor staging in patients with laryngo-hypopharyngeal cancer: a systematic review and meta-analysis. Eur Radiol. 2020 Jul;30(7):3803–12. doi: 10.1007/s00330-020-06718-8. Epub 2020 Mar 9.
46. Becker M, Zbären P, Delavelle J, Kurt AM, Egger C, Rüfenacht DA, Terrier F. Neoplastic invasion of the laryngeal cartilage: reassessment of criteria for diagnosis at CT. Radiology. 1997 May;203(2):521–32. doi: 10.1148/radiology.203.2.9114116.
47. Jensen EC. Technical review, types of imaging, part 4 – magnetic resonance imaging. Anat Rec (Hoboken). 2014 Jun;297(6):973–8. doi: 10.1002/ar.22927. Epub 2014 Apr 19.
48. Hintze JM, Cleere E, Griffin J, O'Riordan I, Timon C, Kinsella J, Fitzgerald C, Lennon P. Primary Site Influences the Ability of Magnetic Resonance Imaging to Assess Cartilage Invasion in Advanced Laryngeal Cancer. Laryngoscope. 2025 Feb;135(2):723–8. doi: 10.1002/lary.31822. Epub 2024 Oct 5.

49. Juliano A, Moonis G. Computed Tomography Versus Magnetic Resonance in Head and Neck Cancer: When to Use What and Image Optimization Strategies. Magn Reson Imaging Clin N Am. 2018 Feb;26(1):63–84. doi: 10.1016/j.mric.2017.08.005. Epub 2017 Oct 18.
50. Razek AA, Tawfik AM, Elsorogy LG, Soliman NY. Perfusion CT of head and neck cancer. Eur J Radiol. 2014 Mar;83(3):537–44. doi: 10.1016/j.ejrad.2013.12.008. Epub 2013 Dec 16.
51. Faggioni L, Neri E, Bartolozzi C. CT perfusion of head and neck tumors: how we do it. AJR Am J Roentgenol. 2010 Jan;194(1):62–9. doi: 10.2214/ajr.09.3187.
52. Preda L, Calloni SF, Moscatelli ME, Cossu Rocca M, Bellomi M. Role of CT perfusion in monitoring and prediction of response to therapy of head and neck squamous cell carcinoma. Biomed Res Int. 2014;2014:917150. doi: 10.1155/2014/917150. Epub 2014 Jul 21.
53. Trojanowska A, Trojanowski P, Drop A, Jargiełło T, Klatka J. Head and neck cancer: value of perfusion CT in depicting primary tumor spread. Med Sci Monit. 2012 Feb;18(2):CR112–118. doi: 10.12659/msm.882466.
54. Forghani R. An update on advanced dual-energy CT for head and neck cancer imaging. Expert Rev Anticancer Ther. 2019 Jul;19(7):633–44. doi: 10.1080/14737140.2019.1626234. Epub 2019 Jun 21.
55. Roele ED, Timmer VCML, Vaassen LAA, van Kroonenburgh AMJL, Postma AA. Dual-Energy CT in Head and Neck Imaging. Curr Radiol Rep. 2017;5(5):19. doi: 10.1007/s40134-017-0213-0. Epub 2017 Mar 29.
56. Sodickson AD, Keraliya A, Czakowski B, Primak A, Wortman J, Uyeda JW. Dual energy CT in clinical routine: how it works and how it adds value. Emerg Radiol. 2021 Feb;28(1):103–17. doi: 10.1007/s10140-020-01785-2. Epub 2020 Jun 1.
57. Tunlayadechanont P, Sananmuang T. Dual-energy CT in head and neck applications. Neuroradiol J. 2025 Oct;38(5):543–52. doi: 10.1177/19714009251313507. Epub 2025 Jan 8.
58. Sananmuang T, Agarwal M, Maleki F, Muthukrishnan N, Marquez JC, Chankowsky J, Forghani R. Dual Energy Computed Tomography in Head and Neck Imaging: Pushing the Envelope. Neuroimaging Clin N Am. 2020 Aug;30(3):311–23. doi: 10.1016/j.nic.2020.04.003. Epub 2020 Jun 10.
59. Forghani R, Levental M, Gupta R, Lam S, Dadfar N, Curtin HD. Different spectral hounsfield unit curve and high-energy virtual monochromatic image characteristics of squamous cell carcinoma compared with nonossified thyroid cartilage. AJNR Am J Neuroradiol. 2015 Jun;36(6):1194–200. doi: 10.3174/ajnr.A4253. Epub 2015 Mar 5.
60. Kuno H, Onaya H, Iwata R, Kobayashi T, Fujii S, Hayashi R, et al. Evaluation of cartilage invasion by laryngeal and hypopharyngeal squamous cell carcinoma with dual-energy CT. Radiology. 2012 Nov;265(2):488–96. doi: 10.1148/radiol.12111719. Epub 2012 Sep 14.
61. Kuno H, Sakamaki K, Fujii S, Sekiya K, Otani K, Hayashi R, Yamanaka T, Sakai O, Kusumoto M. Comparison of MR Imaging and Dual-Energy CT for the Evaluation of Cartilage Invasion by Laryngeal and Hypopharyngeal Squamous Cell Carcinoma. AJNR Am J Neuroradiol. 2018 Mar;39(3):524–31. doi: 10.3174/ajnr.A5530. Epub 2018 Jan 25.
62. Petralia G, Summers PE, Agostini A, Ambrosini R, Cianci R, Cristel G, Calistri L, Colagrande S. Dynamic contrast-enhanced MRI in oncology: how we do it. Radiol Med. 2020 Dec;125(12):1288–300. doi: 10.1007/s11547-020-01220-z. Epub 2020 May 15.

63. Khalifa F, Soliman A, El-Baz A, Abou El-Ghar M, El-Diasty T, Gimel'farb G, Ouseph R, Dwyer AC. Models and methods for analyzing DCE-MRI: a review. Med Phys. 2014 Dec;41(12):124301. doi: 10.1118/1.4898202.
64. Huang B, Wong CS, Whitcher B, Kwong DL, Lai V, Chan Q, Khong PL. Dynamic contrast-enhanced magnetic resonance imaging for characterising nasopharyngeal carcinoma: comparison of semiquantitative and quantitative parameters and correlation with tumour stage. Eur Radiol. 2013 Jun;23(6):1495–502. doi: 10.1007/s00330-012-2740-7. Epub 2013 Feb 2.
65. Karabay N, Bülbül HM, Doğan E, İkiz AÖ, Bülbül G, Sarıoğlu S. The correlations between dynamic contrast enhanced magnetic resonance imaging and immunohistochemical data in head and neck squamous cell carcinomas. Turk J Med Sci. 2022 Dec;52(6):1950–7. doi: 10.55730/1300-0144.5543. Epub 2022 Dec 21.
66. Baba A, Kurokawa R, Rawie E, Kurokawa M, Ota Y, Srinivasan A. Normalized Parameters of Dynamic Contrast-Enhanced Perfusion MRI and DWI-ADC for Differentiation between Posttreatment Changes and Recurrence in Head and Neck Cancer. AJNR Am J Neuroradiol. 2022 Aug;43(8):1184–9. doi: 10.3174/ajnr.A7567. Epub 2022 Jul 14.
67. Yu J, Xu W, Wang L, Jiang N, Dou W, Li C, Sun L. The clinical value of DCE-MRI for differentiating secondary laryngeal cartilage lesions. Medicine (Baltimore). 2023 Mar 31;102(13):e33352. doi: 10.1097/MD.0000000000033352.
68. Zheng D, Chen Y, Chen Y, Xu L, Chen W, Yao Y, Du Z, Deng X, Chan Q. Dynamic contrast-enhanced MRI of nasopharyngeal carcinoma: a preliminary study of the correlations between quantitative parameters and clinical stage. J Magn Reson Imaging. 2014 Apr;39(4):940–8. doi: 10.1002/jmri.24249. Epub 2013 Sep 24.
69. Dietrich CF, Averkiou M, Nielsen MB, Barr RG, Burns PN, Calliada F, Cantisani V, Choi B, Chammas MC, Clevert DA, Claudon M, Correas JM, Cui XW, Cosgrove D, D'Onofrio M, Dong Y, Eisenbrey J, Fontanilla T, Gilja OH, Ignee A, Jenssen C, Kono Y, Kudo M, Lassau N, Lyshchik A, Franca Meloni M, Moriyasu F, Nolsøe C, Piscaglia F, Radzina M, Saftoiu A, Sidhu PS, Sporea I, Schreiber-Dietrich D, Sirlin CB, Stanczak M, Weskott HP, Wilson SR, Willmann JK, Kim TK, Jang HJ, Vezeridis A, Westerway S. How to perform Contrast-Enhanced Ultrasound (CEUS). Ultrasound Int Open. 2018 Jan;4(1):E2–E15. doi: 10.1055/s-0043-123931. Epub 2018 Feb 7.
70. Barr RG, Wilson SR, Lyshchik A, McCarville B, Darge K, Grant E, Robbin M, Wilmann JK, Chong WK, Fleischer A, Paltiel HJ. Contrast-enhanced Ultrasound-State of the Art in North America: Society of Radiologists in Ultrasound White Paper. Ultrasound Q. 2020 Sep;36(4S Suppl 1):S1–S39. doi: 10.1097/RUQ.0000000000000515.
71. Tang MX, Mulvana H, Gauthier T, Lim AK, Cosgrove DO, Eckersley RJ, Stride E. Quantitative contrast-enhanced ultrasound imaging: a review of sources of variability. Interface Focus. 2011 Aug 6;1(4):520–39. doi: 10.1098/rsfs.2011.0026. Epub 2011 May 18.
72. Claudon M, Dietrich CF, Choi BI, Cosgrove DO, Kudo M, Nolsøe CP, Piscaglia F, Wilson SR, Barr RG, Chammas MC, Chaubal NG, Chen MH, Clevert DA, Correas JM, Ding H, Forsberg F, Fowlkes JB, Gibson RN, Goldberg BB, Lassau N, Leen EL, Mattrey RF, Moriyasu F, Solbiati L, Weskott HP, Xu HX. Guidelines and good clinical practice recommendations for contrast enhanced ultrasound (CEUS) in the liver – update 2012: a WFUMB-EFSUMB initiative in cooperation with representatives of AFSUMB, AIUM, ASUM, FLAUS and ICUS. Ultraschall Med. 2013 Feb;34(1):11–29. doi: 10.1055/s-0032-1325499. Epub 2012 Nov 5.

73. Jung EM, Weber MA, Wiesinger I. Contrast-enhanced ultrasound perfusion imaging of organs. Radiologe. 2021 Dec;61(Suppl 1):19–28. doi: 10.1007/s00117-021-00891-7. Epub 2021 Aug 10.
74. Peniaeva EI, Sencha AN, Pomortsev AV, Timofeyeva LA, Patrunov YN, Sencha EA. Technique of CEUS and data analysis. In: Contrast-Enhanced Ultrasound: From Simple to Complex. Springer International Publishing; 2022. p. 21–34. Available from: https://link.springer.com/chapter/10.1007/978-3-030-91764-7_3
75. Claudon M, Cosgrove D, Albrecht T, Bolondi L, Bosio M, Calliada F, Correas JM, Darge K, Dietrich C, D'Onofrio M, Evans DH, Filice C, Greiner L, Jäger K, Jong Nd, Leen E, Lencioni R, Lindsell D, Martegani A, Meairs S, Nolsøe C, Piscaglia F, Ricci P, Seidel G, Skjoldbye B, Solbiati L, Thorelius L, Tranquart F, Weskott HP, Whittingham T. Guidelines and good clinical practice recommendations for contrast enhanced ultrasound (CEUS) – update 2008. Ultraschall Med. 2008 Feb;29(1):28–44. doi: 10.1055/s-2007-963785.
76. Dietrich CF, Albrecht T, Becher H, Harvey CJ, Jenssen C, Lim AK, Möller K, Greis C. History of contrast enhanced ultrasound (CEUS). Med Ultrason. 2024 Dec 19;26(4): 405–16. doi: 10.11152/mu-4366. Epub 2024 Apr 26.
77. Zhang Q, Liang X, Zhang Y, Nie H, Chen Z. A review of contrast-enhanced ultrasound using SonoVue® and Sonazoid™ in non-hepatic organs. Eur J Radiol. 2023 Oct;167:111060. doi: 10.1016/j.ejrad.2023.111060. Epub 2023 Aug 22.
78. Albrecht T, Blomley M, Bolondi L, Claudon M, Correas JM, Cosgrove D, Greiner L, Jäger K, Jong ND, Leen E, Lencioni R, Lindsell D, Martegani A, Solbiati L, Thorelius L, Tranquart F, Weskott HP, Whittingham T; EFSUMB Study Group. Guidelines for the use of contrast agents in ultrasound. January 2004. Ultraschall Med. 2004 Aug;25(4):249–56. doi: 10.1055/s-2004-813245.
79. Shang Y, Xie X, Luo Y, Nie F, Luo Y, Jing X, Liao J, Zheng R, Wu R, Luo X, Chen Z, Xu Y, Zhang R, Wang H, Yuan J, Zhang H, Zhu J, Zhang W, Ruan L, Yang M, Li Z, Luo H, Chen Q, Yan J, Tang C, Liu D, Fang K, Guo Y, He W. Safety findings after intravenous administration of sulfur hexafluoride microbubbles to 463,434 examinations at 24 centers. Eur Radiol. 2023 Feb;33(2):988–95. doi: 10.1007/s00330-022-09108-4. Epub 2022 Oct 7.
80. Rogalska M, Antkowiak L, Kasperczuk A, Scierski W. Contrast-Enhanced Ultrasound in the Differentiation between the Most Common Benign Parotid Gland Tumors: A Systematic Review and Meta-Analysis. J Clin Med. 2022 Dec 12;11(24):7360. doi: 10.3390/jcm11247360.
81. Pucėtaitė M, Farina D, Ryškienė S, Mitraitė D, Tarasevičius R, Lukoševičius S, Padervinskis E, Vaitkus S. The Diagnostic Value of CEUS in Assessing Non-Ossified Thyroid Cartilage Invasion in Patients with Laryngeal Squamous Cell Carcinoma. J Clin Med. 2024 Feb 3;13(3):891. doi: 10.3390/jcm13030891.
82. Turco S, Frinking P, Wildeboer R, Arditi M, Wijkstra H, Lindner JR, Mischi M. Contrast-Enhanced Ultrasound Quantification: From Kinetic Modeling to Machine Learning. Ultrasound Med Biol. 2020 Mar;46(3):518–43. doi: 10.1016/j.ultrasmedbio.2019.11.008. Epub 2020 Jan 8.
83. Cantisani V, Di Leo N, David E, Clevert DA. Role of CEUS in Vascular Pathology. Ultraschall Med. 2021 Aug;42(4):348–66. English. doi: 10.1055/a-1403-2400. Epub 2021 Apr 29.

84. Janu E, Krikavova L, Little J, Dvorak K, Brancikova D, Jandakova E, Pavlik T, Kovalcikova P, Kazda T, Valek V. Prospective evaluation of contrast-enhanced ultrasound of breast BI-RADS 3–5 lesions. BMC Med Imaging. 2020 Jun 17;20(1):66. doi: 10.1186/s12880-020-00467-2.
85. Tang J, He W, Zhang Y, Tang Q, He N, Liang Z, Li S. Extracorporeal high-frequency combined with contrast-enhanced ultrasound: a novel imaging method for detection and treatment evaluation of patients with cervical trachea-associated relapsing polychondritis. Ann Transl Med. 2021 Dec;9(24):1785. doi: 10.21037/atm-21-6175.
86. Wakonig KM, Lerchbaumer MH, Dommerich S, Olze H, Hamm B, Fischer T, Arens P. Assessment of Parotid Gland Tumors by Means of Quantitative Multiparametric Ultrasound (mpUS). Diagnostics (Basel). 2022 Dec 21;13(1):12. doi: 10.3390/diagnostics13010012.
87. Welkoborsky HJ, Albers M, Küstermeyer J. Perfusion analysis of benign parotid gland tumors by contrast-enhanced ultrasonography (CEUS). Eur Arch Otorhinolaryngol. 2022 Aug;279(8):4137–46. doi: 10.1007/s00405-022-07303-z. Epub 2022 Mar 1.
88. Hunt D, Romero J. Contrast-Enhanced Ultrasound. Magn Reson Imaging Clin N Am. 2017 Nov;25(4):725–36. doi: 10.1016/j.mric.2017.06.004.
89. Ajmal S. Contrast-Enhanced Ultrasonography: Review and Applications. Cureus. 2021 Sep 24;13(9):e18243. doi: 10.7759/cureus.18243.
90. D'Onofrio M, Crosara S, De Robertis R, Canestrini S, Mucelli RP. Contrast-Enhanced Ultrasound of Focal Liver Lesions. AJR Am J Roentgenol. 2015 Jul;205(1):W56–66. doi: 10.2214/AJR.14.14203.
91. Zarzour JG, Porter KK, Tchelepi H, Robbin ML. Contrast-enhanced ultrasound of benign liver lesions. Abdom Radiol (NY). 2018 Apr;43(4):848–60. doi: 10.1007/s00261-017-1402-2.
92. Kazmierski B, Deurdulian C, Tchelepi H, Grant EG. Applications of contrast-enhanced ultrasound in the kidney. Abdom Radiol (NY). 2018 Apr;43(4):880–98. doi: 10.1007/s00261-017-1307-0.
93. Ding Z, Deng C, Wang Z, Liu L, Ma X, Huang J, Wang X, Xuan M, Xie H. Comparison of contrast-enhanced ultrasound and contrast-enhanced computed tomography for the diagnosis of cervical lymph node metastasis in squamous cell carcinoma of the oral cavity. Int J Oral Maxillofac Surg. 2021 Mar;50(3):294–301. doi: 10.1016/j.ijom.2020.07.013. Epub 2020 Jul 29.
94. Srivastava S, Dhyani M, Dighe M. Contrast-enhanced ultrasound (CEUS): applications from the kidneys to the bladder. Abdom Radiol (NY). 2024 Nov;49(11):4092–112. doi: 10.1007/s00261-024-04388-4. Epub 2024 Jun 17.
95. Yu M, Liu Q, Song HP, Han ZH, Su HL, He GB, Zhou XD. Clinical application of contrast-enhanced ultrasonography in diagnosis of superficial lymphadenopathy. J Ultrasound Med. 2010 May;29(5):735–40. doi: 10.7863/jum.2010.29.5.735.
96. Huang S, Zhao Y, Jiang X, Lin N, Zhang M, Wang H, Zheng A, Ma X. Clinical Utility of Contrast-enhanced Ultrasound for the Diagnosis of Lymphadenopathy. Ultrasound Med Biol. 2021 Apr;47(4):869–79. doi: 10.1016/j.ultrasmedbio.2020.12.020. Epub 2021 Jan 21.
97. Albers MA, Küstermeyer J, Welkoborsky HJ. Perfusion analysis in parotid gland tumors using contrast-enhanced ultrasound (CEUS). HNO. 2022 Jan 1;70(1):51–9.
98. Salib A, Halpern E, Eisenbrey J, Chandrasekar T, Chung PH, Forsberg F, Trabulsi EJ. The evolving role of contrast-enhanced ultrasound in urology: a review. World J Urol. 2023 Mar;41(3):673–8. doi: 10.1007/s00345-022-04088-y. Epub 2022 Aug 15.

99. Sun D, Wei C, Li Y, Lu Q, Zhang W, Hu B. Contrast-Enhanced Ultrasonography with Quantitative Analysis allows Differentiation of Renal Tumor Histotypes. Sci Rep. 2016 Oct 11;6:35081. doi: 10.1038/srep35081
100. Denham SL, Alexander LF, Robbin ML. Contrast-Enhanced Ultrasound: Practical Review for the Assessment of Hepatic and Renal Lesions. Ultrasound Q. 2016 Jun;32(2):116–25. doi: 10.1097/RUQ.0000000000000182.
101. Ignat RM, Fekete Z, Csutak C, Todor N, Ignat FL, Ignat PD, Badea R. The value of contrast-enhanced ultrasound in cervical cancer assessed in comparison with magnetic resonance imaging. Med Pharm Rep. 2024 Jul;97(3):255–62. doi: 10.15386/mpr-2746. Epub 2024 Jul 30.
102. Gvetadze SR, Xiong P, Lv M, Li J, Hu J, Ilkaev KD, Yang X, Sun J. Contrast-enhanced ultrasound mapping of sentinel lymph nodes in oral tongue cancer-a pilot study. Dentomaxillofac Radiol. 2017 Mar;46(3):20160345. doi: 10.1259/dmfr.20160345. Epub 2017 Feb 17.
103. Spiesecke P, Neumann K, Wakonig K, Lerchbaumer MH. Contrast-enhanced ultrasound (CEUS) in characterization of inconclusive cervical lymph nodes: a meta-analysis and systematic review. Sci Rep. 2022 May 12;12(1):7804. doi: 10.1038/s41598-022-11542-9.
104. Wendl CM, Janke M, Jung W, Stroszczysnski C, Jung EM. Contrast-enhanced ultrasound with perfusion analysis for the identification of malignant and benign tumours of the thyroid gland. Clin Hemorheol Microcirc. 2015 Oct 27;63(2):113–21. doi: 10.3233/CH-151966.
105. Ling W, Nie J, Zhang D, Yang Q, Jin H, Ou X, Ma X, Luo Y. Role of Contrast-Enhanced Ultrasound (CEUS) in the Diagnosis of Cervical Lymph Node Metastasis in Nasopharyngeal Carcinoma (NPC) Patients. Front Oncol. 2020 Jul 17;10:972. doi: 10.3389/fonc.2020.00972.
106. Su S, Huang J, Huang X, Li X, Liu Y, Meng J, et al. The correlation between time-intensity curve parameters of transrectal contrast-enhanced ultrasound and pathological prognostic factors in rectal adenocarcinoma. Med Ultrason. 2024 May 15;26(3):233–241. doi: 10.11152/mu-4375
107. Cui QL, Yin SS, Fan ZH, Yang W, Wang S, Yan K. Diagnostic Value of Contrast-Enhanced Ultrasonography and Time-Intensity Curve in Differential Diagnosis of Cervical Metastatic and Tuberculous Lymph Nodes. J Ultrasound Med. 2018 Jan;37(1):83_92. doi: 10.1002/jum.14311. Epub 2017 Jul 10.
108. Hong YR, Luo ZY, Mo GQ, Wang P, Ye Q, Huang PT. Role of Contrast-Enhanced Ultrasound in the Pre-operative Diagnosis of Cervical Lymph Node Metastasis in Patients with Papillary Thyroid Carcinoma. Ultrasound Med Biol. 2017 Nov;43(11):2567–75. doi: 10.1016/j.ultrasmedbio.2017.07.010. Epub 2017 Aug 12.
109. Trimboli P, Castellana M, Virili C, Havre RF, Bini F, Marinozzi F, D'Ambrosio F, Giorgino F, Giovanella L, Prosch H, Grani G, Radzina M, Cantisani V. Performance of contrast-enhanced ultrasound (CEUS) in assessing thyroid nodules: a systematic review and meta-analysis using histological standard of reference. Radiol Med. 2020 Apr;125(4):406–15. doi: 10.1007/s11547-019-01129-2. Epub 2020 Jan 22.
110. Baugnon KL, Beitler JJ. Pitfalls in the staging of cancer of the laryngeal squamous cell carcinoma. Neuroimaging Clin N Am. 2013 Feb;23(1):81–105. doi: 10.1016/j.nic.2012.08.008.

111. Amin MB, Greene FL, Edge SB, Compton CC, Gershenwald JE, Brookland RK, Meyer L, Gress DM, Byrd DR, Winchester DP. The Eighth Edition AJCC Cancer Staging Manual: Continuing to build a bridge from a population-based to a more "personalized" approach to cancer staging. CA Cancer J Clin. 2017 Mar;67(2):93–9. doi: 10.3322/caac.21388. Epub 2017 Jan 17.
112. Claassen H, Kirsch T, Simons G. Cartilage canals in human thyroid cartilage characterized by immunolocalization of collagen types I, II, pro-III, IV and X. Anat Embryol (Berl). 1996 Aug;194(2):147–53. doi: 10.1007/BF00195008.
113. Leggio A, Introna F. Fully Ossified Thyroid Cartilage Found among the Skeletal Remains of A 21-Year-Old Slavic Soldier: Interpretation of a Case. Forensic Sci. 2021 Dec 1;1(3):213–9. doi: 10.3390/forensicsci1030019
114. Sable N, Kshirsagar R, Shukla S, Thakur M, Mahajan A. Normal mineralization patterns of laryngeal cartilage on computed tomography and their implication for laryngeal and hypopharyngeal cancer management: A cross-sectional retrospective analysis. Cancer Research, Statistics, and Treatment. 2022 Jul 1;5(3):452–60. doi: 10.4103/crst.crst_69_22
115. Jurik AG. Ossification and calcification of the laryngeal skeleton. Acta Radiol Diagn (Stockh). 1984;25(1):17–22. doi: 10.1177/028418518402500104.
116. Hut AR, Boia ER, Para D, Iovanescu G, Horhat D, Mikša L, Chiriac M, Galant R, Motofelea AC, Balica NC. Laryngeal Cancer in the Modern Era: Evolving Trends in Diagnosis, Treatment, and Survival Outcomes. J Clin Med. 2025 May 12;14(10):3367. doi: 10.3390/jcm14103367.
117. Bicci E, Di Finizio A, Calamandrei L, Treballi F, Mungai F, Tamburrini S, Sica G, Nardi C, Bonasera L, Miele V. Head and Neck Squamous Cell Carcinoma: Insights from Dual-Energy Computed Tomography (DECT). Tomography. 2024 Nov 11;10(11): 1780–97. doi: 10.3390/tomography10110131.
118. Thurnher D, Simo R, Succo G, Vilaseca I, Simon C. Open partial or transoral laryngectomy – total laryngectomy today. Front Oncol. 2025 Aug 15;15:1520524. doi: 10.3389/fonc.2025.1520524.
119. Chang BA, Lott DG, Nagel TH, Howard BE, Hayden RE, Hinni ML. Outcomes Following Transoral Laser Microsurgery With Resection of Cartilage for Laryngeal Cancer. Ann Otol Rhinol Laryngol. 2019 Oct;128(10):978–82. doi: 10.1177/00034894 19851521. Epub 2019 May 27.
120. Campo F, Mazzola F, Bianchi G, Manciocco V, Ralli M, Greco A, Sperduti I, de Vincentiis M, Pellini R. Partial laryngectomy for naïve pT3N0 laryngeal cancer: Systematic review on oncological outcomes. Head Neck. 2023 Jan;45(1):243–50. doi: 10.1002/hed.27205. Epub 2022 Sep 30.
121. Forastiere AA, Ismaila N, Lewin JS, Nathan CA, Adelstein DJ, Eisbruch A, Fass G, Fisher SG, Laurie SA, Le QT, O'Malley B, Mendenhall WM, Patel S, Pfister DG, Provenzano AF, Weber R, Weinstein GS, Wolf GT. Use of Larynx-Preservation Strategies in the Treatment of Laryngeal Cancer: American Society of Clinical Oncology Clinical Practice Guideline Update. J Clin Oncol. 2018 Apr 10;36(11):1143–69. doi: 10.1200/JCO.2017.75.7385. Epub 2017 Nov 27.
122. Ravanelli M, Lancini D, Maroldi R, Paderno A, Rondi P, Battocchio S, Ardighieri L, Vezzoli M, Del Bon F, Farina D, Piazza C. Magnetic resonance imaging to assess cartilage invasion in recurrent laryngeal carcinoma after transoral laser microsurgery. Acta Otorhinolaryngol Ital. 2022 Dec;42(6):531–7. doi: 10.14639/0392-100X-N2090.

123. Montenegro C, Paderno A, Ravanelli M, Pessina C, Nassih FE, Lancini D, Del Bon F, Mattavelli D, Farina D, Piazza C. Thyroid cartilage infiltration in advanced laryngeal cancer: prognostic implications and predictive modelling. Acta Otorhinolaryngol Ital. 2024 Jun;44(3):176–82. doi: 10.14639/0392-100X-N2739. Epub 2023 Dec 29.
124. Steuer CE, El-Deiry M, Parks JR, Higgins KA, Saba NF. An update on larynx cancer. CA Cancer J Clin. 2017 Jan;67(1):31–50. doi: 10.3322/caac.21386. Epub 2016 Nov 29.
125. OpenAI. ChatGPT (GPT-5) [internet]. San Francisco (CA): OpenAI; 2025 [cited 2025 Oct 28]. Available from: https://chat.openai.com/.
126. Jiang F, Jiang Y, Zhi H, Dong Y, Li H, Ma S, Wang Y, Dong Q, Shen H, Wang Y. Artificial intelligence in healthcare: past, present and future. Stroke Vasc Neurol. 2017 Jun 21;2(4):230–43. doi: 10.1136/svn-2017-000101.
127. Pucėtaitė M, Mitraitė D, Tarasevičius R, Farina D, Ryškienė S, Lukoševičius S, Padervinskis E, Šarauskas V, Vaitkus S. Time-Intensity Curve Analysis of Contrast-Enhanced Ultrasound for Non-Ossified Thyroid Cartilage Invasion in Laryngeal Squamous Cell Carcinoma. Tomography. 2025 May 16;11(5):57. doi: 10.3390/tomography11050057.
128. James D. Brierley MKGCWU for ICC. TNM Classification of Malignant Tumours. Eitght. James D. Brierley MKG, CW, editor. Chichester, West Sussex, UK: Wiley Blackwell; 2017. p. 25–36 Available from: http://mom.gov.az/resources/content_files/ebook/TNM-Classification-of-Malignant-Tumours-8th-edition.pdf
129. Weinstein S, Obuchowski NA, Lieber ML. Clinical evaluation of diagnostic tests. AJR Am J Roentgenol. 2005 Jan;184(1):14-9. doi: 10.2214/ajr.184.1.01840014.
130. Chiesa-Estomba CM, Ravanelli M, Farina D, Remacle M, Simo R, Peretti G, Sjogren E, Sistiaga-Suarez JA, Gónzalez-García JA, Larruscain E, Piazza C. Imaging checklist for preoperative evaluation of laryngeal tumors to be treated by transoral microsurgery: guidelines from the European Laryngological Society. Eur Arch Otorhinolaryngol. 2020 Jun;277(6):1707–14. doi: 10.1007/s00405-020-05869-0. Epub 2020 Feb 27.
131. Obid R, Redlich M, Tomeh C. The Treatment of Laryngeal Cancer. Oral Maxillofac Surg Clin North Am. 2019 Feb;31(1):1–11. doi: 10.1016/j.coms.2018.09.001.
132. Scherl C, Mantsopoulos K, Semrau S, Fietkau R, Kapsreiter M, Koch M, Traxdorf M, Grundtner P, Iro H. Management of advanced hypopharyngeal and laryngeal cancer with and without cartilage invasion. Auris Nasus Larynx. 2017 Jun;44(3):333–9. doi: 10.1016/j.anl.2016.08.002. Epub 2016 Aug 25.
133. Park CJ, Kim JH, Ahn SS, Lee SK, Koh YW, Kim J. Preoperative MRI Evaluation of Thyroid Cartilage Invasion in Patients with Laryngohypopharyngeal Cancer: Comparison of Contrast-Enhanced 2D Spin-Echo and 3D T1-Weighted Radial Gradient Recalled-Echo Techniques. AJNR Am J Neuroradiol. 2021 Sep;42(9):1690–4. doi: 10.3174/ajnr.A7213. Epub 2021 Jul 22.
134. Ruytenberg T, Verbist BM, Vonk-Van Oosten J, Astreinidou E, Sjögren EV, Webb AG. Improvements in High Resolution Laryngeal Magnetic Resonance Imaging for Preoperative Transoral Laser Microsurgery and Radiotherapy Considerations in Early Lesions. Front Oncol. 2018 Jun 6;8:216. doi: 10.3389/fonc.2018.00216.
135. Dhoot NM, Choudhury B, Kataki AC, Kakoti L, Ahmed S, Sharma J. Effectiveness of ultrasonography and computed tomography in assessing thyroid cartilage invasion in laryngeal and hypopharyngeal cancers. J Ultrasound. 2017 Aug 19;20(3):205–11. doi: 10.1007/s40477-017-0259-0.
136. Xia CX, Zhu Q, Zhao HX, Yan F, Li SL, Zhang SM. Usefulness of ultrasonography in assessment of laryngeal carcinoma. Br J Radiol. 2013 Oct;86(1030):20130343. doi: 10.1259/bjr.20130343. Epub 2013 Sep 4.

137. Folkman J. Tumor angiogenesis: therapeutic implications. N Engl J Med. 1971 Nov 18;285(21):1182–6. doi: 10.1056/NEJM197111182852108.
138. Yousefzadeh DK, Doerger K, Sullivan C. The blood supply of early, late, and nonossifying cartilage: preliminary gray-scale and Doppler assessment and their implications. Pediatr Radiol. 2008 Feb;38(2):146–58. doi: 10.1007/s00247-007-0655-2. Epub 2007 Nov 27.
139. Zhang CC, Yan Z, Giddabasappa A, Lappin PB, Painter CL, Zhang Q, Li G, Goodman J, Simmons B, Pascual B, Lee J, Levkoff T, Nichols T, Xie Z. Comparison of dynamic contrast-enhanced MR, ultrasound and optical imaging modalities to evaluate the antiangiogenic effect of PF-03084014 and sunitinib. Cancer Med. 2014 Jun;3(3):462–71. doi: 10.1002/cam4.215. Epub 2014 Feb 27.
140. Zheng D, Chen Y, Liu X, Chen Y, Xu L, Ren W, Chen W, Chan Q. Early response to chemoradiotherapy for nasopharyngeal carcinoma treatment: Value of dynamic contrast-enhanced 3.0 T MRI. J Magn Reson Imaging. 2015 Jun;41(6):1528–40. doi: 10.1002/jmri.24723. Epub 2014 Aug 18.
141. Ng SH, Liao CT, Lin CY, Chan SC, Lin YC, Yen TC, Chang JT, Ko SF, Fan KH, Wang HM, Yang LY, Wang JJ. Dynamic contrast-enhanced MRI, diffusion-weighted MRI and 18F-FDG PET/CT for the prediction of survival in oropharyngeal or hypopharyngeal squamous cell carcinoma treated with chemoradiation. Eur Radiol. 2016 Nov;26(11):4162–72. doi: 10.1007/s00330-016-4276-8. Epub 2016 Feb 24.

LIST OF SCIENTIFIC PUBLICATIONS

Publications related to the results of the dissertation:

1. **Pucėtaitė M**, Mitraitė D, Tarasevičius R, Farina D, Ryškienė S, Lukoševičius S, Padervinskis E, Šarauskas V, Vaitkus S. *Time-Intensity Curve Analysis of Contrast-Enhanced Ultrasound for Non-Ossified Thyroid Cartilage Invasion in Laryngeal Squamous Cell Carcinoma.* Tomography. 2025;11(5):57. https://doi.org/10.3390/tomography11050057. **This article was selected by editorial board as the cover story of the journal issue.**
2. **Pucėtaitė M**, Farina D, Ryškienė S, Mitraitė D, Tarasevičius R, Lukoševičius S, Padervinskis E, Vaitkus S. *The Diagnostic Value of CEUS in Assessing Non-Ossified Thyroid Cartilage Invasion in Patients with Laryngeal Squamous Cell Carcinoma.* Journal of Clinical Medicine. 2024;13(3):891. https://doi.org/10.3390/jcm1303089.

Other significant scientific publications not related to the results of the dissertation:

1. Touska P, Dudau C, Patel J, Montvila A, **Pucėtaitė M**, Obholzer R, Pai I, Connor S. Computed tomographic features of the proximal petrous facial nerve canal in recurrent Bell's palsy. *Laryngoscope Investigative Otolaryngology*. 2021; 6(4):816–823. https://doi.org/10.1002/lio2.571.
2. **Pucėtaitė M,** Quesnel AM, Juliano A, Curtin HD, Reinshagen KL. The cochlear cleft: CT correlation with histopathology: clinical capsule report. *Otology & Neurotology*. 2020; 41(6):745–749. https://doi.org/10.1097/MAO.0000000000002637.

LIST OF PRESENTATIONS IN SCIENTIFIC CONFERENCES

The results of the dissertation were presented at the scientific conferences:

1. **Pucetaite M,** Ryskiene S, Mitraite D, Sarauskas V, Vaitkus S. *The value of CEUS, CT and MRI in assessing thyroid cartilage invasion in patients with laryngeal squamous cell carcinoma.* In: **VIII Baltic ENT Congress**, Abstracts; 2023 Jun 8–10; Vilnius, Lithuania. Vilnius: Lithuanian Society of Otorhinolaryngology; 2023. p. 1. ISBN: (LSMU ALMA) 991715186807106.
2. **Pucetaite M**, Tarasevicius R, Ryskiene S, Mitraite D, Vaitkus S. *The place of contrast-enhanced ultrasound in assessing thyroid cartilage invasion in laryngeal cancer.* In: **EUROSON 2023 – 34th Congress of the European Federation of Societies for Ultrasound in Medicine and Biology**; 2023 May 25–27; Riga, Latvia. Riga: European Federation of Ultrasound Societies in Medicine and Biology; 2023. p. 169. ISBN: (LSMU ALMA)991715187107106.

COPIES OF PUBLICATIONS RELATED TO THE RESULTS OF THE DISSERTATION

A1

Title: Time-Intensity Curve Analysis of Contrast-Enhanced Ultrasound for Non-Ossified Thyroid Cartilage Invasion in Laryngeal Squamous Cell Carcinoma

Authors: Pucėtaitė Milda, Mitraitė Dalia, Tarasevičius Rytis, Farina Davide, Ryškienė Silvija, Lukoševičius Saulius, Padervinskis Evaldas, Šarauskas Valdas, Vaitkus Saulius.

Tomography (2025)

No special permission is required to reuse all or part of article published by MDPI, including table and figures. Furthermore, no special permission is required for authors to submit their work to external repositories (MDPI | Open Access Information)

tomography

MDPI

Article

Time-Intensity Curve Analysis of Contrast-Enhanced Ultrasound for Non-Ossified Thyroid Cartilage Invasion in Laryngeal Squamous Cell Carcinoma

Milda Pucėtaitė [1,*], Dalia Mitraitė [1], Rytis Tarasevičius [2], Davide Farina [3], Silvija Ryškienė [1], Saulius Lukoševičius [1], Evaldas Padervinskis [4], Valdas Šarauskas [5] and Saulius Vaitkus [4]

[1] Department of Radiology, Faculty of Medicine, Medical Academy, Lithuanian University of Health Sciences, A. Mickevičiaus Str. 9, 44307 Kaunas, Lithuania; dalia.mitraite@lsmu.lt (D.M.); silvija.ryskiene@lsmu.lt (S.R.); saulius.lukosevicius@lsmu.lt (S.L.)
[2] Department of Radiology, Lithuanian University of Health Sciences Kaunas Clinics, Eivenių 2, 50009 Kaunas, Lithuania; rytis.tarasevicius@kaunoklinikos.lt
[3] Department of Radiological Sciences, University of Brescia, Piazzale Spedali Civili 1, 25123 Brescia, Italy; davide.farina@unibs.it
[4] Department of Otorhinolaryngology, Faculty of Medicine, Medical Academy, Lithuanian University of Health Sciences, A. Mickevičiaus Str. 9, 44307 Kaunas, Lithuania; evaldas.padervinskis@lsmu.lt (E.P.); saulius.vaitkus@lsmu.lt (S.V.)
[5] Department of Pathological Anatomy, Faculty of Medicine, Medical Academy, Lithuanian University of Health Sciences, A. Mickevičiaus Str. 9, 44307 Kaunas, Lithuania; valdas.sarauskas@lsmu.lt
* Correspondence: milda.pucetaite@lsmu.lt

check for updates

Academic Editor: Emilio Quaia

Received: 30 March 2025
Revised: 14 May 2025
Accepted: 15 May 2025
Published: 16 May 2025

Citation: Pucėtaitė, M.; Mitraitė, D.; Tarasevičius, R.; Farina, D.; Ryškienė, S.; Lukoševičius, S.; Padervinskis, E.; Šarauskas, V.; Vaitkus, S. Time-Intensity Curve Analysis of Contrast-Enhanced Ultrasound for Non-Ossified Thyroid Cartilage Invasion in Laryngeal Squamous Cell Carcinoma. *Tomography* **2025**, *11*, 57. https://doi.org/10.3390/tomography11050057

Correction Statement: This article has been republished with a minor change. The change does not affect the scientific content of the article and further details are available within the backmatter of the website version of this article.

Copyright: © 2025 by the authors. Licensee MDPI, Basel, Switzerland. This article is an open access article distributed under the terms and conditions of the Creative Commons Attribution (CC BY) license (https://creativecommons.org/licenses/by/4.0/).

Abstract: Objective: This study aimed to assess the diagnostic value of contrast-enhanced ultrasound (CEUS) time–intensity curve (TIC) parameters in detecting non-ossified thyroid cartilage invasion in patients with laryngeal squamous cell carcinoma (SCC). **Methods**: A CEUS TIC analysis was performed on 32 cases from 27 patients with histologically confirmed laryngeal SCC. The diagnostic performance of time to peak (TTP), peak intensity (PI), wash-in slope (WIS), area under the curve (AUC), and their quantitative differences (ΔTTP, ΔPI, ΔWIS, and ΔAUC) to discriminate between the invaded and the non-invaded non-ossified thyroid cartilage was determined using ROC analysis. A logistic regression analysis was employed to identify significant predictors. **Results**: In an ROC analysis, of all TIC parameters analyzed separately, ΔTTP showed the greatest diagnostic performance (AUC: 0.85). A ΔTTP cut-off of $\leq$ 8.9 s differentiated between the invaded and the non-invaded non-ossified thyroid cartilage with a sensitivity of 100%, specificity of 76.9%, and accuracy of 81.3%. A combination of ΔTTP and PI increased the AUC to 0.93, specificity to 100%, and accuracy to 96.8%, but reduced the sensitivity to 83.3%. Meanwhile, the visual assessment of enhancement on CEUS to detect cartilage invasion had 83.3% sensitivity and 84.6% specificity. In a univariate logistic regression, only ΔTTP was a significant predictor of non-ossified thyroid cartilage invasion (OR: 0.80; 95% CI: 0.64–1.00). For every second increase in ΔTTP, the probability of thyroid cartilage invasion decreased by 20%. **Conclusions**: CEUS TIC parameters, particularly a combination of ΔTTP and PI, showed high diagnostic performance in the detection of non-ossified thyroid cartilage invasion in laryngeal SCC.

Keywords: contrast-enhanced ultrasound; laryngeal squamous cell carcinoma; non-ossified thyroid cartilage invasion; diagnostic performance

1. Introduction

Squamous cell carcinoma (SCC) is the most common histological type of carcinomas in the larynx, and laryngeal SCC is the most frequent carcinoma among head and neck SCCs [1,2].

Accurate assessment of thyroid cartilage invasion is essential for precisely determining the extent of disease progression and tailoring appropriate treatment strategies. This evaluation plays a critical role in clinical decision making, particularly when distinguishing between organ-preserving approaches, such as radiation therapy, cordectomy or partial laryngectomy, and more radical interventions like total laryngectomy [3–6].

Conventional imaging modalities, such as computed tomography (CT) and magnetic resonance imaging (MRI), are widely used for staging laryngeal cancer. However, these techniques have limitations, particularly in accurately assessing laryngeal cartilage invasion [7–9]. Despite MRI generally being considered superior to CT for evaluating thyroid cartilage invasion [10–12], a recent study by Mohamad et al. has reported suboptimal diagnostic accuracy [13]. This study found that the overall MRI accuracy in detecting tumor invasion into the inner thyroid cortex and full-thickness thyroid cartilage was 65% and 69%, respectively. These findings raise some concerns and highlight the need to explore alternative diagnostic tools.

Among emerging imaging modalities, contrast-enhanced ultrasound (CEUS) has gained attention in oncologic imaging due to its ability to provide real-time, dynamic assessments of tissue vascularization and perfusion pattern [14,15]. Recent advancements in quantitative CEUS analysis have enabled the extraction of perfusion-based parameters, which play a crucial role in CEUS for distinguishing malignant from benign tissue and lesions [16–20]. Knowing that non-ossified thyroid cartilage is composed of hyaline cartilage, which is avascular, CEUS began to be explored in the scientific field, with the hypothesis that it would show no enhancement if not invaded by a tumor [21,22].

However, despite its promising potential, a limited number of studies have specifically investigated the role of qualitative CEUS in staging laryngeal cancer [23,24]. To our knowledge, no studies have investigated the role of the quantitative assessment of CEUS parameters, which offers a standardized and reproducible approach to evaluate differences in microvascular perfusion, which may be useful for the diagnostic evaluation of non-ossified thyroid cartilage invasion in laryngeal carcinoma. This study aimed to evaluate the diagnostic performance of time–intensity curve (TIC) CEUS-derived parameters in differentiating invaded from non-invaded non-ossified thyroid cartilage and comparing with histopathological assessment used as the gold standard. Our hypothesis is that these quantitative metrics can significantly enhance diagnostic efficacy and may serve as a complementary imaging modality to CT or MRI.

2. Materials and Methods

2.1. Study Design and Subjects

A prospective study was conducted at the Hospital of the Lithuanian University of Health Sciences Kauno Klinikos between 2021 and 2025. Forty-one patients with histopathologically confirmed SCC of the larynx were enrolled in this study. The inclusion criteria included the following: the availability of a contrast-enhanced computed tomography (CECT) scan demonstrating pathological infiltration adjacent to the non-ossified thyroid cartilage or clear cartilage infiltration; no history of laryngeal–hypopharyngeal surgery or chemoradiation; and surgery planned after multidisciplinary team discussion. Ten patients were excluded because some of them refused surgical treatment or did not attend further consultations or did not undergo further surgery.

All 31 male patients meeting the inclusion criteria were subjected to CEUS examination. However, 4 of them had significant motion artifacts during CEUS; therefore, data from only 27 patients were available for TIC analysis. Informed consent was obtained from all participants before the study. The study was conducted according to the guidelines of the

Declaration of Helsinki. Ethical approval was obtained from Kaunas Regional Biomedical Research Ethics Committee (No. BE-2-121; dated 2021).

2.2. Contrast-Enhanced Ultrasound Examination

The analysis of CEUS images was performed by two radiologists with > 4 and > 20 years of experience, respectively. The radiologists were not blinded to the clinical and CECT data during the CEUS examination and image analysis.

CEUS examination was performed using a Philips Epiq 7 (expert-class) US system (Philips Healthcare, Best, The Netherlands) with a 5–12 MHz linear transducer and a mechanical index of 0.08. The target area during CEUS was selected based on CECT images, additionally using the measured distance between the lesion area of contact to the non-ossified thyroid cartilage and the upper border of the thyroid cartilage as coordinates.

During the CEUS examination, an intravenous bolus of 5 mL SonoVue (Bracco SpA, Milan, Italy), followed by saline flush, was administered. The patients were instructed to avoid swallowing or coughing during the examination. The dynamic perfusion of the suspected non-ossified thyroid cartilage invasion area and the adjacent tumor was monitored and recorded on the device hard drive for approximately 1 min. If more than one suspected invasion site was identified, the CEUS procedure was repeated after a 10 min interval.

2.3. Image Analysis

Recorded video loops were processed with Qlab® Quantification software (Qlab 15; Philips Medical Systems, Inc., Best, the Netherlands). Both qualitative and quantitative analysis was employed for the evaluation of blood perfusion of the area of suspected non-ossified thyroid cartilage invasion and adjacent tumor.

For a qualitative analysis, the enhancement of each non-ossified thyroid cartilage area with suspected tumor invasion was evaluated with no enhancement and visible enhancement being the main categories.

For quantitative analysis, the region of interest (ROI) of the tumor and the thyroid cartilage was manually determined. The first ROI was placed in the determined non-ossified thyroid cartilage area with suspected invasion, and the second comparative ROI was placed in the adjacent tumor tissue (Figure 1). The ROI size varied between 0.3 and 1.6 mm^2 for each patient due to differences in the thickness of the non-ossified thyroid cartilage. However, for each patient, the ROI size was selected to be similar to the non-ossified cartilage and that of the region in the adjacent tumor. TICs for the tumor and the non-ossified thyroid cartilage were generated from perfusion data and analyzed with a predefined software function Auto Curve Fit control model. The following 4 parameters of quantitative analysis were produced: TTP (time to peak, s), PI (peak intensity, dB), WIS (wash-in slope, dB/s), AUC (area under curve, dB × s). Quantitative differences in TIC parameters (ΔTTP, ΔPI, ΔWIS, and ΔAUC) between the tumor (t) and the suspected site of thyroid cartilage (tc) invasion were calculated, e.g., ΔPI = $PI_t - PI_{tc}$. The results were written as absolute values assuming that smaller differences should show similarity with vascular tumor tissue, which could be detected in the invaded non-ossified thyroid cartilage.

2.4. Histological Examination

Histopathological assessment was performed by a pathologist with >20-year experience. To ensure accurate correlation between radiological findings and pathological analysis, the radiologist marked the suspected area of non-ossified thyroid cartilage invasion on an anatomical sketch of the larynx in both axial and coronal planes for each case. The macroscopic and microscopic examination was performed for each specimen. The 8th Edition of TNM Classification of Malignant Tumors [25] was used for staging.

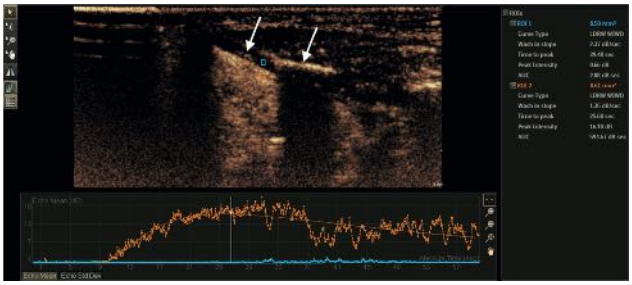

Figure 1. Laryngeal cancer on the left with the partially ossified thyroid cartilage (white arrows). The ROI marked by the blue rectangle frame was placed on the non-ossified thyroid cartilage and the ROI marked by the orange rectangle frame, on the adjacent tumor. Qualitative TIC analysis of wash-out was conducted by describing a wash-out curve as shallow (slow wash-out) or steep (rapid wash-out).

2.5. Statistical Analysis

The IBM SPSS Statistics 29.0 (IBM Corp. in Armonk, NY, USA) and MedCalc 23.1.3 (MedCalc Software Ltd., Ostend, Belgium) statistical software packages were used in this study. Not all quantitative data conformed to the normal distribution. Comparisons of TIC parameters between the histopathologically proven non-ossified thyroid cartilage with and without invasion, and the tumor were performed using nonparametric tests such as the Mann–Whitney U test and the Wilcoxon test (TIC parameters of the thyroid cartilage and the tumor were treated as dependent). The non-parametric chi-square test was used to compare the enhancement of the thyroid cartilage area with and without tumor invasion. Moreover, sensitivity, specificity, and accuracy were calculated according to the formulas used in our previous work [25]. Statistically significant TIC parameters of the non-ossified cartilage with and without invasion were included in a logistic regression analysis (enter method) for calculating odds ratios (OR) with their 95% confidence intervals (CI). The area under the receiver operating characteristic (ROC) curve (AUCROC) along with sensitivity and specificity was analyzed for significant TIC parameters and their combinations. The accuracy of significant parameters was compared using the McNemar's test. On the ROC curves, points with the greatest Youden index (sensitivity + specificity − 1) were considered the most appropriate cut-off values. A p value of <0.05 was considered to indicate a statistically significant difference.

3. Results

This prospective study involved 27 male patients with a mean age of 63.52 years (SD, 7.92; range, 49–84 years). There were 32 cases of suspected sites of non-ossified thyroid cartilage invasion analyzed by CEUS, as 5 patients had two suspected sites of invasion. There were 12 patients (44.4%) with glottic SCC and 15 patients (55.6%) with transglottic SCC with the majority showing a G2 degree of differentiation (77.8%). The patients' distribution by pT staging was as follows: 7 (25.9%) patients had T1 SCC; 7 (25.9%) patients, T2; 9 (33.3) patients, T3; and 4 (14.8) patients, T4. In six cases (18.8%), histological proof of non-ossified thyroid cartilage invasion was obtained.

3.1. CEUS Imaging Features of Non-Ossified Thyroid Cartilage

The contrast enhancement of the non-ossified thyroid cartilage with suspected tumor invasion (according to CECT) was analyzed. The thyroid cartilage with invasion showed visible strong or moderate enhancement in 5 cases, and there was only 1 case of no enhancement. Moreover, the non-invaded cartilage did not show enhancement in 22 cases, and there were 4

cases with visible poor enhancement ($p < 0.05$) (Table 1). CEUS was able to discriminate between the invaded (visible enhancement) and the non-invaded (no enhancement) non-ossified thyroid cartilage with 83.3% sensitivity, 84.6% specificity, and 84.4% accuracy. Figure 2 is a representative CEUS scan showing poor enhancement of the thyroid cartilage.

Table 1. Contrast enhancement of the non-ossified thyroid cartilage with suspected tumor invasion.

Feature	Thyroid Cartilage Without Invasion (n = 26)	Thyroid Cartilage with Invasion (n = 6)	p Value
No enhancement	22 (84.6)	1 (16.7)	<0.05
Visible enhancement	4 (15.4)	5 (83.3)	

Values are number (percentage).

Figure 2. Right laryngeal SCC on CEUS. The red arrows indicate poor enhancement of thyroid cartilage. Postoperative histopathological analysis confirmed the absence of invasion.

3.2. TIC Analysis of Non-Ossified Thyroid Cartilage and Tumor Tissue

Parameters of hemodynamics and perfusion for 3 groups of histopathologically proven tumor, invaded non-ossified thyroid cartilage, and non-invaded non-ossified thyroid cartilage were investigated and compared (Figure 3). The comparison showed statistically significant differences in TTP and PI between these 3 groups ($p < 0.05$) (Table 2). The AUC of the thyroid cartilage with and without invasion differed significantly ($p < 0.05$); however, no significant difference in the WIS was found ($p > 0.05$). AUC and WIS results differed significantly between thyroid cartilage without invasion and tumor ($p < 0.05$) and did not differ between tumor and thyroid cartilage with invasion ($p > 0.05$). Comparison of quantitative differences in TIC parameters (ΔTTP, ΔPI, ΔWIS, ΔAUC) between the invaded and the non-invaded non-ossified thyroid cartilage is shown in Table 3. The median of the ΔTTP parameter in cases with thyroid cartilage invasion was statistically significantly lower than in cases with intact thyroid cartilage ($p < 0.05$).

Table 2. TIC parameters of the tumor and the thyroid cartilage with and without invasion.

Parameter	Thyroid Cartilage Without Invasion	Thyroid Cartilage with Invasion	p Value [1]	Tumor	p Value [2]
TTP, s	44.4 (30.99–58.31)	32.83 (29.02–58.70)	<0.05	28.44 (10.95–49.80)	<0.05 [n] <0.05 [i]
PI, dB	1.85 (0.00–7.22)	12.27 (0.30–21.80)	<0.05	13.59 (4.65–46.41)	<0.05 [n] <0.05 [i]
AUC, dB × s	10.30 (0.30–58.54)	69.05 (3.85–330.12)	<0.05	313.00 (61.05–657.89)	<0.05 [n] >0.05 [i]
WIS, dB/s	3.64 (0.00–19.51)	11.89 (0.60–46.77)	>0.05	1.74 (0.48–10.06)	<0.05 [n] >0.05 [i]

Values are median (min–max). Abbreviations: TTP = time to peak; PI = peak intensity; AUC = area under curve; WIS = wash-in slope. [1] Comparisons made using Mann–Whitney *U* test. [2] Comparisons made using Wilcoxon test. [n] Thyroid cartilage without invasion; [i] thyroid cartilage with invasion.

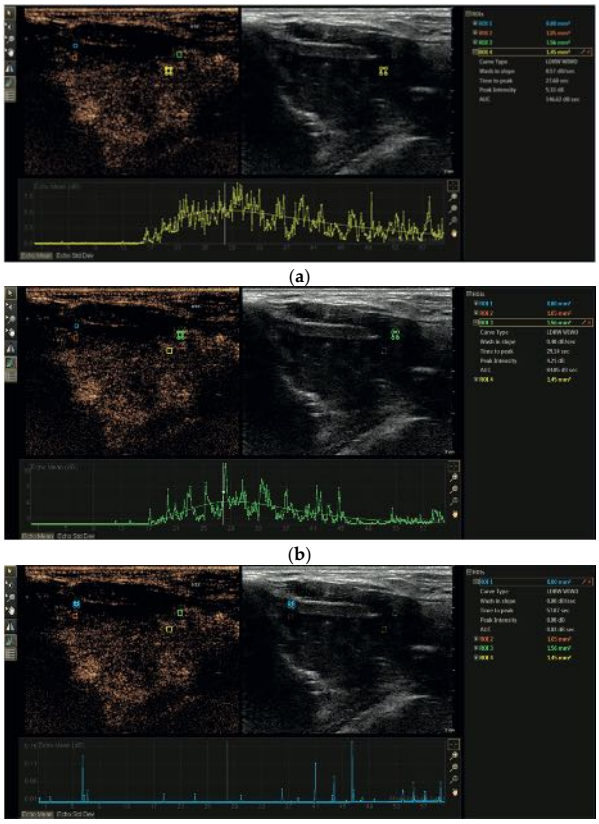

(**a**)

(**b**)

(**c**)

Figure 3. Time–intensity curve analysis of left laryngeal SCC at 28 s. (**a**) The ROI marked by the yellow rectangle frame indicates the enhancing tumor adjacent to the thyroid cartilage; (**b**) the ROI marked by the green rectangle frame shows the histologically proven invaded thyroid cartilage with enhancement; (**c**) the ROI marked by the blue rectangle frame shows non-ossified, non-enhanced cartilage without invasion.

Table 3. Quantitative differences in TIC parameters (ΔTTP, ΔPI, ΔWIS, and ΔAUC) between the tumor and the non-invaded or the invaded non-ossified thyroid cartilage.

Parameter	Thyroid Cartilage Without Invasion	Thyroid Cartilage with Invasion	*p* Value
ΔTTP, s	15.19 (2.02–36.54)	5.10 (1.83–8.90)	<0.05
ΔPI, dB	11.60 (3.33–37.11)	4.15 (1.60–24.61)	>0.05
ΔAUC, dB × s	333.75 (67.18–650.42)	199.55 (85.39–303.46)	>0.05
ΔWIS, dB/s	5.11 (0.24–15.92)	11.18 (0.27–45.87)	>0.05

Values are absolute and expressed as median (min–max). Abbreviations: TTP = time to peak; PI = peak intensity; AUC = area under the curve; WIS = wash-in slope.

3.3. *TIC Morphology Analysis of Non-Ossified Thyroid Cartilage and Tumor Tissue*

TICs of tumors indicated that all 32 tumor cases (100%) had shallow wash-out curves. TICs of non-ossified thyroid cartilages with and without histologically proven invasion showed that

there was no statistically significant difference between wash-out curve morphology as 13 cases of thyroid cartilage without invasion and 3 cases with invasion (50% of both groups) had shallow and other 50% had steep curves ($p > 0.05$). Significant differences in the TIC wash-out shapes were observed between the tumor and non-ossified thyroid cartilage groups ($p < 0.05$).

3.4. Logistic Regression Analysis for Non-Ossified Thyroid Cartilage Invasion

A univariate logistic regression was carried out to determine statistically significant parameters for non-ossified thyroid cartilage invasion. Only ΔTTP was found to be statistically significant associated with non-ossified thyroid cartilage invasion. For every second increase in ΔTTP, the probability of thyroid cartilage invasion decreased by 20%. No other parameters were significant in univariate regression analysis; however, *p* values of TTP and PI were close to 0.05. Further two pairs from univariate logistic regression models of TTP + ΔTTP as Model 1 and PI + ΔTTP as Model 2 were analyzed in a multivariate logistic regression. These models did not show statistically significant results in predicting non-ossified thyroid cartilage invasion. The results of the logistic regression analysis are summarized in Table 4.

Table 4. Logistic regression for diagnosis of non-ossified thyroid cartilage invasion.

Univariate Logistic Regression		**Odds Ratio**	**95% CI**	***p* Value**
TTP (1 s)		0.88	0.76–1.01	0.067
PI (1 dB)		1.59	0.97–2.62	0.067
AUC (1 dB × s)		1.03	0.99–1.07	0.103
ΔTTP (1 s)		0.80	0.64–1.00	0.047
Multivariate logistic regression models				
Model 1	TTP (1 s)	1.04	0.87–1.25	0.64
	ΔTTP (1 s)	0.76	0.56–1.05	0.09
Model 2	PI (1 dB)	1.66	0.87–3.14	0.12
	ΔTTP (1 s)	0.82	0.64–1.06	0.12

Abbreviations: TTP = time to peak; PI = peak intensity; AUC = area under curve.

3.5. ROC Analysis of TIC Parameters and Their Combinations

Figure 4 shows the ROC curves generated for statistically significant TIC parameters (TTP, PI, AUC, and ΔTTP). Based on the greatest Youden index, the following cut-off values were obtained: ≤36.3 s for TTP, ≥3.65 dB for PI, ≥18.36 dB × s for AUC, and ≤8.9 s for ΔTTP. Diagnostic performance of all the above-mentioned parameters and their combinations (using cut-off values) were compared (Table 5). ΔTTP (AUCROC = 0.85, 95% CI: 0.68–0.95) and PI (AUCROC = 0.83, 95% CI: 0.65–0.94) were found to have the highest AUCs. ΔTTP with a higher sensitivity (100%) than specificity (76.9%) had a better ability to detect non-ossified thyroid cartilage invasion. Meanwhile, PI and TTP had better ability to exclude non-ossified thyroid cartilage invasion as their specificity reached 88.0% and 88.5%, respectively, but sensitivity was lower (83.3% each). The combination of PI and ΔTTP parameters in Model 2 increased the area under the ROC curve by 8.0% (AUCROC = 0.93, 95% CI: 0.77–0.99) when compared to the parameter with the highest AUCROC (ΔTTP).

Model 2 increased the specificity (ability to exclude non-ossified thyroid cartilage invasion) to 100% and accuracy to 96.8%; however, Model 2's accuracy did not differ significantly from that of the parameter with highest accuracy (87.5% for TTP) ($p = 0.25$).

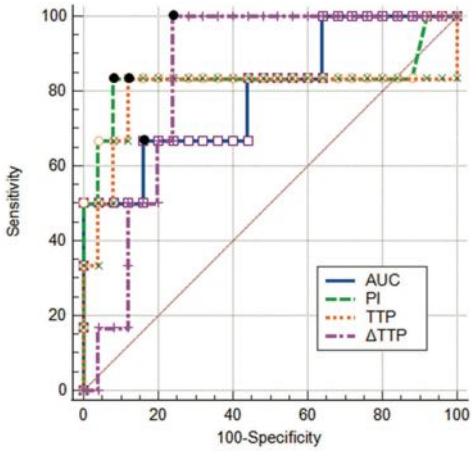

Figure 4. Receiver operating characteristics analysis of the time–intensity curve parameters of non-ossified thyroid cartilage with suspected tumor invasion. PI = peak intensity; AUC = area under the curve; TTP = time to peak; ΔTTP = quantitative difference in TTP between the tumor and the thyroid cartilage; black dots represent the Youden index.

Table 5. Diagnostic performance of TIC perfusion parameters in predicting thyroid cartilage invasion.

Parameter	AUCROC	95% CI	Sensitivity (%)	Specificity (%)	Accuracy (%)	Cut-Off	*p* Value
TTP (s)	0.80	0.62–0.92	83.3	88.5	87.5	≤36.3	0.047
PI (dB)	0.83	0.65–0.94	83.3	88.0	87.1	≥3.65	0.015
AUC (dB × s)	0.79	0.61–0.92	66.7	80.0	77.4	≥18.36	0.008
ΔTTP (s)	0.85	0.68–0.95	100.0	76.9	81.3	≤8.9	<0.001
Model 1 (TTP + ΔTTP)	0.82	0.65–0.93	88.5	76.9	87.5	–	<0.0001
Model 2 (PI + ΔTTP)	0.93	0.77–0.99	83.3	100	96.8	–	<0.0001

Abbreviations: TTP = time to peak; PI = peak intensity; AUC = area under curve; AUCROC = area under the receiver operating characteristic curve.

4. Discussion

In recent years, CEUS has been widely studied, and its application has expanded, especially in the diagnosis and differentiation of tumor types and inflammatory diseases [14,15]. CEUS provides real-time, dynamic imaging with high spatial and temporal resolution, making it a valuable tool for assessing tumor vascularity and perfusion characteristics [26]. Its utility has been demonstrated in various oncological entities, such as liver, breast, and prostate cancers, etc. [27].

However, despite its advantages, there is no current standardized CEUS recommendation for laryngeal cancer staging according to the European Federation of Societies for Ultrasound in Medicine and Biology [14]. Given the lack of established guidelines and the limited scientific literature on this topic, we aimed to investigate the value of quantitative CEUS in assessing the invasion of the non-ossified thyroid cartilage in patients with laryngeal cancer. Specifically, our study focused on quantitative perfusion parameters such as TTP, PI, AUC, and WIS derived from a TIC analysis to explore microcirculatory changes in laryngeal SCC and the non-ossified thyroid cartilage. These findings represent a pioneering approach in utilizing CEUS to evaluate laryngeal SCC and emphasize its value in non-ossified thyroid cartilage perfusion analysis, establishing a basis for further research in this field.

In line with our expectations, we found statistically significant differences in the TIC parameters of thyroid cartilage invasion with high sensitivity and specificity, as follows: TTP (83.3%, 88.5%), PI (83.3%, 88.0%), and ΔTTP (100%, 76.9%). A visual assessment of CEUS discriminated the invaded from the non-invaded non-ossified thyroid cartilage with similar sensitivity (83.3%) and specificity (84.6%). The combination of ΔTTP and PI parameters increased the specificity, reaching 100% in excluding non-ossified thyroid cartilage invasion, while sensitivity for detecting non-ossified thyroid cartilage invasion remained the same as for PI alone. According to our results, CEUS may lead to improved pre-operative staging of the tumoral "T" component in the TNM classification of laryngeal tumors, especially in cases with equivocal CECT and/or MRI findings.

This study was based on the differences in tissue perfusion. Tumor vascularization exhibits distinct differences from normal tissue vascularization. Unlike the orderly and efficient structure of normal vasculature, tumor vessels are highly irregular, disorganized, and leaky, which results in chaotic blood flow and increased permeability. Tumor angiogenesis driven by factors such as tumor angiogenesis factor enables rapid endothelial cell division and new capillary formation, often in response to tumor-specific signals. This abnormal vascular environment can support tumor growth by facilitating nutrient delivery and waste removal, yet it also contributes to the heterogeneous microenvironment observed in a tumor [28]. Because the non-ossified cartilage is considered avascular or poorly vascularized, we can generally expect higher perfusion in areas invaded by a tumor [29,30]. This knowledge has already been employed in the evaluation of laryngeal cartilage invasion in patients with laryngeal carcinoma using multiple radiological imaging modalities [23,24,31–35].

Dynamic contrast-enhanced CT (DCECT), based on tissue perfusion, has been studied in the head and neck field, with the aim of achieving better diagnostic performances. DCECT uses several sequential acquisitions after intravenous contrast administration and calculated tissue perfusion parameters [35]. However, researchers found no significant added benefit of DCECT in assessing cartilage invasion, and the sensitivity of routine CECT was better than that of DCECT (85% and 75%, respectively) [35]. Some results of the latter study are in line with the findings of the study by Trojanowska et al. [33] that reported CECT being superior to DCECT (sensitivity of 66.6% and 33.3%, specificity of 96.5% of 96.5%, PPV of 80.0% and 66.6%, and NPV of 93.33% and 87.5%, respectively) in detecting malignant infiltration into the thyroid cartilage. These results suggest that DCECT is not so suitable for diagnosing laryngeal cartilage invasion as expected.

There is a growing interest in advanced MRI techniques, such as dynamic contrast-enhanced magnetic resonance imaging (DCE-MRI), a noninvasive approach used to assess microvascular perfusion by tracking changes in MRI contrast agents within targeted tissues. Since vascular irregularities are a hallmark of malignant tumors, DCE-MRI has been widely studied for its applications in cancer diagnosis, prognosis, and treatment monitoring [32,36–41]. Additionally, DCE-MRI proves to be effective in distinguishing laryngeal cartilage lesions and accurately assessing neoplastic invasion in the laryngeal cartilage [34]. According to Citil et al., the sensitivity, specificity, and accuracy of DCE-MRI for cartilage involvement was 100% [32]. However, these results need to be confirmed in larger-scale research, highlighting the necessity of further studies.

CEUS is another diagnostic tool that has been employed just in few studies for visual assessment of thyroid cartilage invasion [23,24]. They found that CEUS was superior to CECT and MRI in assessing thyroid cartilage invasion. To the best of our knowledge, we were the first to perform the quantitative analysis of laryngeal SCC and non-ossified thyroid cartilage, by extending the work of Hu et al. [23] and our previous study [24]. A study by Hu et al. reported high sensitivity, specificity, and accuracy of CEUS in the visual detection of thyroid cartilage invasion (92.9%, 87.5%, and 90.0%, respectively); meanwhile, our

quantitative analysis using a combined model of ΔTTP and PI parameters showed higher specificity and accuracy (100% and 96.8%, respectively), but lower sensitivity (83.33%).

In our previous published study [24], CEUS showed a sensitivity of 100%, specificity of 84.0%, and accuracy of 87.1% in the detection of laryngeal cancer invasion into the non-ossified thyroid cartilage. In this study, due to the inclusion and exclusion of some patients, the sensitivity and accuracy of CEUS to discriminate enhancement pattern between non-invaded and invaded non-ossified thyroid cartilage decreased to 83.3% and 84.4%, respectively, while the specificity slightly increased to 84.6%. In the suspected site of cartilage invasion, visual moderate/severe accumulation of contrast agent was observed only in cases with histologically confirmed cartilage invasion. In one of the confirmed cases of cartilage invasion, no visual accumulation of contrast agent in the ROI was seen, resulting in a sensitivity of 83.3%. This could be caused by a human error in not precisely targeting the area of interest or by microinvasion of the inner cartilage plate. In 15.4% of cases without cartilage invasion, poor accumulation was observed, which could be attributed to early ossification phase, hyperemia, or mild peritumoral infiltration, leading to a specificity of 84.6%.

Based on the obtained results, we were the first to determine the values of TIC parameters for laryngeal SCC and the non-ossified thyroid cartilage. This contributes to the scientific literature for future research, as to the best of our knowledge, no similar studies have been published, thus making the comparison difficult. After performing statistical calculations, we obtained several statistically significant TIC parameters in assessing the invasion of thyroid cartilage. In our study, we identified laryngeal SCC and observed a trend demonstrating a relatively rapid accumulation (median TTP of 28.44 s). In contrast, the non-invaded non-ossified thyroid cartilage exhibited a prolonged median TTP as compared to that of the invaded thyroid cartilage (44.40 s and 32.83 s, respectively). These differences were statistically significant. Using a TTP cut-off value of 36.3 s, we can accurately differentiate (87.5%) between the invaded and the non-invaded non-ossified thyroid cartilage with a sensitivity of 83.3% and a specificity of 88.5%.

The maximum signal intensity reached with the contrast agent showed the higher mean PI value for the tumor and the invaded non-ossified thyroid cartilage than that for the non-invaded non-ossified thyroid cartilage (13.59 dB and 12.27 dB vs. 1.85 dB, respectively). The cut-off PI value for distinguishing between the non-invaded and invaded non-ossified thyroid cartilages was 3.65 dB with the sensitivity, specificity, and accuracy of 83.33%, 88.00%, and 87.1%, respectively.

We confirmed our hypothesis that the TIC parameters of the non-ossified thyroid cartilage with and without invasion differ significantly. During the study, we observed a trend indicating that the TIC parameter values of the invaded thyroid cartilage were closer to those of the tumor. Based on this observation, we decided to calculate derived values expressed as the absolute difference between the tumor and cartilage parameters. From all derivates, only ΔTTP differed significantly when comparing the thyroid cartilage without and with tumor invasion. A ROC curve analysis showed that a ΔTTP cut-off value of $\leq$8.9 s can accurately (81.3%) determine non-ossified thyroid cartilage invasion with a sensitivity of 100% and a specificity of 76.9%, suggesting its better ability to detect non-ossified cartilage invasion. As we hypothesized, the logistic regression analysis showed that an increase in the ΔTTP value statistically significantly decreased the probability of invasion. The combination of ΔTTP and PI slightly improved the ability to exclude non-ossified thyroid cartilage invasion with a specificity of 100%. However, an increased accuracy of this combination did not statistically significantly differ from that of the PI parameter. Our results suggest that by utilizing the main TIC parameters—ΔTTP and the combination of ΔTTP, TTP, and PI—we can more confidently rule out the invasion of non-ossified thyroid cartilage.

As the first study of its kind, certain limitations are inherent. First, the study sample size was small, and it was a single-center study. Second, the technique is highly operator-dependent, requiring an experienced professional in CEUS as well as in MRI and CT imaging. Third, motion artifacts were a challenge in patients with an advanced disease as they struggled to maintain shallow breathing or to remain still in a supine position for extended periods. Additionally, the accurate identification of ROI (according to CECT) posed difficulties, and perfusion data were derived from a single tissue slice, which may limit generalizability. Finally, anatomical variations, such as a thin, non-ossified thyroid cartilage, could have influenced TIC parameters due to the small ROI size, increasing sensitivity to movement.

In summary, this study is the first to address the CEUS quantitative analysis of the evaluation of non-ossified thyroid cartilage invasion in patients with laryngeal cancer, providing a critical starting point for further research. Understanding that further research on CEUS is needed, it should focus on larger patient samples and should ideally adopt a multicentric approach to enhance reliability. Additionally, exploring the feasibility of fusing CEUS images with MRI or CT scans may further improve diagnostic accuracy and clinical utility.

5. Conclusions

The results obtained enhance the diagnostic value of the CEUS examination by assessing and utilizing quantitative parameters, particularly a combination of ΔTTP and PI, to rule out and detect non-ossified thyroid cartilage invasion. Our study highlights CEUS as a suitable and easily accessible complementary method to MRI or CT for cases where non-ossified thyroid cartilage invasion remains unclear.

Author Contributions: Conceptualization M.P.; methodology, M.P., S.V., D.M., and S.R.; statistical analysis, R.T.; investigation, M.P., S.V., D.M., S.R., V.Š. and E.P.; data curation, M.P. and R.T.; writing—original draft preparation, M.P.; writing—review and editing, D.M. and S.V.; visualization, M.P., D.M. and R.T.; supervision S.V.; consulting, D.F.; project administration, S.L. All authors have read and agreed to the published version of the manuscript.

Funding: This research received no external funding.

Institutional Review Board Statement: The study was conducted in accordance with the Declaration of Helsinki and approved by Kaunas Regional Biomedical Research Ethics Committee of Lithuanian University of Health Sciences (No. BE-2-121, dated 13 December 2021).

Informed Consent Statement: Informed consent was obtained from all subjects involved in the study.

Data Availability Statement: The data that support the findings of this study are available from the corresponding author upon reasonable request. The data are not publicly available due to privacy or ethical restrictions.

Conflicts of Interest: The authors declare no conflicts of interest.

Abbreviations

The following abbreviations are used in this manuscript:

SCC	Squamous cell carcinoma
CT	Computed tomography
MRI	Magnetic resonance imaging
CEUS	Contrast-enhanced ultrasound
TIC	Time–intensity curve
CECT	Contrast-enhanced computed tomography
ROI	Region of interest
TTP	Time to peak

PI	Peak intensity
WIS	Wash-in slope
AUC	Area under the curve
DCECT	Dynamic contrast-enhanced computed tomography
ROC	Receiver operating characteristic

References

1. Doğan, S.; Vural, A.; Kahriman, G.; İmamoğlu, H.; Abdülrezzak, Ü.; Öztürk, M. Non-squamous cell carcinoma diseases of the larynx: Clinical and imaging findings. *Braz. J. Otorhinolaryngol.* **2020**, *86*, 468–482. [CrossRef] [PubMed]
2. Machiels, J.P.; René Leemans, C.; Golusinski, W.; Grau, C.; Licitra, L.; Gregoire, V. Squamous cell carcinoma of the oral cavity, larynx, oropharynx and hypopharynx: EHNS–ESMO–ESTRO Clinical Practice Guidelines for diagnosis, treatment and follow-up. *Ann. Oncol.* **2020**, *31*, 1462–1475. [CrossRef] [PubMed]
3. Choi, Y.S.; Park, S.G.; Song, E.K.; Cho, S.H.; Park, M.R.; Park, K.U.; Lee, K.-H.; Song, I.-C.; Lee, H.J.; Jo, D.-Y.; et al. Comparison of the therapeutic effects of total laryngectomy and a larynx-preservation approach in patients with T4a laryngeal cancer and thyroid cartilage invasion: A multicenter retrospective review. *Head Neck* **2016**, *38*, 1271–1277. [CrossRef]
4. Connor, S. Laryngeal cancer: How does the radiologist help? *Cancer Imaging* **2007**, *7*, 93–103. [CrossRef] [PubMed]
5. Hermans, R. Staging of laryngeal and hypopharyngeal cancer: Value of imaging studies. *Eur. Radiol.* **2006**, *16*, 2386–2400. [CrossRef]
6. Shoushtari, S.T.; Gal, J.; Chamorey, E.; Schiappa, R.; Dassonville, O.; Poissonnet, G.; Aloi, D.; Barret, M.; Safta, I.; Saada, E.; et al. Salvage vs. Primary Total Laryngectomy in Patients with Locally Advanced Laryngeal or Hypopharyngeal Carcinoma: Oncologic Outcomes and Their Predictive Factors. *J. Clin. Med.* **2023**, *12*, 1305. [CrossRef]
7. Dadfar, N.; Seyyedi, M.; Forghani, R.; Curtin, H.D. Computed Tomography Appearance of Normal Nonossified Thyroid Cartilage Implication for Tumor Invasion Diagnosis. *J. Comput. Assist. Tomogr.* **2015**, *39*, 240–243. Available online: www.jcat.org (accessed on 1 February 2025). [CrossRef]
8. Li, B.; Bobinski, M.; Gandour-Edwards, R.; Farwell, D.G.; Chen, A.M. Overstaging of cartilage invasion by multidetector CT scan for laryngeal cancer and its potential effect on the use of organ preservation with chemoradiation. *Br. J. Radiol.* **2011**, *84*, 64–69. [CrossRef]
9. Kuno, H.; Sakamaki, K.; Fujii, S.; Sekiya, K.; Otani, K.; Hayashi, R.; Yamanaka, T.; Sakai, O.; Kusumoto, M. Comparison of MR imaging and dual-energy ct for the evaluation of cartilage invasion by laryngeal and hypopharyngeal squamous cell carcinoma. *Am. J. Neuroradiol.* **2018**, *39*, 524–531. [CrossRef]
10. Cho, S.J.; Lee, J.H.; Suh, C.H.; Kim, J.Y.; Kim, D.; Lee, J.B.; Lee, M.K.; Chung, S.R.; Choi, Y.J.; Baek, J.H. Comparison of diagnostic performance between CT and MRI for detection of cartilage invasion for primary tumor staging in patients with laryngo-hypopharyngeal cancer: A systematic review and meta-analysis. *Eur. Radiol.* **2020**, *30*, 3803–3812. [CrossRef]
11. Becker, M.; Zbären, P.; Casselman, J.W.; Kohler, R.; Dulguerov, P.; Becker, C.D. Neoplastic invasion of laryngeal cartilage: Reassessment of criteria for diagnosis at MR imaging. *Radiol. Soc. North Am.* **2008**, *249*, 551–559. [CrossRef] [PubMed]
12. Becker, M.; Monnier, Y.; de Vito, C. MR Imaging of Laryngeal and Hypopharyngeal Cancer. *Magn. Reson. Imaging Clin. North Am.* **2022**, *30*, 53–72. [CrossRef] [PubMed]
13. Mohamad, I.; Hejleh, T.A.; Qandeel, M.; Al-Hussaini, M.; Koro, S.; Taqash, A.; Almousa, A.; Abuhijla, F.; Abuhijlih, R.; Ajlouni, F.; et al. Concordance between head and neck MRI and histopathology in detecting laryngeal subsite invasion among patients with laryngeal cancer. *Cancer Imaging* **2023**, *23*, 99. [CrossRef] [PubMed]
14. Sidhu, P.S.; Cantisani, V.; Dietrich, C.F.; Gilja, O.H.; Saftoiu, A.; Bartels, E.; Bertolotto, M.; Calliada, F.; Clevert, D.-A.; Cosgrove, D.; et al. The EFSUMB guidelines and recommendations for the clinical practice of contrast-enhanced ultrasound (CEUS) in non-hepatic applications: Update 2017 (long version). *Ultraschall Der Med.* **2018**, *39*, e2–e44.
15. Dietrich, C.F.; Nolsoe, C.P.; Barr, R.G.; Berzigotti, A.; Burns, P.N.; Cantisani, V.; Chammas, M.C.; Chaubal, N.; Choi, B.I.; Clevert, D.-A.; et al. Guidelines and good clinical practice recommendations for contrast enhanced ultrasound (CEUS) in the liver-Update 2020-WFUMB in cooperation with EFSUMB, AFSUMB, AIUM, and FLAUS. *Ultrasound Med. Biol.* **2020**, *41*, 562–585.
16. Petrasova, H.; Slaisova, R.; Rohan, T.; Stary, K.; Kyclova, J.; Pavlik, T.; Kovalcikova, P.; Kazda, T.; Valek, V. Contrast-Enhanced Ultrasonography for Differential Diagnosis of Benign and Malignant Thyroid Lesions: Single-Institutional Prospective Study of Qualitative and Quantitative CEUS Characteristics. *Contrast Media Mol. Imaging* **2022**, *2022*, 8229445. [CrossRef]
17. Wu, M.; Hu, Y.; Hang, J.; Peng, X.; Mao, C.; Ye, X.; Li, A. Qualitative and Quantitative Contrast-Enhanced Ultrasound Combined with Conventional Ultrasound for Predicting the Malignancy of Soft Tissue Tumors. *Ultrasound Med. Biol.* **2022**, *48*, 237–247. [CrossRef]
18. Badiu, M.S.; Gheorghe, E.C.; Nicolau, C.; Săftoiu, A. Quantitative time intensity curve analysis of contrast-enhanced ultrasound (CEUS) examinations for the assessment of focal liver lesions. *Med. Ultrason.* **2024**, *26*, 63–71. [CrossRef]
19. Schwarz, S.; Clevert, D.A.; Ingrisch, M.; Geyer, T.; Schwarze, V.; Rübenthaler, J.; Armbruster, M. Quantitative analysis of the time–intensity curve of contrast-enhanced ultrasound of the liver: Differentiation of benign and malignant liver lesions. *Diagnostics* **2021**, *11*, 1244. [CrossRef]

20. Chen, L.; Chen, L.; Liu, J.; Wang, B.; Zhang, H. Value of Qualitative and Quantitative Contrast-Enhanced Ultrasound Analysis in Preoperative Diagnosis of Cervical Lymph Node Metastasis From Papillary Thyroid Carcinoma. *J. Ultrasound Med.* **2020**, *39*, 73–81. [CrossRef]
21. Krishnan, Y.; Grodzinsky, A.J. Cartilage diseases. *Matrix Biol.* **2018**, *71–72*, 51–69. [CrossRef] [PubMed]
22. Danišovič, L.; Varga, I.; Zamborský, R.; Böhmer, D. The tissue engineering of articular cartilage: Cells, scaffolds and stimulating factors. *Exp. Biol. Med.* **2012**, *237*, 10–17. [CrossRef] [PubMed]
23. Hu, Q.; Zhu, S.Y.; Liu, R.C.; Zheng, H.Y.; Lun, H.M.; Wei, H.M.; Weng, J.J. Contrast-enhanced ultrasound for the preoperative assessment of laryngeal carcinoma: A preliminary study. *Acta Radiol.* **2021**, *62*, 1016–1024. [CrossRef] [PubMed]
24. Pucėtaitė, M.; Farina, D.; Ryškienė, S.; Mitraitė, D.; Tarasevičius, R.; Lukoševičius, S.; Padervinskis, E.; Vaitkus, S. The Diagnostic Value of CEUS in Assessing Non-Ossified Thyroid Cartilage Invasion in Patients with Laryngeal Squamous Cell Carcinoma. *J. Clin. Med.* **2024**, *13*, 891. [CrossRef]
25. Brierley, J.D.; Gospodarowicz, M.K.; Wittekind, C.H. (Eds.) *TNM Classification of Malignant Tumours*, 8th ed.; Wiley Blackwell: Chichester, UK, 2017; pp. 25–36.
26. Dietrich, C.F.; Averkiou, M.; Nielsen, M.B.; Barr, R.G.; Burns, P.N.; Calliada, F.; Cantisani, V.; Choi, B.; Chammas, M.C.; Clevert, D.-A.; et al. How to perform Contrast-Enhanced Ultrasound (CEUS). *Ultrasound Int. Open* **2018**, *4*, E2–E15. [CrossRef]
27. Jung, E.M.; Weber, M.A.; Wiesinger, I. Contrast-enhanced ultrasound perfusion imaging of organs. *Radiologe* **2021**, *61*, 19–28. Available online: https://link.springer.com/article/10.1007/s00117-021-00891-7 (accessed on 28 December 2024). [CrossRef]
28. Folkman, J. Tumor angiogenesis: Therapeutic implications. *N. Engl. J. Med.* **1971**, *285*, 1182–1186. [CrossRef]
29. Olszewski, E. Blood Vascular System in Cancer of the Larynx. Available online: http://archotol.jamanetwork.com/ (accessed on 1 February 2025).
30. Wangaryattawanich, P.; Agarwal, M.; Rath, T. Imaging features of cartilaginous tumors of the head and neck. *J. Clin. Imaging Sci.* **2021**, *11*, 66. [CrossRef]
31. Yousefzadeh, D.K.; Doerger, K.; Sullivan, C. The blood supply of early, late, and nonossifying cartilage: Preliminary gray-scale and Doppler assessment and their implications. *Pediatr. Radiol.* **2008**, *38*, 146–158. [CrossRef]
32. Citil, S.; Dogan, S.; Atilgan, H.I.; Menzilcioglu, M.S.; Sahin, T.; Abdulrezzak, U.; Duymus, M.; Ozturk, M. Comparison of dynamic contrast-enhanced MRI and PET/CT in the evaluation of laryngeal cancer after inadequate CT results. *Pol. J. Radiol.* **2015**, *80*, 428–432. [CrossRef]
33. Trojanowska, A.; Trojanowski, P.; Drop, A.; Jargiełło, T.; Klatka, J. Head and neck cancer: Value of perfusion CT in depicting primary tumor spread. *Med. Sci. Monit.* **2012**, *18*, CR112–CR118. [CrossRef]
34. Yu, J.; Xu, W.; Wang, L.; Jiang, N.; Dou, W.; Li, C.; Sun, L. The clinical value of DCE-MRI for differentiating secondary laryngeal cartilage lesions. *Medicine* **2023**, *102*, E33352. [CrossRef] [PubMed]
35. Dankbaar, J.W.; Oosterbroek, J.; Jager, E.A.; de Jong, H.W.; Raaijmakers, C.P.; Willems, S.M.; Terhaard, C.H.; Philippens, M.E.; Pameijer, F.A. Detection of cartilage invasion in laryngeal carcinoma with dynamic contrast-enhanced CT. *Laryngoscope Investig. Otolaryngol.* **2017**, *2*, 373–379. [CrossRef] [PubMed]
36. Zheng, D.; Chen, Y.; Liu, X.; Chen, Y.; Xu, L.; Ren, W.; Chen, W.; Chan, Q. Early response to chemoradiotherapy for nasopharyngeal carcinoma treatment: Value of dynamic contrast-enhanced 3.0 T MRI. *J. Magn. Reson. Imaging* **2015**, *41*, 1528–1540. [CrossRef] [PubMed]
37. Zheng, D.; Chen, Y.; Chen, Y.; Xu, L.; Chen, W.; Yao, Y.; Du, Z.; Deng, X.; Chan, Q. Dynamic contrast-enhanced MRI of nasopharyngeal carcinoma: A preliminary study of the correlations between quantitative parameters and clinical stage. *J. Magn. Reson. Imaging* **2014**, *39*, 940–948. [CrossRef]
38. Huang, B.; Wong, C.S.; Whitcher, B.; Kwong, D.L.W.; Lai, V.; Chan, Q.; Khong, P.-L. Dynamic contrast-enhanced magnetic resonance imaging for characterising nasopharyngeal carcinoma: Comparison of semiquantitative and quantitative parameters and correlation with tumour stage. *Eur. Radiol.* **2013**, *23*, 1495–1502. [CrossRef]
39. Zhang, C.C.; Yan, Z.; Giddabasappa, A.; Lappin, P.B.; Painter, C.L.; Zhang, Q.; Li, G.; Goodman, J.; Simmons, B.; Pascual, B.; et al. Comparison of dynamic contrast-enhanced MR, ultrasound and optical imaging modalities to evaluate the antiangiogenic effect of PF-03084014 and sunitinib. *Cancer Med.* **2014**, *3*, 462–471. [CrossRef]
40. Baba, A.; Kurokawa, R.; Rawie, E.; Kurokawa, M.; Ota, Y.; Srinivasan, A. Normalized Parameters of Dynamic Contrast-Enhanced PerfusionMRI and DWI-ADC for Differentiation between Posttreatment Changes and Recurrence in Head and Neck Cancer. *Am. J. Neuroradiol.* **2022**, *43*, 1184–1189. [CrossRef]
41. Ng, S.H.; Liao, C.T.; Lin, C.Y.; Chan, S.C.; Lin, Y.C.; Yen, T.C.; Li, G.; Goodman, J.; Simmons, B.; Pascual, B.; et al. Dynamic contrast-enhanced MRI, diffusion-weighted MRI and 18F-FDG PET/CT for the prediction of survival in oropharyngeal or hypopharyngeal squamous cell carcinoma treated with chemoradiation. *Eur Radiol.* **2016**, *26*, 4162–4172. [CrossRef]

Disclaimer/Publisher's Note: The statements, opinions and data contained in all publications are solely those of the individual author(s) and contributor(s) and not of MDPI and/or the editor(s). MDPI and/or the editor(s) disclaim responsibility for any injury to people or property resulting from any ideas, methods, instructions or products referred to in the content.

A2

Title: The Diagnostic Value of CEUS in Assessing Non-Ossified Thyroid Cartilage Invasion in Patients with Laryngeal Squamous Cell Carcinoma

Authors: Pucėtaitė Milda, Farina Davide, Ryškienė Silvija, Mitraitė Dalia, Tarasevičius Rytis, Lukoševičius Saulius, Padervinskis Evaldas, Vaitkus Saulius.

Journal of Clinical Medicine (2024)

No special permission is required to reuse all or part of article published by MDPI, including table and figures. Furthermore, no special permission is required for authors to submit their work to external repositories (MDPI | Open Access Information)

Journal of
Clinical Medicine

MDPI

Article

The Diagnostic Value of CEUS in Assessing Non-Ossified Thyroid Cartilage Invasion in Patients with Laryngeal Squamous Cell Carcinoma

Milda Pucėtaitė [1,*], Davide Farina [2], Silvija Ryškienė [1], Dalia Mitraitė [1], Rytis Tarasevičius [3], Saulius Lukoševičius [1], Evaldas Padervinskis [4] and Saulius Vaitkus [4]

[1] Department of Radiology, Medical Academy, Lithuanian University of Health Sciences, A. Mickevičiaus Str. 9, 44307 Kaunas, Lithuania; silvija.ryskiene@lsmu.lt (S.R.); dalia.mitraite@lsmu.lt (D.M.)
[2] Department of Radiological Sciences, University of Brescia, Piazzale Spedali Civili 1, 25123 Brescia, Italy; davide.farina@unibs.it
[3] Department of Radiology, Lithuanian University of Health Sciences Kaunas Clinics, Eivenių 2, 50009 Kaunas, Lithuania
[4] Department of Otorhinolaryngology, Medical Academy, Lithuanian University of Health Sciences, A. Mickevičiaus Str. 9, 44307 Kaunas, Lithuania; evaldas.padervinskis@lsmu.lt (E.P.); saulius.vaitkus@lsmu.lt (S.V.)
* Correspondence: milda.pucetaite@lsmu.lt

check for updates

Citation: Pucėtaitė, M.; Farina, D.; Ryškienė, S.; Mitraitė, D.; Tarasevičius, R.; Lukoševičius, S.; Padervinskis, E.; Vaitkus, S. The Diagnostic Value of CEUS in Assessing Non-Ossified Thyroid Cartilage Invasion in Patients with Laryngeal Squamous Cell Carcinoma. *J. Clin. Med.* **2024**, *13*, 891. https://doi.org/10.3390/jcm13030891

Academic Editor: Erich Sorantin

Received: 24 November 2023
Revised: 24 January 2024
Accepted: 30 January 2024
Published: 3 February 2024

Correction Statement: This article has been republished with a minor change. The change does not affect the scientific content of the article and further details are available within the backmatter of the website version of this article.

Copyright: © 2024 by the authors. Licensee MDPI, Basel, Switzerland. This article is an open access article distributed under the terms and conditions of the Creative Commons Attribution (CC BY) license (https://creativecommons.org/licenses/by/4.0/).

Abstract: Background: Accurate assessment of thyroid cartilage invasion in squamous cell carcinoma (SCC) of the larynx remains a challenge in clinical practice. The aim of this study was to assess the diagnostic performance of contrast-enhanced ultrasound (CEUS), contrast-enhanced computed tomography (CECT), and magnetic resonance imaging (MRI) in the detection of non-ossified thyroid cartilage invasion in patients with SCC. **Methods:** CEUS, CECT, and MRI scans of 27 male patients with histologically proven SCC were evaluated and compared. A total of 31 cases were assessed via CEUS and CECT. The MR images of five patients and six cases were excluded (one patient had two suspected sites), leaving twenty-five cases for analysis via MRI. **Results:** CEUS showed the highest accuracy and specificity compared with CECT and MRI (87.1% vs. 64.5% and 76.0% as well as 84.0% vs. 64.0% and 72.7%, respectively). The sensitivity and negative predictive value of CEUS and MRI were the same (100%). CEUS yielded four false-positive findings. However, there were no statistically significant differences among the imaging modalities ($p > 0.05$). **Conclusions:** CEUS showed better diagnostic performance than CECT and MRI. Therefore, CEUS has the potential to accurately assess non-ossified thyroid cartilage invasion and guide appropriate treatment decisions, hopefully leading to improved patient outcomes.

Keywords: non-ossified thyroid cartilage; CEUS; CECT; MRI; laryngeal cancer

1. Introduction

Imaging of the local spread of laryngeal cancer plays an important role in choosing a suitable treatment strategy, such as organ-sparing therapy, radical surgery, or combined therapy. The decision regarding which treatment strategy to employ affects the effectiveness of treatment and quality of life [1–3]. The role of imaging is more crucial in discriminating between T3 and T4 stages than between T1 and T2 stages according to the tumor-node-metastasis (TNM) classification. As reported in the review by Deganello et al. [4], patients with T4 stage tumors have a higher risk of developing lymph node metastases, which also affects both prognosis and treatment planning. Therefore, radiologists often face great challenges in evaluating subtle findings.

Both contrast-enhanced computed tomography (CECT) and magnetic resonance imaging (MRI) are the main and most widely used modalities for laryngeal imaging; most

guidelines leave the choice between the two techniques up to local protocols and scanner availability. In CECT, one of the most controversial issues in the assessment of the tumor invasion of non-ossified thyroid cartilage is a similar post-contrast density of the tumor and the non-ossified thyroid cartilage [5]. In these cases, dual-energy computed tomography (DECT) or MRI may provide added value. In particular, the study published by Becker et al. [6] demonstrated that the application of revised MRI criteria led to an overall statistically significant improvement in the assessment of thyroid cartilage invasion. However, none of the cross-sectional techniques outperform the others on the specific issue of non-ossified thyroid cartilage [5–10].

Contrast-enhanced ultrasound (CEUS) can be used to assess and quantify microcirculation in normal and pathological conditions with a good acoustic window [11]. Moreover, it has been widely used in clinical practice to diagnose hepatic and renal pathologies [12,13]. In a recent publication, CEUS showed potential in assessing non-ossified thyroid cartilage invasion [14]. Non-ossified thyroid cartilage and adjacent laryngeal cancer are well visualized on CEUS due to the differences between non-enhancing non-ossified thyroid cartilage and enhancing adjacent laryngeal cancer. Therefore, the detection of enhancement along the course of a thyroid lamina contacting a tumor suggests infiltration. However, there is currently a lack of studies and data that can strongly support the use of CEUS as an additional imaging modality in the diagnostic algorithms for determining the local spread of laryngeal cancer more accurately.

Therefore, the purpose of this study was to assess the diagnostic value of CEUS, compared with that of CECT and MRI, in the detection of non-ossified thyroid cartilage invasion in SCC of the larynx.

2. Materials and Methods

2.1. Patients

Between 2021 and 2023, a prospective comparative study was carried out at the Hospital of Lithuanian University of Health Sciences Kaunas Clinics. A total of 38 patients with histopathologically proven SCC of the larynx were enrolled in this study. The inclusion criteria were as follows: an available CECT scan demonstrating pathological infiltration adjacent to the non-ossified tract of the thyroid cartilage or its clear infiltration; no history of previous laryngeal–hypopharyngeal surgery or chemoradiation; and having undergone surgery planned after multidisciplinary team discussion. Eleven patients were excluded because they refused surgical treatment or did not attend further consultations or undergo further surgery.

All 27 male patients meeting the inclusion criteria were subjected to CEUS and MRI. Informed consent was obtained from all participants before the study. The study was conducted according to the guidelines of the Declaration of Helsinki. Ethical approval was obtained from Kaunas Regional Biomedical Research Ethics Committee (protocol No. 2021-BE-10-00016; dated 2021).

2.2. CECT Examination

Multislice CT examinations were performed using an Aquilion ONE TSX-301 scanner (Toshiba, Tokyo, Japan) with the following parameters: 120 kVp; specific effective mAs for each patient based on the patient's size and tissue thickness; collimation, 128 × 0.625 mm; field of view, 260 mm; and matrix, 512 × 512. The patients were asked to assume a supine position, breathe quietly, and avoid coughing and swallowing. The field of view was from the skull base to the aortic arch. Scanning was performed without and with intravenous contrast media (65–100 mL) with a 50 mL saline flush to obtain contrast-enhanced images with a 60–80 s delay after administration; the concentration of iodine in the contrast agent was 320–370 mg/mL. Images were reconstructed for axial (parallel to the plane of the true vocal cords), sagittal, and coronal (perpendicular to the plane of the true vocal cords) planes with soft tissue and bone algorithms (2 mm in thickness).

2.3. CEUS Examination

CEUS examination was performed using a Philips Epiq 7 (expert-class) US system (Philips Healthcare, Best, The Netherlands) with a 5–12-MHz linear transducer. The patients were asked to assume the supine position with their necks extended. The larynx and its surrounding structures were evaluated in the transverse and longitudinal sections. The distance between the area of lesion contact to the non-ossified thyroid cartilage seen via CECT and the upper border of the thyroid lamina was measured via CECT and then used as a reference to target the same area through CEUS.

CEUS examination was performed by administering an intravenous bolus of SonoVue (Bracco SpA, Milan, Italy) (5 mL, followed by saline flush) [14]. The scan was performed with a frequency of 12 MHz and a mechanical index of 0.08. The patients were asked to refrain from swallowing and coughing during the examination. Dynamic perfusion of the tumor and peritumoral tissues was observed and recorded in the hard drive of the device for about 1 min. If there was more than one suspected site of invasion, the CEUS procedure was repeated after 10 min.

2.4. MRI Examination

MRI examination was performed using a Philips Ingenia 3.0T scanner (Philips Healthcare, Best, The Netherlands) with dedicated head–neck 20-channel parallel imaging array coils. The patients were imaged in the supine position and asked to breathe quietly and refrain from swallowing and coughing during the scanning. Axial images were captured parallel to the plane of the true vocal cords; coronal images were obtained perpendicular to this plane. The MRI protocol employed is specified in Table 1.

Table 1. MRI protocol.

Sequence	Plane	Slice Thickness, mm	Repetition Time, ms	Time to Echo, ms	Field of View, mm
High-resolution T2-weighted turbo spin echo Dixon	Axial, coronal, sagittal	2.5–3	2888	80	190–210
High-resolution T1-weighted turbo spin echo Dixon	Axial	2.1–2.5	634	8	190–210
DWI and ADC	Axial	2	14,439; 220	66	250
Contrast-enhanced high-resolution T1-weighted turbo spin echo Dixon	Axial, coronal	2.1–2.5	634	8	190–210

DWI, diffusion-weighted imaging; ADC, apparent diffusion coefficient.

2.5. Image Analysis

The analysis of CEUS images was performed by two radiologists with >4 and >20 years of experience, respectively. The findings from the CECT and MRI examinations were interpreted by one head-and-neck radiologist with >20 years of experience in head-and-neck imaging. The radiologists were not blinded to the clinical and CECT information during the analysis of CEUS and MRI images.

2.5.1. CEUS Imaging

CEUS images were evaluated and interpreted by both radiologists during examination and post-processing. The non-ossified thyroid cartilage was considered infiltrated by a tumor when contrast enhancement was observed (Figure 1). When the cases were evaluated, there was no disagreement between the radiologists.

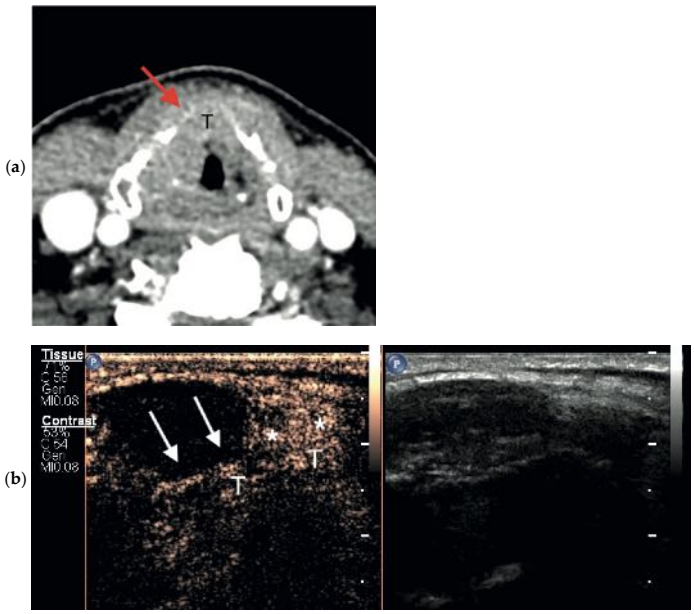

Figure 1. True-positive findings through axial CECT and CEUS. (**a**) In this CECT image, a partial bilateral ossification of the thyroid cartilage with a similar tissue density between the tumor (T) and the non-ossified thyroid cartilage (red arrow) can be seen; (**b**) CEUS image taken after intravenous contrast material administration showing the enhancement of the tumor (T) with invasion of the right anterior part of the non-ossified thyroid cartilage (asterisks); the adjacent hypoechogenic cartilage is non-invaded (white arrows).

2.5.2. Cross-Sectional Imaging

CECT and MRI images were evaluated and interpreted according to previous articles [6,7,9,15].

In CECT images, non-ossified thyroid cartilage invasion was positive when the following criteria were met: a focal cartilage defect in close proximity to the tumor was found; replacement of the cartilage by soft tissue with enhancement matching that adjacent to the cartilage occurred; and the lesion was in direct contact with the thyroid cartilage and densities were indistinguishable (Figure 2). Findings obtained via CECT were considered negative if the densities between the tumor/pathologic infiltration and the non-ossified cartilage were distinguishable.

When conducting MRI, thyroid cartilage invasion was diagnosed when the thyroid lamina showed abnormal signal intensity matching the signal of the tumor in T2-weighted image (T2WI), T1-weighted image (T1WI) (before and after contrast administration), DWI, and ADC map (Figure 3). When the thyroid lamina showed a T2WI signal, enhancement, and an ADC value higher than those of the tumor, the abnormal signal was classified as inflammation.

2.6. Histologic Examination

A pathologist with >20 years of experience evaluated the surgical specimens according to the existing guidelines described elsewhere [16]. To ensure precise correspondence

between radiological findings and pathology, the suspected area of invasion was indicated by radiologists on an anatomical sketch of the larynx that accompanied each specimen.

2.7. Statistical Analysis

The IBM SPSS Statistics 20.0 (IBM Corp. in Armonk, NY, USA) statistical software package was used in this study. Sensitivity, specificity, accuracy, negative predictive value (NPV), and positive predictive value (PPV) of CEUS, CECT, and MRI in evaluating non-ossified laryngeal cartilage involvement were assessed by comparing results with histopathological findings [17,18]. Accuracy was calculated according to the following formula:

$$\text{Accuracy} = \frac{\text{TP} + \text{TN}}{\text{TP} + \text{TN} + \text{FP} + \text{FN}}$$

where TP is true positive; TN denotes true negative; FP denotes false positive; and FN denotes false negative.

McNemar's test was used to compare the accuracy of imaging modalities. A p value of <0.05 was considered statistically significant.

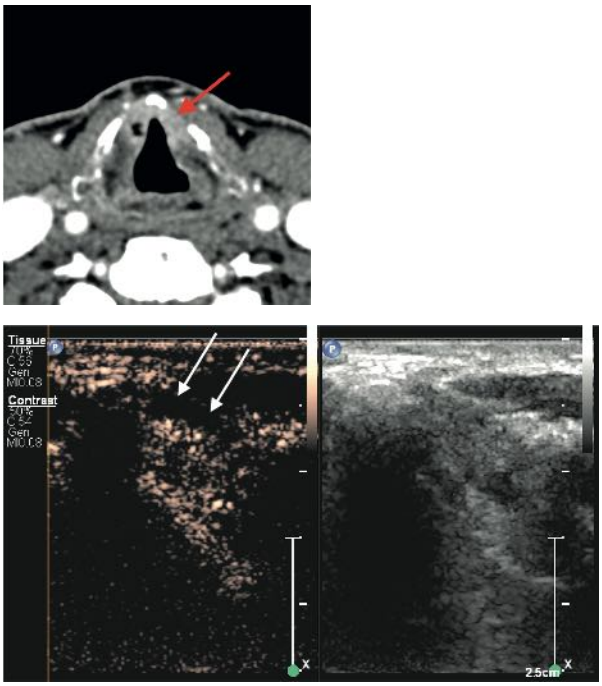

Figure 2. Bilateral glottic cancer adjacent to the non-ossified thyroid cartilage lamina. (**a**) Axial CECT findings on the left side were false-positive for tumor invasion (red arrow). (**b**) CEUS image of the left side at the same level as (**a**) in the transverse plane shows true-negative findings, i.e., non-enhanced non-ossified cartilage (white arrows).

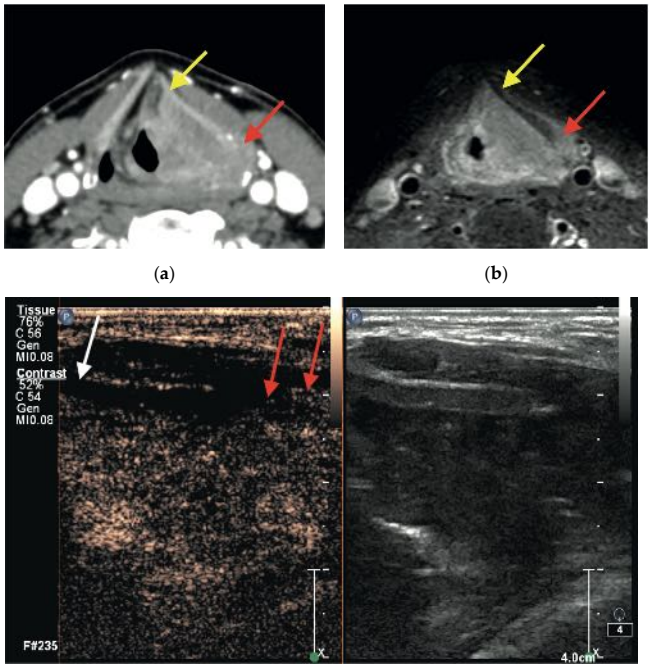

(**a**) (**b**)

(**c**)

Figure 3. Supraglottic squamous cell carcinoma on the left side. (**a**) Axial CECT represents two sites, namely, sites that were false-positive anteriorly (yellow arrow) and true-positive posteriorly (red arrow), whereas MRI (**b**) contrast-enhanced high-resolution T1-weighted turbo spin echo Dixon and CEUS (**c**) findings were true-negative anteriorly (white arrow) and true-positive posteriorly (red arrows), respectively.

3. Results

In this prospective study, 27 male patients with a mean age of 63 years (SD, 8.7; range, 46–84 years) were enrolled.

Overall, there were 31 cases, as four patients had two suspected sites of non-ossified thyroid cartilage invasion. All 31 cases were assessed using CEUS and CECT. The MR images of five patients (corresponding to 6 cases, as one patient had two suspected sites) were non-diagnostic due to major artifacts, leaving 25 cases for analysis via MRI.

There were 14 cases (51.9%) of glottic SCC and 13 cases (48.1%) of transglottic SCC with the majority showing a G2 degree of differentiation (85.2%). The patients' distribution by pT staging is shown in Table 2.

In six cases (19.4%), histological proof of non-ossified thyroid cartilage invasion was obtained. The diagnostic performance of imaging studies is shown in Table 3. There were no statistically significant differences among the modalities ($p > 0.05$). CEUS and MRI showed a NPV of 100%. CEUS had four false-positive findings (Figure 4); however, the PPV was higher than those of CECT and MRI (60% vs. 30.8% and 33.3%, respectively).

Table 2. Distribution of the patients according to pT staging.

pT Group	n (%)
pTis	1 (3.7)
pT1	7 (25.9)
pT2	7 (25.9)
pT3	8 (29.6)
pT4	4 (14.8)

Staging was performed according to the American Joint Committee on Cancer/Union for International Cancer Control (AJCC/UICC), 8th Edition, guidelines.

Table 3. Diagnostic performance of CEUS, CECT, and MRI in the assessment of non-ossified thyroid cartilage invasion.

Imaging Modality	TP, n	TN, n	FP, n	FN, n	Sensitivity, % (95% CI)	Specificity, % (95% CI)	Accuracy, % (95% CI)	PPV, %	NPV, %
CEUS (n = 31)	6	21	4	0	100.0 (54.1–100.0)	84.0 (63.2–95.5)	87.1 (70.2–96.4)	60.0	100.0
CECT (n = 31)	4	16	9	2	66.7 (22.3–95.7)	64.0 (42.5–82.0)	64.5 (45.4–80.8)	30.8	88.9
MRI (n = 25)	3	16	6	0	100.0 (29.2–100.0)	72.7 (49.8–89.3)	76.0 (54.9–90.6)	33.3	100.0

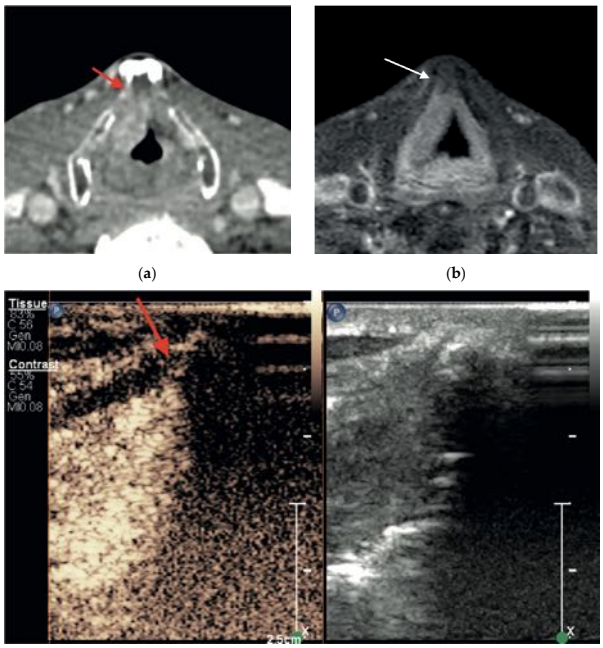

(**a**) (**b**)

(**c**)

Figure 4. Supraglottic squamous cell carcinoma on the right side anteriorly adjacent to non-ossified cartilage inner lamina. (**a**) Axial CECT and (**c**) CEUS findings were false positive (red arrow) for tumor invasion of the thyroid cartilage, whereas MRI findings, as shown in (**b**), in axial contrast-enhanced high-resolution T1-weighted turbo spin echo Dixon images were true negative (white arrow).

There were no statistically significant differences between these imaging modalities ($p > 0.05$). CEUS, contrast-enhanced ultrasound; CECT, contrast-enhanced computed tomography; MRI, magnetic resonance imaging; TP, true positive; TN, true negative; FP, false positive; FN, false negative; PPV, positive predictive value; NPV, negative predictive value.

4. Discussion

In the current study, we aimed at evaluating the diagnostic performance of CEUS, CECT, and MRI in detecting non-ossified thyroid cartilage tumor invasion, taking postoperative histopathological examination as the gold standard. Our results show that based on the presence of enhancement, CEUS allows for the discrimination of invaded (i.e., enhancing) from normal (i.e., non-enhancing) non-ossified thyroid cartilage. CEUS, CECT, and MRI evaluation demonstrated high accuracy (87.1%, 64.5%, and 76%, respectively) with minor differences. Moreover, CEUS was slightly superior to other modalities employed in this study in detecting non-ossified thyroid cartilage tumor invasion.

The detection of laryngeal cartilage invasion can significantly influence the choice of optimal treatment strategy and the prognosis of SCC of the larynx. Currently, the choice of optimal treatment strategy is controversial. However, in the case of thyroid cartilage invasion or its suspicion, transoral laryngeal microsurgery (TOLMS) should be ruled out due to possible non-radical tumor removal, and in such cases, open partial horizontal laryngectomy (OPHL), total laryngectomy, or non-surgical treatments should be considered [2,3,19–21]. In addition, deep tumor invasion into the thyroid cartilage leads to negative outcomes through treatment with radiation therapy [21]. Therefore, for the selection of an optimal treatment plan avoiding complications and incomplete resection as well as improving disease control and survival, an accurate clinical and radiological assessment of local spread, especially the most controversial invasion of the cartilage, is necessary.

Cross-sectional imaging with multi-slice CT or MRI is designed to map deep tumor spread to the submucosal soft tissues and cartilaginous framework. CECT examination can be quickly performed, is widely available, and allows volumetric acquisition with a submillimetric voxel size: the short acquisition time minimizes the risk of motion artifacts, while the high spatial resolution allows the detection of subtle areas of tumor invasion of soft tissue spaces and cartilage [9,22,23].

MRI has higher contrast resolution, which is boosted by the possibility of combining different pulse sequences. In the literature, this potential has mainly been exploited to assess cartilage invasion [6,24], and MRI is reported to have significantly higher sensitivity than CECT for cartilage invasion [22]. A recent meta-analysis of studies involving patients with laryngo–hypopharyngeal cancer reported pooled sensitivities of 88% for MRI and 66% for CT, with specificities of 81% and 90%, respectively, in the detection of cartilage invasion [22]. Expectedly, CT's performance was more heterogeneous than that of MRI, as it differed when taking into account which type of cartilage was involved: when only thyroid cartilage was analyzed, the sensitivity was 69%, which was close to that in our study (66%), but the specificity was higher (86% vs. 64%). Based on the results of the above-mentioned meta-analysis and our current study, we can assume that the diagnosis of thyroid cartilage invasion poses significant challenges that are better handled by MRI than CT.

However, most studies evaluating the diagnostic performance of imaging techniques in the detection of cartilage invasion tend to focus—intentionally or unintentionally—on the ossified cartilage. This occurs for several reasons: first, because, in most cases, invasion involves the ossified parts, and second, because CT and MRI better visualize the invasion of ossified cartilage, manifesting with a panel of findings including sclerosis, erosion, or destruction with cartilage replacement by tumor tissue [5]. This is mainly due to the lack of differences in density in CT images between the tumor and the non-ossified thyroid cartilage and because of the overlapping features of the tumor and non-neoplastic changes such as reactive inflammation, edema, and fibrosis in MRI images [22,24]. Peritumoral

inflammation is another potential confounding factor at the interface between a tumor and cartilage, although the combination of different sequences may improve differentiation when conducting MRI.

DECT is another promising imaging modality that has been analyzed in recent years. One research group [25] used DECT to evaluate the spectral attenuation curves of tumor tissue and non-ossified thyroid cartilage. Virtual monochromatic images (VMIs) of different energy levels showed that tumor tissue density dropped in higher-kiloelectron-volt VMIs, while the non-ossified cartilage maintained high attenuation, allowing distinguishment between the two. However, this study did not directly evaluate non-ossified cartilage invasion by tumor tissue.

US was also previously investigated for its possible role in solving the problem of thyroid cartilage invasion. Indeed, US seemed to uniquely take a place among cross-sectional modalities for evaluating non-ossified cartilage invasion, as the larynx is a superficial structure, and because it best visualizes the non-ossified parts, which present the most diagnostic challenges when conducting CT and MRI scans [14,26,27]. One study involving 62 patients with laryngeal or hypopharyngeal cancer showed that US and CECT had sensitivities of 98% and 91%, respectively, and equal specificities of 75% [26]. The authors speculated that clear visualization of the fat plane between the tumor and the cartilage as well as independent movement of the thyroid cartilage and adjacent tumor tissues contributed to the higher sensitivity of US [26]. The results of the previously mentioned studies prompted the cited researchers to further analyze the possibilities of US examination by incorporating CEUS.

Our study aligns with the study by Hu et al. [14] in terms of showing a higher accuracy of CEUS than CECT (90% and 83%, respectively) in detecting thyroid cartilage invasion, even though there were the following relevant differences in the methodological part: In our study, the exact site of possible non-ossified thyroid cartilage invasion as indicated by CECT examination was further investigated using CEUS and MRI and postoperative histopathological examination. Moreover, the radiologist who carried out the CEUS and MRI examinations and the pathologist were not blinded to the CECT findings. To the best of our knowledge, this is the first study comparing CEUS, CECT, and MRI regarding the specific topic of non-ossified cartilage invasion. Although we did not observe statistically significant differences among the three imaging modalities ($p > 0.05$), based on the promising results, we suggest that CEUS may be considered a usable imaging modality complementary to CECT and MRI for the assessment of non-ossified thyroid cartilage in the non-infrequent event of equivocal CECT and/or MRI findings. One of the limitations of this study is its small sample size. A second limitation is that the CECT and MRI images were assessed by a single expert/observer. Moreover, in our practice, in some cases, matching the suspected site seen in CECT images to the site observed in CEUS images was difficult due to the small region of interest. In the future, this issue could be solved by fusing CECT with US, and this should be performed by a head-and-neck radiologist due to their comprehensive knowledge of laryngeal anatomy and CECT imaging. Moreover, only one region of interest can be investigated at a time; therefore, we reinjected a contrast agent for the evaluation of another site of tumor invasion, leading to the extended examination time.

5. Conclusions

CEUS showed slightly higher diagnostic values in the detection of non-ossified thyroid cartilage invasion in laryngeal and hypopharyngeal cancer than CECT and MRI. This may result in CEUS being an important problem-solving tool in routine clinical practice that can be used to confidently assess non-ossified thyroid cartilage invasion and guide appropriate treatment decisions, hopefully leading to improved patient outcomes. Further studies are needed to increase the number of observations and confirm the evidence obtained.

Author Contributions: Conceptualization M.P.; methodology, M.P., S.V. and S.R.; statistical analysis, R.T.; investigation, M.P., S.V., D.M., S.R. and E.P.; data curation, M.P. and R.T.; writing—original draft preparation, M.P.; writing—review and editing, D.F. and S.R.; visualization, M.P., S.R. and D.M.; supervision S.V.; consulting, D.F.; project administration, S.L. All authors have read and agreed to the published version of the manuscript.

Funding: This research received no external funding.

Institutional Review Board Statement: The current study was conducted according to the guidelines of the Declaration of Helsinki. Ethical approval was obtained from Kaunas Regional Biomedical Research Ethics Committee (protocol No. 2021-BE-10-00016; dated 2021).

Informed Consent Statement: Informed consent was obtained from all subjects involved in the study.

Data Availability Statement: The data that support the findings of this study are available from the corresponding author upon reasonable request. The data are not publicly available due to privacy or ethical restrictions.

Conflicts of Interest: The authors declare no conflicts of interest.

References

1. Shoushtari, S.T.; Gal, J.; Chamorey, E.; Schiappa, R.; Dassonville, O.; Poissonnet, G.; Aloi, D.; Barret, M.; Safta, I.; Saada, E.; et al. Salvage vs. Primary Total Laryngectomy in Patients with Locally Advanced Laryngeal or Hypopharyngeal Carcinoma: Oncologic Outcomes and Their Predictive Factors. *J. Clin. Med.* **2023**, *12*, 1305. [CrossRef]
2. Connor, S. Laryngeal cancer: How does the radiologist help? *Cancer Imaging* **2007**, *7*, 93–103. [CrossRef]
3. Hermans, R. Staging of laryngeal and hypopharyngeal cancer: Value of imaging studies. *Eur. Radiol.* **2006**, *16*, 2386–2400. [CrossRef]
4. Deganello, A.; Ruaro, A.; Gualtieri, T.; Berretti, G.; Rampinelli, V.; Borsetto, D.; Russo, S.; Boscolo-Rizzo, P.; Ferrari, M.; Bussu, F. Central Compartment Neck Dissection in Laryngeal and Hypopharyngeal Squamous Cell Carcinoma: Clinical Considerations. *Cancers* **2023**, *15*, 804. [CrossRef] [PubMed]
5. Dadfar, N.; Seyyedi, M.; Forghani, R.; Curtin, H.D. Computed Tomography Appearance of Normal Nonossified Thyroid Cartilage Implication for Tumor Invasion Diagnosis. *J. Comput. Assist. Tomogr.* **2015**, *39*, 240–243. [CrossRef] [PubMed]
6. Becker, M.; Zbären, P.; Casselman, J.W.; Kohler, R.; Dulguerov, P.; Becker, C.D. Neoplastic invasion of laryngeal cartilage: Reassessment of criteria for diagnosis at MR imaging. *Radiology* **2008**, *249*, 551–559. [CrossRef]
7. Becker, M.; Burkhardt, K.; Dulguerov, P.; Allal, A. Imaging of the larynx and hypopharynx. *Eur. J. Radiol.* **2008**, *66*, 460–479. [CrossRef]
8. Dankbaar, J.W.; Oosterbroek, J.; Jager, E.A.; de Jong, H.W.; Raaijmakers, C.P.; Willems, S.M.; Terhaard, C.H.; Philippens, M.E.; Pameijer, F.A. Detection of cartilage invasion in laryngeal carcinoma with dynamic contrast-enhanced CT. *Laryngoscope Investig. Otolaryngol.* **2017**, *2*, 373–379. [CrossRef]
9. Kuno, H.; Onaya, H.; Fujii, S.; Ojiri, H.; Otani, K.; Satake, M. Primary staging of laryngeal and hypopharyngeal cancer: CT, MR imaging and dual-energy CT. *Eur. J. Radiol.* **2014**, *83*, e23–e35. [CrossRef]
10. Li, B.; Bobinski, M.; Gandour-Edwards, R.; Farwell, D.G.; Chen, A.M. Overstaging of cartilage invasion by multidetector CT scan for laryngeal cancer and its potential effect on the use of organ preservation with chemoradiation. *Br. J. Radiol.* **2011**, *84*, 64–69. [CrossRef] [PubMed]
11. Tamas-Szora, A.; Badea, A.F.; Opincariu, I.; Badea, R.I. Noninvasive Evaluation of Microcirculation under Normal and Pathological Conditions Using Contrast-Enhanced Ultrasonography (CEUS). In *Microcirculation Revisited—From Molecules to Clinical Practice*; InTech: Vienna, Austria, 2016.
12. D'Onofrio, M.; Crosara, S.; De Robertis, R.; Canestrini, S.; Mucelli, R.P. Contrast-enhanced ultrasound of focal liver lesions. *Am. J. Roentgenol.* **2015**, *205*, W56–W66. [CrossRef] [PubMed]
13. Furrer, M.A.; Spycher, S.C.; Büttiker, S.M.; Gross, T.; Bosshard, P.; Thalmann, G.N.; Schneider, M.P.; Roth, B. Comparison of the Diagnostic Performance of Contrast-enhanced Ultrasound with That of Contrast-enhanced Computed Tomography and Contrast-enhanced Magnetic Resonance Imaging in the Evaluation of Renal Masses: A Systematic Review and Meta-analysis. *Eur. Urol. Oncol.* **2020**, *3*, 464–473. [CrossRef] [PubMed]
14. Hu, Q.; Zhu, S.Y.; Liu, R.C.; Zheng, H.Y.; Lun, H.M.; Wei, H.M.; Weng, J.J. Contrast-enhanced ultrasound for the preoperative assessment of laryngeal carcinoma: A preliminary study. *Acta Radiol.* **2021**, *62*, 1016–1024. [CrossRef] [PubMed]
15. Maroldi, R.; Ravanelli, M.; Farina, D. Magnetic resonance for laryngeal cancer. *Curr. Opin. Otolaryngol. Head Neck Surg.* **2014**, *22*, 131–139. [CrossRef] [PubMed]
16. Westra, W.H. *Surgical Pathology Dissection: An Illustrated Guide*, 2nd ed.; Springer: New York, NY, USA, 2003; pp. 38–42.
17. Šimundić, A.M. Measures of Diagnostic Accuracy: Basic Definitions. *EJIFCC* **2009**, *19*, 203–211. [PubMed]
18. Baratloo, A.; Hosseini, M.; Negida, A.; El Ashal, G. Part 1: Simple Definition and Calculation of Accuracy, Sensitivity and Specificity. *Emergency* **2015**, *3*, 48–49.

19. Scherl, C.; Mantsopoulos, K.; Semrau, S.; Fietkau, R.; Kapsreiter, M.; Koch, M.; Traxdorf, M.; Grundtner, P.; Iro, H. Management of advanced hypopharyngeal and laryngeal cancer with and without cartilage invasion. *Auris Nasus Larynx* **2017**, *44*, 333–339. [CrossRef]
20. Chiesa-Estomba, C.M.; Ravanelli, M.; Farina, D.; Remacle, M.; Simo, R.; Peretti, G.; Sjogren, E.; Sistiaga-Suarez, J.A.; Gónzalez-García, J.A.; Larruscain, E.; et al. Imaging checklist for preoperative evaluation of laryngeal tumors to be treated by transoral microsurgery: Guidelines from the European Laryngological Society. *Eur. Arch. Oto-Rhino-Laryngol.* **2020**, *277*, 1707–1714. [CrossRef]
21. Obid, R.; Redlich, M.; Tomeh, C. *The Treatment of Laryngeal Cancer. Oral and Maxillofacial Surgery Clinics of North America*; W.B. Saunders: Philadelphia, PA, USA, 2019; Volume 31, pp. 1–11.
22. Cho, S.J.; Lee, J.H.; Suh, C.H.; Kim, J.Y.; Kim, D.; Bin Lee, J.; Lee, M.K.; Chung, S.R.; Choi, Y.J.; Baek, J.H. Comparison of diagnostic performance between CT and MRI for detection of cartilage invasion for primary tumor staging in patients with laryngo-hypopharyngeal cancer: A systematic review and meta-analysis. *Eur. Radiol.* **2020**, *30*, 3803–3812. [CrossRef]
23. Juliano, A.; Moonis, G. Computed Tomography Versus Magnetic Resonance in Head and Neck Cancer: When to Use What and Image Optimization Strategies. *Magn. Reson. Imaging Clin. N. Am.* **2018**, *26*, 63–84. [CrossRef] [PubMed]
24. Becker, M.; Monnier, Y.; de Vito, C. MR Imaging of Laryngeal and Hypopharyngeal Cancer. *Magn. Reson. Imaging Clin. N. Am.* **2022**, *30*, 53–72. [CrossRef] [PubMed]
25. Forghani, R.; Levental, M.; Gupta, R.; Lam, S.; Dadfar, N.; Curtin, H. Different spectral Hounsfield unit curve and high-energy virtual monochromatic image characteristics of squamous cell carcinoma compared with nonossified thyroid cartilage. *Am. J. Neuroradiol.* **2015**, *36*, 1194–1200. [CrossRef]
26. Dhoot, N.M.; Choudhury, B.; Kataki, A.C.; Kakoti, L.; Ahmed, S.; Sharma, J. Effectiveness of ultrasonography and computed to-mography in assessing thyroid cartilage invasion in laryngeal and hypopharyngeal cancers. *J. Ultrasound* **2017**, *20*, 205–211. [CrossRef] [PubMed]
27. Xia, C.-X.; Zhu, Q.; Zhao, H.-X.; Yan, F.; Li, S.-L.; Zhang, S.-M. Usefulness of ultrasonography in assessment of laryngeal carcinoma. *Br. J. Radiol.* **2013**, *86*, 20130343. [CrossRef] [PubMed]

Disclaimer/Publisher's Note: The statements, opinions and data contained in all publications are solely those of the individual author(s) and contributor(s) and not of MDPI and/or the editor(s). MDPI and/or the editor(s) disclaim responsibility for any injury to people or property resulting from any ideas, methods, instructions or products referred to in the content.

APPENDICES

Appendix 1

Lokalaus išplitimo ištyrimo schema

PILDO RADIOLOGAS

Paciento KK kodas: **a.k:**

Deš.

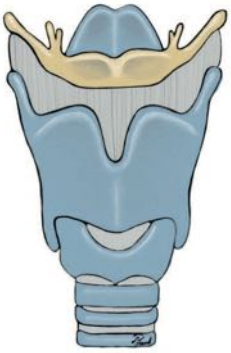

Kair.

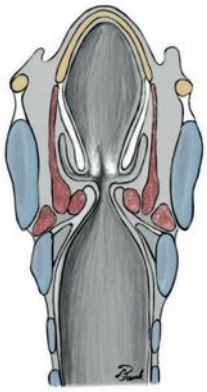

1 ir 2 pav. Pažymėti skydinės kremzlės esamo/įtariamo pažeidimo vietą. 3pav. pažymėti pažeidimo aukštį gerklų atžvilgiu.

Kremzlės pažeidimas: nėra □ yra □ įtariamas □

Pusė: dešinė □ kairė □

Trečdaliai: priekinis □ vidurinis □ užpakalinis □

Kremzlės pažeidimo pobūdis:

Infiltracija □ Invazija □ Penetracija □

Kremzlės dalis: neosifikuota □ osifikuota □

Nuo tikrųjų balso klosčių (TBK): aukštyn □ žemyn □ BK aukštyje □

Nuo TBK cm: _____

Papildoma informacija: .....

Papildomi klausimai patologui:

KT tyrime:

Infiltracija – pažeidimas vetinamas, kai ties kremzlės vidinės plokštelės dalimi betarpiškai stebėti navikiniai pakitimai arba šios dalies abejotini struktūros pokyčiai.

Invazija – pažeista vidinė kremzlės plokštelė, tačiau nėra aiškiaus išorinės plokštelės pažeidimo.

Penetracija – vidinės ir išorinės kremzlės plokštelių pažeidimas be ir su navikinių masių plitimu į ekstralaringinius audinius.

Appendix 2

PATVIRTINTA
Lietuvos bioetikos komiteto
biomedicininių tyrimų ekspertų grupės
2016 m. lapkričio 15 d. sprendimu
PAKEISTA
Lietuvos bioetikos komiteto
biomedicininių tyrimų ekspertų grupės
2020 m. birželio 16 d. sprendimu

Informuoto asmens sutikimo forma, versija Nr. 3, data: 2021 12 13

INFORMUOTO ASMENS SUTIKIMO FORMA

Biomedicininio tyrimo pavadinimas: Pacientų, sergančių gerklų ir gerklaryklės vėžiu ultragarsinio tyrimo be ir su intraveniniu kontrastavimu diagnostinė reikšmė, vertinant lokalų naviko išplitimą.

Protokolo Nr.: 001

Užsakovas: Lietuvos sveikatos mokslų universitetas

Užsakovo atstovas: Prof. Hab. Dr. Vaiva Lesauskaitė

LSMU asmens duomenų pareigūno kontaktai : Jūratė Karpavičienė

Adresas: A. Mickevičiaus g. 7, Kaunas,

Tel nr: + 37063071046,

El. paštas: jurate. karpaviciene@lsmu.lt

Atsakingas tyrėjas[1]: Prof. Dr. Saulius Vaitkus

Tyrimo centro pavadinimas: Lietuvos sveikatos mokslų universiteto ligoninė, Kauno klinikos.

Kauno klinikų asmens duomenų pareigūno kontaktai : Tomas Kuzmarskas

Adresas: Eivenių g. 2, Kaunas,

Tel. nr: +37037326268,

El. paštas: tomas.kuzmarskas@kaunoklinikos.lt.

[1] Jeigu tyrėjo adresas nesutampa su tyrimo centro adresu – nurodykite abu

1. Kokia šio dokumento paskirtis?

Šioje formoje pateikiama Jums skirta informacija apie biomedicininį tyrimą, aptariamos tyrimo atlikimo priežastys, mokslinio tyrimo procedūros, nauda, rizika, galimi nepatogumai ir kita svarbi informacija. Jei nuspręsite dalyvauti, prašysime Jūsų pasirašyti šią sutikimo formą, kuria sutinkate tyrimo metu vykdyti gydytojo tyrėjo ir tyrimo komandos nurodymus. Pasirašydami šį dokumentą, sutinkate dalyvauti moksliniame tyrime. Neskubėkite ir atidžiai perskaitykite šį dokumentą, jei nesupratote kokio nors žodžio ar teiginio, visus iškilusius klausimus būtinai užduokite tyrimo gydytojui ar kitiems tyrimo komandos nariams. Prieš priimdami sprendimą, galite pasitarti su šeimos nariais, draugais ar savo gydytoju.

2. Kodėl atliekami biomedicininiai tyrimai?

Svarbu suprasti, kad nors biomedicininio tyrimo metu Jums bus skiriamos medicininės procedūros, biomedicininis tyrimas iš esmės skiriasi nuo įprastos (kasdienės) klinikinės praktikos. Įprastos (kasdienės) klinikinės praktikos tikslas yra Jus (t. y. konkretų asmenį, pacientą) išgydyti ir/ar pagerinti Jūsų sveikatos būklę. Pagrindinis biomedicininio (mokslinio) tyrimo tikslas – gauti naujų medicinos mokslo žinių, kurios ateityje padėtų kitų šia liga sergančių pacientų sveikatai. Kitaip tariant, pagrindinis šio tyrimo tikslas nėra tiesioginė nauda Jūsų sveikatai.

3.Kodėl atliekamas šis tyrimas?

Šio tyrimo tikslas – nustatyti ir palyginti ultragarso (UG) be ir su intraveniniu (i/v) kontrastavimu, kompiuterinės tomografijos (KT), magnetinio rezonanso tomografijos (MRT) be ir su i/v kontrastavimu diagnostines vertes, vertinant lokalų gerklų ir gerklaryklės vėžio (GGV) išplitimą. Nors sparčiai tobulėjant gydymo ir diagnostikos technologijoms pacientų sergančių gerklų ir gerklaryklės vėžiu mirštamumas siekia 60 proc., o šiuolaikinių radiologinių tyrimų tikslumas, vertinat lokalaus naviko išplitimo ribas nėra toks aukštas. Todėl GGV lokalaus išplitimo diagnostika išlieka rimta problema, lemianti optimalaus gydymo pasirinkimą, paciento gyvenimo kokybę ir išgyvenamumą. Klinikinėje ir mokslinėje praktikoje vis dar ieškoma naujų radiologinio tyrimo metodų, leidžiančių tiksliau stadijuoti gerklų ir gerklaryklės vėžį.

Šiuo metu gana plačiai ir sėkmingai taikomas UG tyrimas su intravenine kontrastine medžiaga, diferencijuojant kepenų, kasos, inkstų darinius. Pagrindinis tyrimo uždavinys - nustatyti kontrastinio UG tyrimo specifiškumą ir jautrumą, lyginant su KT ir MRT, vertinant gerklų ir gerklaryklės vėžio lokalų išplitimą. Šis diagnostinis metodas, nustatant ar patikslinant lokalų vėžio išplitimą, būtų KT papildantis, naujas, pigesnis, bei mažiau nuo kvėpavimo artefaktų priklausantis tyrimo metodas, lyginant su MRT.

4. Kokie asmenys pasirenkami dalyvauti šiame tyrime?

Kviečiame Jus dalyvauti biomedicininiame tyrime, nes esate gerklų ir gerklaryklės vėžio įtarimo grupėje ar jau histologiškai patvirtinto gerklų ir gerklaryklės vėžio grupėje ir atitinkate pagrindinius išvardytus įtraukimo į tyrimą kriterijus.

Pagrindiniai įtraukimo į šį tyrimą kriterijai yra šie: 1. Įtariamas ar patvirtintas gerklų ir gerklaryklės navikinis procesas. 2. Anksčiau nėra diagnozuotas ar gydytas gerklų ir gerklaryklės vėžys. 3. Vyras vyresnis nei 18 metų amžiaus.

5. Kas atlieka/užsako šį biomedicininį tyrimą?

Šio biomedicininio tyrimo užsakovas yra Lietuvos sveikatos mokslų universiteto Kauno klinikų Radiologijos klinika. Šiam tyrimui atlikti reikalingos papildomos lėšos bus skiriamos iš LSMU KK Radiologijos klinikos klinikinių tyrimų lėšų, Lietuvos sveikatos mokslų universiteto Mokslo Fondo.

6. Tikimybė patekti į skirtingas tiriamųjų grupes ir dalyvavimo šiose grupėse ypatybės.

Šiame moksliniame tyrime pacientai vyrai, kuriems įtariamas ir/ar patvirtintas gerklų ir gerklaryklės vėžys, nebus išskiriami į skirtingas grupes, galinčias įtakoti jų gydymo pasirinkimą ir eigą. Palyginamoji kontrolinė grupė bus sudaryta iš pacientų, kuriems nenustatyta gerklų ir gerklaryklės patologija, tačiau dėl kitų priežaščių rutiniškai atliktas KT tyrimas.

7. Kiek truks Jūsų dalyvavimas šiame tyrime?

Bendra tyrimo trukmė – 10 metų. Jūs dalyvausite 3-6 savaites, t. y., kai pasirašysite informuoto asmens sutikimo formą, tiek kiek įprastai laiko užtrunka nuo pirmo radiologinio tyrimo atlikimo iki operacinio gydymo pradžios, remiantis esama praktika. Papildomai pas gydantį gydytoją nei įprastai atvykti nereikės.

8. Kokiose šalyse bus vykdomas šis tyrimas?

Tyrimas bus atliekamas Lietuvoje.

9. Kiek tiriamųjų dalyvaus numatyta šiame tyrime?

Tikimasi, kad šiame biomedicininiame tyrime dalyvaus 183 žmonių.

Numatyta įtraukti 122 pacientus sergančius gerklų ir gerklaryklės vėžiu.

Į kontrolinę grupę įtraukiami pacientai santykiu 1:2 lyginant su tiriamąja grupe. Planuojama įtraukti - 61.

10. Ką Jums reikės daryti?

Prašome leisti naudotis Jūsų medicininiais dokumentais (ligos istorija), kuriais remiantis bus renkami duomenys apie gerklų ir gerklaryklės pakitimus, gyvenimo kokybę.

Jei sutiksite dalyvauti tyrime, Jums nereikės papildomai atvykti.

Tyrimo metu bus atliekami rutininiai KT ir MRT tyrimai, bei papildomas kontrastinis UG tyrimas, kuris įprastai nebūtų atliekamas pacientams sergantiems gerklų ir gerklaryklės vėžiu.

Įprastai kontrastinis UG tyrimas trunka apie 20-40 min., bet atliekant šį biomedicininį tyrimą reikia surinkti daugiau informacijos, todėl prašytume Jūsų leisti atlikti 10 min. ilgiau trunkančią procedūrą.

11. Ar dalyvavimas biomedicininiame tyrime Jums bus naudingas?

Jums bus atliekamas papildomas kontrastinis UG tyrimas, galimai suteiksiantis papildomos vertingos informacijos, apie Jūsų ligą, bet nebūtinai. Papildomas tyrimas Jūsų sveikatai jokios įtakos neturės. Tyrimo metu gauta informacija mokslininkams padės sukurti patikimiausią gerklų ir gerklaryklės vėžio lokalaus išplitimo diagnostikos protokolą, kuris ateityje gali būti naudingas šia liga sergantiems pacientams.

12. Kokia su dalyvavimu šiame tyrime susijusi rizika ir nepatogumai?

Dalyvaudami šiame tyrime galite patirti ir kitų nepatogumų, tokių kaip sugaištas laikas vykstant į tyrimo vietą, nemalonios asociacijos, psichologinis diskomfortas.

Atliekant papildomą kontrastinį UG tyrimą intraveninės injekcijos vietoje galite jausti nedidelį diskofortą, paraudimą, kuris praeina savaime. Ultragarsinių tyrimų kontrastinės medžiagos paprastai yra saugios, dauguma reakcijų yra nesunkios (pvz., galvos skausmas, pykinimas, karščio pojūtis, pakitęs skonio pojūtis) ir praeina savaime. Sunkesnės reakcijos pasireiškia retai ir yra panašios į medžiagų, pagamintų jodo ir gadolinio pagrindu, sukeliamas reakcijas t.y, dilgėlinė, niežėjimas, paraudimas, pykinimas, nedidelis vėmimas, nerimas, vazovaginė reakcija, sunkiais atvejais: aritmija, traukuliai, hipotenzinis šokas, kvėpavimo sustojimas, širdies sustojimas.

Tyrime dalyvaujantiems pacientams neskiriamas joks papildomas gydymas galintis neigiamai paveikti ligos ar gydymo eigą.

Jei dėl nenumatytų aplinkybių (force majore ar nenugalima jėga, trečiųjų asmenų nusikalstamos veikos ir pan.), kurios tyrėjui nėra žinomos ir kurioms įtakos tyrėjas negali daryti, konfidenciali informacija taptų prieinama tretiesiems asmenims, kuriems ją suteikti nebuvote davęs sutikimo, tyrėjas iš karto Jus apie tai informuos. Tačiau tyrėjas visais būdais stengsis užtikrinti, kad Jūsų asmens duomenys, tvarkomi šio biomedicininio tyrimo tikslu, nebūtų prieinami tretiesiems asmenims, kuriems jos suteikti nebuvote davęs sutikimo ir įgyvendins–duomenų saugumo priemones, skirtas apsaugoti asmens duomenis nuo atsitiktinio ar neteisėto atskleidimo, taip pat nuo bet kokio kito neteisėto tvarkymo.

13. Jei atsitiktų kas nors negero? (Informacija apie draudimą)

Šio biomedicininio tyrimo metu bus taikomi tik neintervenciniai tyrimo metodai, kurie nekelia

rizikos Jūsų sveikatai, todėl biomedicininis tyrimas nėra apdraustas biomedicininio tyrimo užsakovų ir pagrindinių tyrėjų civilinės atsakomybės draudimu.

Jūs turite teisę į žalos sveikatai ir su tuo susijusios neturtinės žalos, patirtos dalyvaujant šiame tyrime, atlyginimą.

Su draudimo taisyklėmis galite susipažinti tyrimo vietoje, kreipdamiesi į gydytoją tyrėją. Jei manote, kad tyrimo metu patyrėte žalą, taip pat kreipkitės į gydytoją tyrėją.

14. Kokias pasirinkimo galimybes turėsite, jeigu nesutiksite dalyvauti šiame tyrime arba atšauksite sutikimą jame dalyvauti?

Tyrime dalyvaujate savanoriškai, todėl turite teisę atsisakyti, o pradėjęs galite bet kada iš jo pasitraukti.

Jei atsisakysite dalyvauti biomedicininiame tyrime arba atšauksite sutikimą dalyvauti biomedicininiame tyrime, užtikrinsime Jūsų asmens teisę gauti įprastinę sveikatos priežiūrą.

15. Ar galėsite nutraukti dalyvavimą tyrime?

Jei nuspręsite pasitraukti iš tyrimo šiam nepasibaigus, tyrėjas pateiks ir paprašys parašyti laisvos formos atsisakymo prašymą arba užpildyti atsisakymo formą.

Norėtume atkreipti dėmesį, kad šio tyrimo rezultatai, t. y. tyrimo dokumentuose iki Jūsų sutikimo dalyvauti biomedicininiame tyrime atšaukimo įrašyti duomenys nebus sunaikinti.

Jeigu dėl pablogėjusios sveikatos būklės negalėsite spręsti apie tolesnes galimybes dalyvauti tyrime, į Jūsų norą atšaukti sutikimą dalyvauti tyrime bus atsižvelgta, bet teisiškai šį sprendimą priims sutuoktinis, jeigu jo nėra – vienas iš tėvų, pilnamečių vaikų, globėjas ar rūpintojas.

Jūs turite teisę nesutikti, kad biomedicininio tyrimo tikslu toliau būtų naudojama Jūsų sveikatos informacija, gauta šio biomedicininio tyrimo metu[2].

16. Jūsų dalyvavimo tyrime nutraukimo aplinkybės ir kriterijai

Jei nesilaikysite gydytojo tyrėjo nurodymų ar dalyvaujant tyrime smarkiai pablogės Jūsų sveikatos būklė, Jūs daugiau nebegalėsite dalyvauti tyrime.

Tyrimo gydytojas ar užsakovas turi teisę bet kuriuo metu sustabdyti tyrimą ar Jūsų dalyvavimą jame. Jūs nebegalėsite dalyvauti tyrime, jei neatvyksite į suplanuotus vizitus ar nesilaikysite kitų tyrėjų nurodymų.

17. Ar dalyvaudami šiame tyrime patirsite kokių nors išlaidų?

Už dalyvavimą šiame biomedicininiame tyrime atlygis ir kompensacijos nėra numatytos. Dalyvaudami šiame tyrime negausite finansinės naudos.

[2]Taikoma, kai tiriamasis Biomedicininių tyrimų etikos įstatymo 7 straipsnio 6 dalyje nustatyta tvarka buvo įtrauktas be sutikimo.

18. Ar Jūsų asmens duomenys bus konfidencialūs?

Biomedicininį tyrimą atliekant gauta sveikatos informacija, leidžianti nustatyti asmens tapatybę, yra konfidenciali ir gali būti teikiama tik pacientų teises ir asmens duomenų apsaugą reglamentuojančių įstatymų nustatyta tvarka, remiantis ES bendruoju duomenų apsaugos reglamento 6 straipsniu (2016/679).

Duomenų valdytojas yra VšĮ Lietuvos sveikatos mokslų universiteto ligoninė, Kauno klinikos, įmonės kodas: 135163499, adresas: .Eivenių g. 2, LT-50161, Kaunas.

Siekiant apsaugoti duomenų konfidencialumą, Jums bus suteiktas specialus kodas, kuris bus nurodomas visuose dokumentuose, išskyrus sutikimo formą. Sąrašą, kuriame Jūsų vardas ir pavardė susiejami su kodu, saugos pagrindinis tyrėjas seife, į kurį prieigą turi tik jis ir įgaliotas tyrėjas.

Kompiuteriai, kuriuose saugomi elektroniniai tyrimo dokumentai ir duomenys, apsaugoti slaptažodžiu. Prisijungimo kodus žino tik tyrėjai, šie duomenys atnaujinami kas mėnesį.

Dokumentai saugomi rakinamoje spintoje, kurios raktą turi tik tyrėjai.

Jei sutiksite dalyvauti šiame tyrime, gydytojas tyrėjas ir tyrimo darbuotojai naudos tyrimui atlikti reikalingus Jūsų asmeninius duomenis, bei mediciniius duomenis (ligos istorija, vaizdiniai tyrimai (KT,MRT, kontrastinis UG), histologinis tyrimas) iš dokumentų esančių mūsų, LSMU KK įstaigoje taip pat, duomenys bus renkami remiantis ir Jūsų pateikta informacija, kuri saugoma ligoninės informacinėje sistemoje: gretutinės ligos, ar anksčiau buvo diagnozuota gerklų ir gerklaryklės karcinoma, KT ir MRT tyrimo rezultatai (lokalaus išplitimo vertinimas: skydinės kremzlės struktūra, pažeidimas, pažeidimo vieta (priekinis, vidurinis ar užpakalinis 1/3-daliai, kuriame gerklų aukšte ir pusėje) paraglotinių audinių infiltracija), UG su ir be kontrasto duomenys (neosifikuotos skydinės kremzlės, paraglotinių audinių, patologinės infiltracijos k/m kaupimas, jo intesyvumas, k/m kaupimo intensyvumo pikas (sekundėmis)), histologinio tyrimo rezultatai (skydinės kremzlės pažeidimas, paraglotinių audinių infiltracija).

Atliekant šį tyrimą gauta sveikatos informacija nelaikoma konfidencialia ir gali būti paskelbta be Jūsų sutikimo, jeigu ją paskelbus nebus galima tiesiogiai ar netiesiogiai nustatyti Jūsų tapatybės.

19. Kas ir kokiu tikslu galės susipažinti su Jūsų asmens duomenimis?

Pasirašydami šią formą sutinkate, kad tyrimo centro tyrėjai, tyrimus kontroliuojančios institucijos (tokios kaip etikos komitetai) ir įgalioti tyrimo užsakovo tyrimą prižiūrintys asmenys galės susipažinti su visa šio tyrimo tikslais apie Jus surinkta informacija. Kitiems asmenims ar įmonėms bus teikiami tik užkoduoti sveikatos duomenys, neleidžiantys tiesiogiai nustatyti Jūsų tapatybės. („Užkoduoti“ reiškia, kad dokumentuose bus nurodomas ne Jūsų vardas ir pavardė, o specialus numeris, kurį susieti su Jūsų asmeniu galės tik gydytojas tyrėjas).

Surinktus duomenis tyrimo gydytojai naudos tik šio biomedicininio tyrimo tikslais. Užsakovas užkoduotus sveikatos duomenis gali naudoti atlikdamas tyrimą, pateikdamas prašymus dėl mokslinio tyrimo, diagnostikos ar norėdamas kurti medicinines priemones.

Jūs turite teisę sužinoti, kokie duomenys buvo surinkti, taip pat galite reikalauti ištaisyti, sunaikinti ar sustabdyti savo asmens duomenų tvarkymo veiksmus, jei nuspręsite pasitraukti iš tyrimo anksčiau numatyto laiko. Tada tyrėjai apie Jus neberinks naujos informacijos, bet negalės sunaikinti iki tol surinktų duomenų.

20. Kiek laiko bus saugomi tyrimo metu surinkti duomenys ir kas už tai bus atsakingas?

Visa informacija bus užrašoma specialiai klinikiniam tyrimui sudaromuose elektroniniuose ir popieriniuose dokumentuose ir tyrimo centre saugoma 5 metus nuo biomedicininio tyrimo pabaigos datos. Tiek laiko saugoti duomenis įpareigoja teisės aktai, siekiant užtikrinti duomenų kokybę ir kontrolę. Vėliau Jūsų asmens duomenys bus sunaikinti tyrimo centro nustatyta tvarka. Už dokumentų saugojimą tyrimo centre bus atsakingas pagrindinis tyrėjas.

Kontaktai: Saulius Vaitkus, el.paštas: saulius.vaitkus@kaunoklinikos.lt, buveinės adresas: Eivenių g. 2, Kaunas LT-50161).

21. Kas įvertino šį biomedicininį? / Į ką kreiptis, jeigu iškiltų klausimų?

Dėl savo kaip tyrimo dalyvio teisių galite kreiptis į leidimą atlikti šį biomedicininį tyrimą išdavusį Kauno regioninį biomedicininių tyrimų etikos komitetą, Lietuvos sveikatos mokslų universitetas, Mickevičiaus g. 9, LT-44307, Kaunas, tel. (8-37) 326889, el. paštas: kaunorbtek@lsmuni.lt.>

Iškilus bet kokiems su biomedicininiu tyrimu susijusiems klausimams galite kreiptis į pagrindinio tyrėjo atstovą – gyd. Mildą Pucėtaitę, telefonu +37064588543 arba el. paštu: milda.pucetaite@kaunoklinikos.lt

Jūs turite teisę pateikti skundą dėl asmens duomenų tvarkymo Valstybinei duomenų apsaugos inspekcijai. Skundą galite pateikti paštu (adresu: L. Sapiegos g. 17, 10312 Vilnius) arba naudodamiesi Valstybinės duomenų apsaugos inspekcijos elektroninių paslaugų sistema: /go.php/lit/Prisijungti/37L. Valstybinės duomenų apsaugos inspekcijos kontaktinis telefono numeris (8-5) 212 7532, el. paštas: ada@ada.lt.

SUTIKIMAS DALYVAUTI BIOMEDICININIAME TYRIME

Aš perskaičiau šią Informuoto asmens sutikimo formą ir supratau man pateiktą informaciją.

Man buvo suteikta galimybė užduoti klausimus ir gavau mane tenkinančius atsakymus.

Supratau, kad galiu bet kada pasitraukti iš tyrimo, nenurodydama(s) priežasčių[3].

Supratau, kad asmuo, dėl kurio dalyvavimo biomedicininiame tyrime aš duodu sutikimą, gali bet kada pasitraukti iš tyrimo, nenurodydamas priežasčių.[4]

Supratau, kad norėdama(s) atšaukti sutikimą dalyvauti biomedicininiame tyrime, raštu turiu apie tai informuoti tyrėją/kitą jo įgaliotą biomedicininį tyrimą atliekantį asmenį.

Patvirtinu, kad turėjau užtektinai laiko apsvarstyti man suteiktą informaciją apie biomedicininį tyrimą.

Supratau, kad dalyvavimas šiame tyrime yra savanoriškas.

Patvirtinu, kad sutikimą dalyvauti šiame biomedicininiame tyrime duodu laisva valia.

Leidžiu naudoti asmens duomenis ta apimtimi ir būdu, kaip nurodyta Informuoto asmens sutikimo formoje.

Patvirtinu, kad gavau Informuoto asmens sutikimo formos egzempliorių, pasirašytą tyrėjo/ kito jo įgalioto biomedicininį tyrimą atliekančio asmens.

Asmuo (ar kitas sutikimą turintis teisę duoti asmuo)

_____	_____	_____	_____	_____	_:_
vardas	pavardė	atstovavimo pagrindas	parašas	pasirašymo data	pasirašymo laikas

Patvirtinu, kad suteikiau informaciją apie biomedicininį tyrimą aukščiau nurodytam asmeniui.

Patvirtinu, kad asmeniui (ar kitam sutikimą duoti turinčiam teisę asmeniui) buvo skirta pakankamai laiko apsispręsti dalyvauti biomedicininiame tyrime, atsižvelgiant į biomedicininio tyrimo pobūdį, taip pat įvertinus kitas aplinkybes, galinčias daryti įtaką priimamam sprendimui.

Aš skatinau asmenį (ar kitą sutikimą turintį teisę duoti asmenį) užduoti klausimus ir į juos atsakiau.

Tyrėjas ar kitas jo įgaliotą biomedicininį tyrimą atliekantis asmuo

_____	_____	_____	_____	_____	_:_
vardas	pavardė	pareigos tyrime	parašas	pasirašymo data	pasirašymo laikas

[3] Jei sutikimą dalyvauti tyrime duoda pats asmuo

[4] Jei sutikimą dalyvauti tyrime duoda kitas asmuo

CURRICULUM VITAE

Name, Surname:	**Milda Pucėtaitė**
Address:	Department of Radiology, Hospital of Lithuanian University of Health Sciences Kauno klinikos, Eivenių 2, LT-50009 Kaunas, Lithuania
E-mail:	milda.pucetaite@lsmu.lt

Workplace:

August 2015 – present	Radiologist, Department of Radiology, Hospital of Lithuanian University of Health Sciences Kauno klinikos
September 2024 – present	Junior assistant, Lithuanian University of Health Sciences
September 2024 – present	Junior scientific assistant, Kaunas University of Technology

Education:

August 2019 – July 2025	PhD student, Lithuanian University of Health Sciences
September 2015 – June 2019	Medical resident, Hospital of Lithuanian University of Health Sciences Kauno klinikos
September 2009 – June 2015	Master's degree in Medicine, Lithuanian University of Health Sciences, Lithuania
September 2007 – June 2011	Bachelor's degree in Public Health, Lithuanian University of Health Sciences, Lithuania

Professional experience:

October 2023 – November 2023	*Observership.* Radiology Unit 2 of the ASST Spedali Civili di, Brescia, Italy
June 2019 – July 2023	*Observership.* Guy's and St. Thomas NHS Trust, London, UK
July 2018 – October 2018	*Observership.* Massachusetts Eye and Ear, Harvard Medical School, Boston, USA

April 2018 – June 2018 *Internship.* The Champalimaud Clinical Centre, Lisbon, Portugal

Participation in Research Projects and Clinical Trials:

"Precision Medicine: MRI-Guided Stereotactic Ablative Radiotherapy for Early-Stage Laryngeal Cancer (SMART)" (funded by the Research Council of Lithuania)

"A phase 3 open-label, randomized, controlled study to evaluate the efficacy and safety of petosemtamab compared with investigator's choice monotherapy treatment in previously treated patients with incurable, metastatic/recurrent head and neck squamous cell carcinoma" (international multicenter clinical trial)

"A phase 3 randomized, open-label study to evaluate the efficacy and safety of petosemtamab plus pembrolizumab vs pembrolizumab in first-line treatment of recurrent or metastatic PD-L1+ head and neck squamous cell carcinoma" (international multicenter clinical trial)

Membership at professional societies:

European Society of Head and Neck Radiology

PADĖKA

Nuoširdžiai dėkoju mokslinio darbo vadovui prof. dr. Sauliui Vaitkui už pasitikėjimą manimi ir šio darbo idėja. Dėkoju už nuolatinį palaikymą, kūrybiškumo skatinimą, mentorystę, profesionalias įžvalgas, pagalbą vykdant tyrimą ir rengiant mokslinius pranešimus.

Dėkoju nuostabiems šio darbo tyrėjams ir savo srities profesionalams, su kuriais galėjau ne tik dirbti, bet ir augti kaip specialistė: lekt. Valdui Šarauskui, prof. dr. Evaldui Padervinskiui, o ypač doc. Daliai Mitratei ir lekt. Silvijai Ryškienei. Dėkoju gyd. Ryčiui Tarasevičiui už pagalbą rengiant statistinę disertacijos dalį, ir prof. dr. Renatai Paukštaitienei už geranorišką sutikimą konsultuoti.

Nuoširdžiai dėkoju konsultantui prof. Davide Farina už palaikymą profesiniame kelyje ir perduotas žinias, kurios ypač pravertė rašant mokslinius straipsnius.

Dėkoju buvusiam Lietuvos sveikatos mokslų universiteto ligoninės Kauno klinikų Radiologijos klinikos vadovui prof. dr. Algidui Basevičiui už paskatinimą studijuoti doktorantūroje bei nuoširdų rūpestį ir žmogiškumą studijų laikotarpiu.

Taip pat dėkoju Kauno klinikų Ausų, nosies ir gerklės ligų klinikos gydytojams ir rezidentams, Radiologijos klinikos registratorėms, radiologijos technologams, bei bendrosios praktikos slaugytojai Kristinai Lapinskienei ir klinikos vyriausiajam inžinieriui Valdemarui Vingeliui už papildomas pastangas ir sklandų bendradarbiavimą. Kolegei ir draugei Laimai Tamkevičiūtei dėkoju už nupieštus „Lokalaus išplitimo ištyrimo schemos“ paveikslėlius.

Didžiausią padėką skiriu visai šeimai, ypač mamai Lidijai, už besąlygišką palaikymą ir tikėjimą manimi – tai buvo esminis motyvacijos šaltinis, padėjęs įveikti šį sudėtingą, tačiau prasmingą ir neįkainojamos patirties suteikusį etapą. Nuoširdžiai dėkoju mylimam vyrui Edvinui už palaikymą ir kantrybę disertacijos rašymo laikotarpiu.

Galiausiai dėkoju visiems nepaminėtiems kolegoms, artimiesiems ir draugams už palaikymą bei šiltus padrąsinimus.